Finite Element Analysis of Surface Acoustic Wave Resonators

A Thesis Submitted to the

College of Graduate Studies and Research

in Partial Fulfillment of the Requirements for the Degree of

Master of Science

in the Department of Electrical Engineering

University of Saskatchewan

Saskatoon, Saskatchewan

by

Thirumalai Kannan

PERMISSION TO USE

In presenting this thesis in partial fulfillment of the requirements for a Postgraduate degree from the University of Saskatchewan, I agree that the Libraries of this University may make it freely available for inspection. I further agree that permission for copying of this thesis in any manner, in whole or in part, for scholarly purposes may be granted by the professor or professors who supervised my thesis work or, in their absence, by the Head of the Department or the Dean of the College in which my thesis work was done. It is understood that any copying or publication or use of this thesis or parts thereof for financial gain shall not be allowed without my written permission. It is also understood that due recognition shall be given to me and to the University of Saskatchewan in any scholarly use which may be made of any material in my thesis.

Requests for permission to copy or to make other use of material in this thesis in whole or in part should be addressed to:

Head of the Department of Electrical Engineering
University of Saskatchewan
Saskatoon, Saskatchewan, Canada
S7N 5A9

ABSTRACT

Surface Acoustic Wave (SAW) devices are key components in RF and IF stages of many electronic systems. A Surface Acoustic wave is a mechanical wave, which is excited on the surface of a piezoelectric substrate, when an alternating electric voltage is applied through a comb-like interdigital transducer (electrodes) patterned on it. Most SAW applications to date have been in the sub-2GHz region, but emerging applications require SAW devices at higher frequencies. The traditional models are inadequate to account for pronounced second order effects at the GHz range and also new microfabrication techniques are required to obtain quality devices as the critical dimensions shrink into the nano-scale range at these frequencies. The finite element method (a numerical method of solving differential equations) has the potential to account for these effects and ever increasing sub-micron processing capabilities of LIGA (X-ray lithography) present a promising outlook for high frequency SAW device modeling and fabrication respectively.

A finite element model has been developed using commercial software ANSYS for one port SAW resonators and is presented in this thesis. The one port SAW resonators are generally connected in form of ladder networks to form low-loss SAW filters. The spacing between the electrodes and the velocity of the SAW determine the frequency of operation of these devices. A finite element model has been developed for three different types of SAW devices namely Rayleigh, leaky and longitudinal leaky SAW (LLSAW). The LLSAW has higher velocity as compared to other two types and hence considered in this work as a good prospect for high frequency SAW devices.

A full finite element model could not be solved due to high computing requirements and hence some assumptions were made and the results were validated against published results in the literature. The results indicate that even with simplifying as-

sumptions and approximations FE model provides reasonably accurate results, that can be used in device design. Some of the simulations (in LLSAW based devices) in this work were also done with a view towards using LIGA (X-ray lithography) for fabrication of high frequency devices as they have the capability for high aspect ratios.

ACKNOWLEDGEMENTS

I would like to thank my supervisor, Dr. David M. Klymyshyn for providing me this wonderful opportunity to do my Masters degree and conduct some useful research. His unwavering support, invaluable guidance and suggestions in performing this research and presenting the thesis are greatly appreciated.

I would also like to thank TRLABS for providing research equipment and nice work environment without which smooth conduct of research work would not have been possible. In particular, I would like to thank Jack Hanson for helping me with computing resources whenever I approached him with a problem. Technical inputs from Anton Kachayev and Venkat Subramanian needs a special mention and their help was vital for this project.

Also, I would once again like to express my gratitude to Dr. David M. Klymyshyn and the University of Saskatchewan for providing me with financial assistance for this project.

Finally, I would like to thank my parents and siblings for their constant encouragement and support during this course. I am greatly indebted to Subramanian maama for his special efforts in helping me prepare documents required for Canadian visa/study permit. I would also like to extend my thanks to all my friends who kept me in good spirits during my stay here.

TABLE OF CONTENTS

LIST OF FIGURES

LIST OF TABLES

LIST OF ABBREVIATIONS

2D	2 dimensional
3D	3 dimensional
BAW	Bulk acoustic wave
BEM	Boundary element method
COM	Coupling of modes
DOF	Degree(s) of freedom
FE	Finite Element
FEA	Finite element analysis
FEM	Finite element method
GUI	Graphical user interface
HS	Homogeneous solution
IDT	Inter-digital transducer
IF	Intermediate frequency
LIGA	German acronym for lithography, electroplating and moulding
LLSAW	Longitudinal leaky surface acoustic wave
MR	Metallization ratio
PDE	Partial differential equation
PS	Particular solution
PSAW	Pseudo surface acoustic wave
Q-factor	Quality factor
RF	Radio frequency
SAW	Surface acoustic wave
SGI	Silicon Graphics, Inc
STW	Surface transverse wave

UV	Ultra violet
WLAN	Wireless local area network
XRL	X-ray lithography

1. Introduction

1.1 Surface Acoustic Wave Devices - An Introduction

There has been a tremendous growth in the telecommunications industry over the past few decades with a subsequent increase in demand for high quality components. Surface Acoustic Wave (SAW) devices have emerged as a key component in radio-frequency (RF) and intermediate-frequency (IF) stages of many communication systems such as satellite receivers, remote control units, keyless entry systems, television sets, and mobile phones, thereby greatly contributing to the growth. Worldwide production of SAW devices counts to hundreds of millions annually. As the SAW devices evolved, their complexity grew many fold with the requirement for better performance and models for prediction. In particular, usage of SAW devices in wireless communication systems demands higher operating frequencies, wider bandwidths, smaller sizes and lower insertion losses. Consequently, there is a pressing need for improved techniques in device fabrication and response prediction.

Surface acoustic waves are essentially mechanical waves (conventionally called acoustic waves) which propagate on the surface of an elastic medium with most of its energy concentrated near the substrate surface. In general, piezoelectric substrates such as lithium niobate, lithium tantalate, and quartz are used as elastic medium. The physical phenomenon on which the SAW devices is based is piezoelectricity, i.e. the virtue by which certain materials produce electrical charge when mechanically strained or vice versa. The most important part of a SAW device is the interdigital transducer (or electrodes as shown in Figure 1.1), IDT, that are patterned on the surface of the piezoelectric substrate using lithographic techniques. When an alternating electric input signal is applied to the electrodes, the electric

field penetrates the piezoelectric substrate and surface acoustic waves are induced due to piezoelectric coupling. Similarly, charge accumulates on the electrodes in response to the acoustic waves, which in turn induces secondary acoustic waves. In this manner, IDTs can act as transmitters, receivers and reflectors collectively [1].

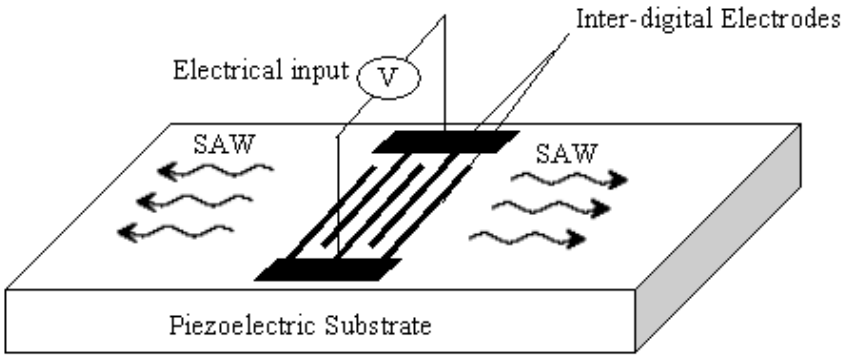

Figure 1.1: IDT in a SAW device

1.1.1 Classification of Acoustic Devices

SAW devices can be grouped under a broader classification of microwave acoustic devices [2]. Microwave acoustic devices can be defined as the ones which convert electromagnetic waves into acoustic waves for useful functions. They can be primarily divided into 3 groups depending on the type of primary waves that propagate.

- **Bulk Acoustic Wave (BAW) devices:** Waves in these type of devices propagate through the bulk and their frequency of operation depends on the thickness of the piezoelectric film. Although their velocity of propagation (phase) is higher than that of SAW, their frequency of operation is much lower due to the need for ultra thin films. But a significant advantage of these kind of devices is that they have high power handling capability and lower losses.

- **Surface Acoustic Wave (SAW) devices:** Surface acoustic waves are excited by interdigital electrodes and propagate on the surface of the piezoelectric

substrate. These are often called Rayleigh waves after their discoverer. Due to compatibility with microfabrication techniques, mass production is possible and also the capability of small features (with microfabrication) makes higher frequencies achievable. But compared to devices based on other waves, the limitations are lower phase velocity which limits the frequency of operation and lower power handling capabilities.

- **Pseudo SAW (PSAW) devices:** This type of wave propagation combines both the attributes of BAW and SAW. They have a component of bulk wave radiating into the substrate which can be controlled or trapped to the surface by interdigital electrodes or gratings on the surface. They have higher phase velocity and better power handling capabilities than SAW and at the same time are suitable for production by lithographic techniques. These features make PSAW devices attractive for higher operating frequencies.

1.1.2 Features of SAW and PSAW Devices

A single SAW device package with piezoelectric substrate and interdigital electrodes can perform complex signal processing such as bandpass filtering in a very compact physical package, which otherwise might require bulky high quality resonators. They are small, rugged and light weight which makes them a good choice for highly integrated wireless tranceivers. PSAW devices possess some additional merits in addition to the ones shared with the SAW counterparts. In addition to having higher phase velocity as compared to SAW, they have higher piezoelectric coupling (better ability to convert the electrical energy into mechanical and vice versa) which translates into wider operational bandwidth and lower insertion losses. Mass production is possible using techniques similar to semiconductor microfabrication which enables excellent reproducibility of these devices [3].

Acoustic wavelength λ is given by v/f where v is the velocity of SAW and f the frequency. The periodicity of the required interdigital electrodes is related to the acoustic wavelength λ, and is typically $\lambda/2$ as shown in Figure 1.2. The surface wave velocity is typically five orders of magnitude smaller than that of electromagnetic

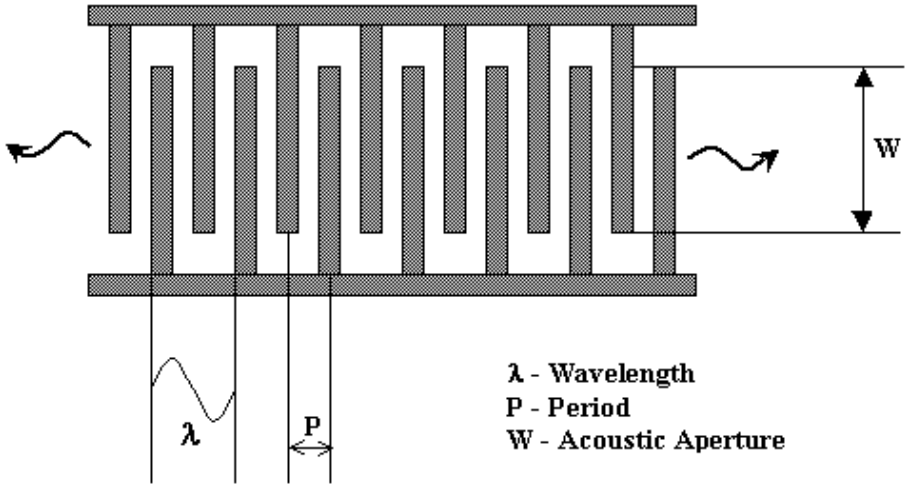

Figure 1.2: IDT periodicity and wavelength

waves in free space and therefore the wavelength is also much smaller at the same frequency, which translates into smaller device sizes. Contrastingly, these devices becomes unmanageably large at low frequencies and unmanageably small at high frequencies. For instance, SAW propagating with a velocity of 3000 m/s at 1 MHz will have wavelength of 3 mm or finger widths around 0.75 mm and wavelength of 300 nm or finger widths of 75 nm at 10 GHz. Both of these extremes represent fabrication challenges using contemporary fabrication technologies and hence SAW devices to date have mainly been realized from a few MHz to a couple GHz.

1.1.3 SAW Devices - Applications

Surface acoustic wave devices can be broadly categorized into 4 divisions based on their type of device operation and applications [3].

1. Bi-directional IDTs: This device operates with waves propagating in both the directions and includes devices such as delay lines and transversal filters. The device shown in Figure 1.3 is a basic delay line with distance between the input and output IDTs dictating the delay time. Since surface acoustic waves travel much slower than electromagnetic waves, longer delays are possible with small

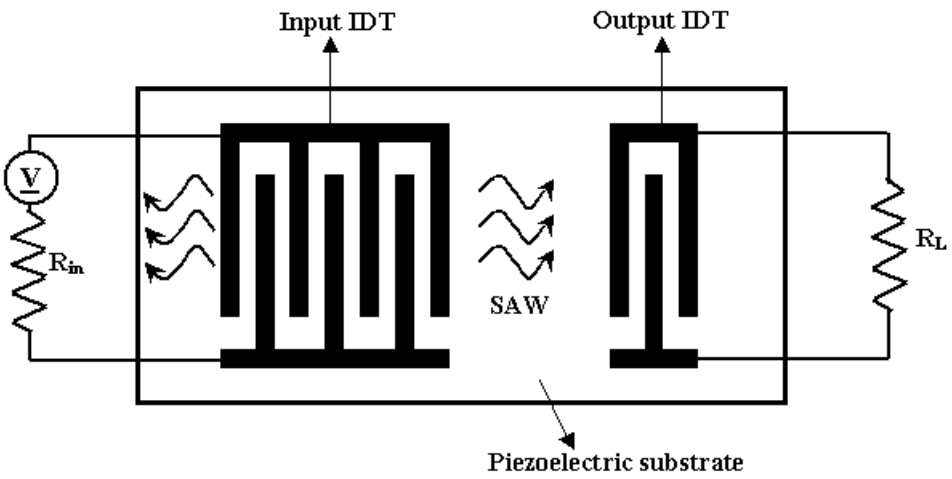

Figure 1.3: Bidirectional IDT: Delay line and transversal filter

device sizes. A similar configuration can also be used as a transversal bandpass filter with the IDT pitch as half the SAW wavelength. When the frequency is varied, the waves generated by the IDT pairs will not be in phase and the wave amplitude will decrease giving rise to bandpass action. The frequency response can further be synthesized by apodizing the IDTs, i.e. changing the finger overlap length with distance and also by altering the distance between the IDTs [2]. The waves are generated on both sides of the IDT and subsequently only half the power reaches the output IDT. Similarly, by reciprocity only half the acoustic power is reconverted into electrical energy at the output IDT. The other half is re-converted into SAW and sent back towards the source due to the piezoelectric effect. This causes a 6 dB loss and together with other second order effects, such as load mismatch and resistive losses, the losses typically increase to 15-20 dB. Bi-directional IDT devices are often employed as delay lines for oscillators, clock recovery filters for fiber optics communications repeater stages, IF filters for mobile/wireless receivers and pagers, etc.

2. Resonators and resonator filters: The SAW resonator shown in Figure 1.4 is of one port configuration with only one set of IDT and 2 sets of reflectors on either side. The waves generated by the IDTs at a particular frequency (deter-

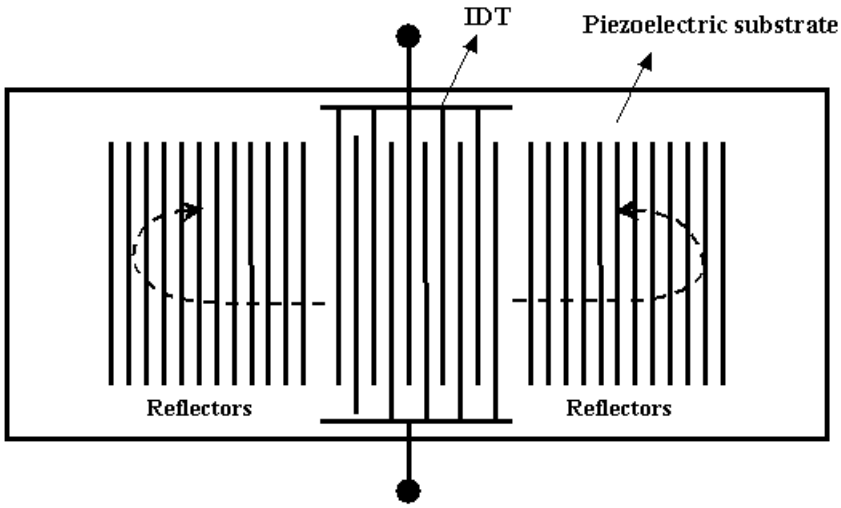

Figure 1.4: SAW resonator with reflectors

mined by the period of the IDT) are constructively reflected by reflectors. The distance between the reflector centres is set to be half of the SAW wavelength enabling in-phase reflections at that particular frequency. At other frequencies, the waves get reflected out-of-phase and consequently die out resulting in a highly frequency selective resonator. The reflected waves form a standing wave pattern which is fundamental to device operation and such resonators are widely used in oscillators and ladder filters. The ladder filters are constructed by connecting the SAW resonators as impedance elements in the form of a ladder network [2]. The series arm resonant frequency is selected together with the parallel arm anti-resonant frequency to get bandpass filter action. Resonator filters are often used in automotive keyless entry, medical alert transmitter circuits and in RF front-ends for wireless and mobile receivers.

3. Unidirectional IDTs: High losses incurred due to the bi-directionality of the IDT can be partially compensated by excitation of waves in one direction only. This is made feasible by smart use of the reflectivity of the IDT fingers. Generally some degree of asymmetry is introduced in the IDT such as two thickness metallization, use of reflectors between electrodes, electrodes with

different widths, etc, [4]. These techniques attempt to reinforce the waves launched in one direction by virtue of internal reflections. High frequencies (as compared to the bi-directional case) are not always attainable because ultra thin electrodes are required at times for unidirectional SAW excitation. Unidirectional IDTs are employed in low-loss IF filters (typically $<$ 3dB) for mobile and wireless circuits and RF front-end filters for mobile communications.

4. Nonlinear devices: Increased power densities at the substrate surface results in a nonlinear response between the input and output signals. The mechanical deformation caused by the electrical input is no longer perfectly elastic. When the power levels are sufficiently high, SAW devices start to operate in nonlinear mode. Since the penetration depth is low for SAW as compared to PSAW and BAW, higher power densities are easier to achieve and consequently these devices are often employed for nonlinear operation. SAW convolvers are often used in spread spectrum communications and a simple unit consists of 2 IDTs, one for the coded input signal and another for the reference signal with a metal film in between them acting as the third port delivering a correlated output.

1.2 Research Motivation and Focus

The ever-increasing growth of telecommunication devices and technologies, causing a demand for bandwidth, has forced the emerging applications to move further up in the frequency scale. Bluetooth and Wireless Local Area Networks (WLANs) operating at 2.45 GHz and 5-6 GHz are telling examples of this trend [5]. The features, merits and applications described in the previous section make the SAW devices attractive in the high frequency range and this has led to increase in demand, especially above the 2 GHz range. The velocity of propagation and linewidth of electrodes (directly linked to the wavelength of SAW being excited) are the two parameters on which the accomplishment of higher operating frequencies depend as specified by the relation $f = v/\lambda$. Clearly, an increase in velocity of propagation of SAW or a decrease in wavelength of IDT patterns corresponding to the SAW

being excited, increases the frequency of operation. This opens up three avenues for research towards acquiring higher frequencies of operation, namely, searching for materials propagating SAW at a higher velocity, by effective utilization of different surface modes that travel with higher velocities, and developing new reproducible techniques for fabrication of high quality sub-micron electrode fingers.

1.2.1 Materials for Higher Velocities and Performance

Piezoelectric materials like quartz and lithium-niobate have been traditionally used in SAW device production, but recently there has been increased activity in the search for materials that propagate SAW more effectively and swiftly, with an eye towards achieving higher frequencies. Non-piezoelectric substrates such as silicon and sapphire have been employed in SAW devices for quite some time facilitated by the deposition of thin film piezoelectric materials [6] such as ZnO (Zinc Oxide) for electrical excitation of acoustic waves. But since the materials have propagation velocities close to the conventional values, they did not offer much of an improvement in frequency ranges. But recently, usage of diamond film [7] in combination with a ZnO piezoelectric layer has shown promise towards realization of high frequency devices without crossing the sub-micron fabrication barrier. With diamond having propagation velocities around $10,000$ m/s, Nakahata et al. have fabricated a narrow band filter at 2.45 GHz with electrode widths around 1 μm. Nitride film based devices such as GaN (Gallium nitride) thin film filters [8] and AlN (Aluminum Nitride) on SiC (Silicon Carbide) [6] substrates, propagating SAW at 5803 m/s and around 6000 m/s respectively, have also been reported in the literature. Thin films of dielectric materials are also often deposited on the substrates for useful modification of SAW propagation properties, improved coupling and reduced temperature effects [6]. With improved methods to process high quality materials and effectively apply them in device production, the prospects for production of high frequency SAW components looks bright.

1.2.2 Modes for Higher Frequencies

Rayleigh waves that die out within two to three wavelengths in depth from the surface, typically have velocities around 3000 m/s. But there are some crystal cuts (explained in Chapter 3) such as YX-128° Lithium niobate ($LiNbO_3$) which propagate Rayleigh SAW at velocities close to 4000 m/s. Nevertheless, to achieve frequencies of operation above 1 GHz, linewidths less than 1 μm are needed. So, pseudo-SAW modes with higher velocities such as leaky SAWs and surface transverse waves (STW) are getting increased attention due to their potential for achieving higher operating frequencies. Table 1.1 shows a comparison of leaky and surface transverse wave to that of Rayleigh wave velocities in different materials. With

Table 1.1: Rayleigh and pseudo-SAW velocities in different materials [3]

Wave type	Material and cut	Velocity (m/s)
Rayleigh	Quartz-ST	3158
SAW	YZ-$LiNbO_3$	3488
	YX-128° $LiNbO_3$	3992
Leaky	LST-Quartz	3948
SAW	64°YX $LiNbO_3$	4478
	36°YX $LiTaO_3$	4112
Surface	Y-cut ST quartz	4990
transverse	36°YX $LiTaO_3$	4211
wave (STW)	35.5°(AT)Y-cut Quartz	5100

velocities above 4000 m/s, devices based on leaky and surface transverse waves are being increasingly employed in the lower GHz (1-3 GHz) region. In particular, STW based devices above 2 GHz have been reported by Avramov et al. [9].

More recently, a second order leaky SAW mode called longitudinal leaky SAW

(LLSAW) with velocities above 6000 m/s have been reported to exist in several substrates. Longitudinal leaky waves with a velocity of 6700 m/sec on lithium tetraborate ($Li_2B_4O_7$) have been reported by Sato and Abe [10]. They have also fabricated filters at 1.2 GHz and 1.5 GHz without using sub-micron fabrication techniques [11]. Similarly, LLSAW on YZ-$LiNbO_3$ with velocities around 6100 m/s have been used at 2.5 GHz [12] and 5.2 GHz [13] by Makonnen et al. Also, different crystal cuts of the same materials are also often explored in order to strike a balance with velocity, temperature effects, insertion losses and other propagation issues.

1.2.3 Sub-micron Fabrication for High Frequency SAW Devices

SAW devices are predominantly built using similar photolithographic patterning techniques used in the semiconductor industry. SAW devices are typically produced by a simple repeatable technique called lift-off process as depicted in Figure 1.5 (subsequent steps are indicated by block arrows). The process involves coating the substrate with resist material and subsequently exposing areas of interest to optical light using a mask produced by a similar process. The exposed regions are washed away using suitable chemicals forming the development step after which the whole area is metallized and the remaining resist is dissolved chemically and lifted off, leaving metal conductors standing on the substrate. Also other techniques such as etching are used in fabrication wherein, the metal is deposited on the substrate directly after which it is patterned using a resist and then etched away. Fabricating sub-micron electrodes is quite challenging using optical lithography, for instance Ultra-Violet (UV) and deep UV lithography, but by useful techniques such as off-axis illumination, SAW resonators have been fabricated at 2.45 GHz [14] and 3.15 GHz [15]. Electron beam (e-beam) lithography has been used to fabricate SAW resonators at 10 GHz with electrode widths below 100 nm [16]. But fabrication using e-beam lithography is an extremely slow serial writing process with low throughput which is suitable only for prototyping and not mass production.

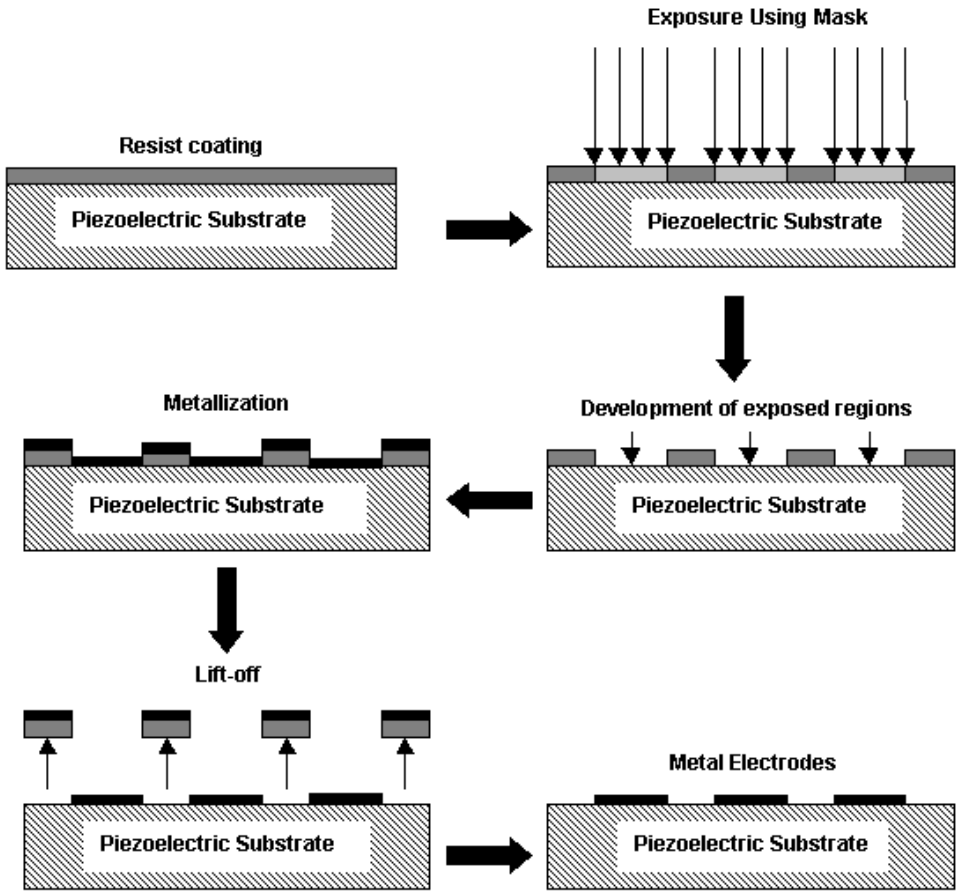

Figure 1.5: Lift-off process

Fabrication Using X-ray Lithography

A relatively unexplored technique for SAW device fabrication is X-ray Lithography, which is also sometimes part of the LIGA process (German Acronym for X-ray Lithography, Electroplating and Moulding). Short wavelength hard X-rays are used for lithography which is generally sourced from a synchrotron. An X-ray sensitive polymeric material coated on top of the substrate is exposed to high energy X-rays through a patterned mask. The exposed regions can be washed away using suitable chemicals and a metal layer could be deposited on it. Lift-off process explained in the previous section could be used to produce free standing electrodes on top of the substrate. The additional promising feature of LIGA, the prospect of high

throughput and mass fabrication using "hot embossing" could be pursued later. In this process, a metal mould obtained using electroplating could be used to replicate SAW structures on softened resist without exposure. Well defined structures with excellent sidewall quality and sub-micron features, around 400 nm are currently possible using X-ray lithography (XRL) [17]

X-ray lithography with etching technique has been used by Yoshioka et al. to fabricate SAW filters with linewidths in the range of 1.7-0.6 μm [18]. The typical electrode thickness of SAW devices would be around 5% (height to wavelength ratio) but for the high velocity LLSAW, the optimal thickness ratio is often around 10% which is easily attainable using XRL technology, which specializes in high aspect ratio structures, even at reduced metallization ratios as opposed to some other technologies. Although the extremely high aspect ratio capabilities (height to width ratio as high as 100:1) possible with XRL is not likely required for traditional modes, they could present some interesting structural possibilities for research into new architectures. And finally, the possible finer resolution that is improving all the time and the mass production potential make XRL a good choice for SAW device fabrication.

1.2.4 Need for Better Models

As the frequency of operation increases, the electrode thickness is no longer negligible compared to the SAW wavelength. Rather, the electrode mass (thickness) affects the centre frequency of the device to a great extent. With newer modes like Longitudinal Leaky SAW, the electrode thickness becomes even more critical. Also, operations of these kind of devices clearly belong to two realms namely, mechanical and electrical (piezoelectric). So models which are not completely derived from first principles (or based on electrical aspects alone), such as equivalent-circuit models and matrix models do not fully characterize the physics of SAW propagation and would fail to capture the high frequency effects. So a model which takes into account the complete set of partial differential equations (PDE) defining the problem, is needed.

Finite element modeling is one such method which solves the partial differential equations numerically by subdividing the whole domain into finer meshes called el-

ements. Finite element method (FEM) is a powerful technique to solve PDEs and has long been used by engineers to solve mechanical, structural, and electrical problems. There are also other pure numerical solvers such as Green's function method, boundary element method and finite difference methods. But they are not as popular as FEM to have fully developed commercial softwares to help in easier modeling of devices. There exists a lot of literature on usage of FEM to model Acoustic wave devices, but many of them are limited to Bulk wave type. BAW resonators in piezoelectric media have been modeled by Lerch [19] , Makkonen [20] and others using FEM formulation. Even though extension of such models to SAW devices is straightforward and potentially as accurate, not much progress has been made due to intensive computational and consequent memory requirement. BAW devices are generally made of thin films whereas SAW devices are generally constructed on thicker substrates and sometimes on layered substrates,making the computational requirements shoot up exponentially. But the imminent widespread usage of 64 bit computing and solving of 111 million degrees of freedom (number of unknowns) by SGI, Intel and ANSYS [21] presents good prospects for solving full scale SAW models using FEM in the near future.

Coupling-of-Modes (COM) model is another successful model which is widely used in the industry because of its speed and effectiveness to model SAW and PSAW modes. But parameters needed to model the devices using COM theory, need to be introduced from outside. Often, one port SAW resonators are fabricated [22] and parameters are measured to be input as COM parameters in a simulation. But analyzing structures with different metallization ratio and thickness becomes an expensive and time consuming approach if devices were to be fabricated every time in order to extract the parameters. Numerical models such as FEM can be used in place of real-device-fabrication, to extract the required parameters for further micro-acoustic device design and can be an efficient tool in the design of new SAW devices and structures.

1.3 Thesis - Objectives

The purpose of this thesis is to develop an accurate finite element model for one-port SAW resonators. Even though the potential accuracy of finite element calculations has been known for sometime, they were not applied to SAW devices due to lack of computing resources and time constraints. But recent advances in computing technology and promising future improvements warrants a fresh look at the capabilities of finite element modeling in SAW device design. The research work was focussed on the following specific objectives for this thesis work:

- Review existing models that are used for SAW device design and illustrate the need for simulators that are based on first principles to account for high frequency and structural effects.
- Development of a finite element model using commercial software ANSYS and verification and validation of results with the ones in literature.
- Extension of the finite element model to more complex leaky SAW resonators and comparison with measured resonator results.
- Modeling of longitudinal leaky SAW resonators in the perspective that the high mode velocity can be used in the realization of high frequency SAW resonators.

1.4 Thesis Organization

This thesis work has been organized in to 6 chapters and the contents are briefly outlined as follows:

Chapter 2 provides the mathematical base for the problem at hand and discusses the properties of various waves, which would be useful in FE modeling of the devices based on them.

In Chapter 3, the existing SAW device models are briefly discussed along with their shortcomings. The assumptions approximations and other basic details about finite element modeling of SAW resonators is also provided in this chapter.

In Chapter 4, the results are presented for Rayleigh SAW and leaky SAW based devices. The results are compared to published as well as some measured test results.

Chapter 5 deals with the FE modeling of LLSAW based SAW devices and the effect of metallization ratio and electrode height on the resonator response.

In Chapter 6, the summary of this thesis, conclusions of this research and some future research directions in this field are provided.

2. Surface Acoustic Waves - Physics

2.1 Elastic Waves

A basic understanding of elastic wave propagation and brief overview of differential equations governing it explains the complexity in solving surface acoustic wave problems. It is also highly useful in the simulation of SAW resonators using the finite element method, as it helps in making valid assumptions and approximations. The material types and properties also dictate what kind of waves propagate on the substrate warranting a brief overview.

Waves are nothing but propagation of energy from one point to another in a medium. Elastic waves in particular are the ones which propagate through a medium without causing permanent deformation to it. A very basic classification of elastic waves yields two types namely, longitudinal and shear waves [23]. The classification is based on the polarization of particle displacement in the medium. It is also worth mentioning that polarization is the direction (in a particular co-ordinate system) of the displacement of the particles in the medium, vibrating to aid in wave propagation.

- **Longitudinal waves:** These are also known as compression waves and the wave propagation takes place by particle displacement (polarization) in the direction of wave vector as shown in Figure 2.1. During longitudinal wave propagation, the distance between planes containing a certain number of particles varies and consequently, the volume occupied by a given number of particles is not a constant.

- **Shear waves:** Shear or transverse wave propagation is due to particle displacement in the direction perpendicular to wave vector (Figure 2.1) and is

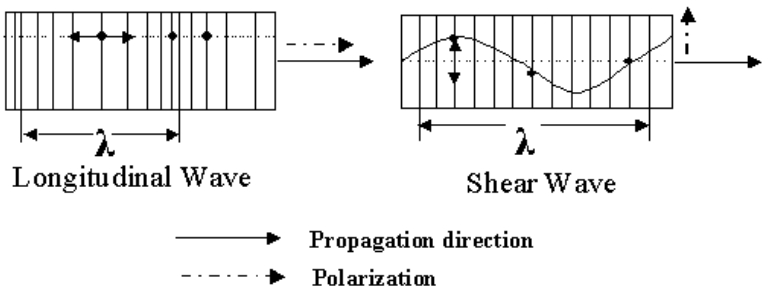

Figure 2.1: Elastic waves - Types [23]

not accompanied by variation in volume as opposed to the longitudinal case.

But in many practical cases such as surface acoustic waves, simple wave propagation explained above is not possible. The displacements are often complex and a mixture of these two types of wave propagation. A closer look at the wave propagation equations reveals some of the issues pertaining to surface wave propagation.

2.2 Acoustic Wave Terminologies

The understanding of wave propagation equations and subsequent solving of them involves some basic understanding of the concepts involved in it. So, a set of terms, variables and indices used in acoustic wave propagation are explained in this section.

Stress may be defined as the force acting on a unit area (N/m^2). The strain is the deformation per unit length and hence a dimensionless quantity. The stress is linearly proportional to the strain and is related by a proportionality constant called the stiffness coefficient C, and is termed as the Hooke's law. If all the quantities are considered with a co-ordinate axes as reference, components of stress and strain arise. The strain is given by,

$$S_{ij} = \frac{1}{2}\left(\frac{\partial U_i}{\partial j} + \frac{\partial U_j}{\partial i}\right) \tag{2.1}$$

where, S_{ij} are the strain components and $i, j = X, Y, Z$ co-ordinate directions. Also, it is worth mentioning that the indices or subscripts with i, j, k, l in this work always represents the X, Y, Z co-ordinate directions. In the Equation 2.1, if $i = j$ it is the normal strain and if not it is the shear strain. This gives rise to three normal strains and six shear strains in a three dimensional co-ordinate system. These elements can be arranged in a matrix form with normal strains as diagonal elements and shear strains as off-diagonal elements constituting a second order tensor (indicates the two subscripts of the strain).

The stress being linearly proportional to strain, must also be a second order tensor with normal and shear stress components and is given by T_{ij}. The relation between corresponding stress and strain components is given by,

$$T_{ij} \;=\; C_{ijkl}\, S_{kl} \tag{2.2}$$

where C_{ijkl} $(ijkl = X, Y, Z)$ are stiffness constants. Each subscript index can have 3 values (X,Y,Z) and hence the total number of stiffness constant is equal to $3 \times 3 \times 3 \times 3 = 81$. In elastic non-ferroelectric materials the stress matrix is symmetric in nature and consequently $T_{ij} = T_{ji}$ [24]. Due to this symmetry, the stiffness constants obey the following relation:

$$C_{ijkl} \;=\; C_{jikl} \;=\; C_{ijlk} \;=\; C_{jilk} \;=\; C_{klij} \tag{2.3}$$

This symmetry in turn reduces the number of independent stiffness constants to 21 [24]. In isotropic materials only two independent constants exist and in the most piezoelectric materials the number of independent constants is only six or seven.

It is useful to provide one stress component in Equation 2.2 as an example, that would help in understanding the summation of repeated subscripts in the equation and is given by,

$$\begin{aligned} T_{xx} \;=\; & C_{xxxx}S_{xx} + C_{xxxy}S_{xy} + C_{xxxz}S_{xz} + \\ & C_{xxyx}S_{yx} + C_{xxyy}S_{yy} + C_{xxyz}S_{yz} + \\ & C_{xxzx}S_{zx} + C_{xxzy}S_{zy} + C_{xxzz}S_{zz} \end{aligned} \tag{2.4}$$

The tensors discussed being symmetric, can be represented by one subscript rather than two (components with 4 subscripts will represented by 2). The notation that is generally followed is given in Table 2.1 [24].

Table 2.1: Reduction of subscripts

I	ij
1	xx
2	yy
3	zz
4	yz,zy
5	xz,zx
6	xy,yx

With this reduction in subscript notation, Equation 2.4 can be rewritten as,

$$T_1 \;=\; C_{11}S_1 + C_{12}S_2 + C_{13}S_3 + 2C_{14}S_4 + 2C_{15}S_5 + 2C_{16}S_6 \tag{2.5}$$

All other stress components can be written in a similar way and it is worthwhile to note that there are 36 components in stiffness matrix from C_{11} to C_{66} (a 6×6 matrix). This matrix is symmetric in nature and therefore could have only 21 independent constants, as noted previously.

In addition to the stress and strain components, the electrical constitutive relation of $D = \epsilon E$ also has corresponding components and is given by,

$$D_i \;=\; \epsilon_{ij}\, E_j \tag{2.6}$$

where $i, j = X, Y, Z$, D is the electric displacement field vector, ϵ the permittivity matrix and E the electric field vector. The permittivity matrix is a 3×3 matrix with mostly diagonal elements. Due to rotations for crystal cuts it might have off diagonal elements often, but nevertheless remains symmetrical.

A brief description about the terminologies involved in the acoustic wave equations was explained in this section and if more details are required about these topics, the reader is referred to [24].

2.3 Wave Propagation Equation

In this section, the basic wave equation formulation for a non-piezoelectric elastic medium is discussed. The reduction in subscript order (explained for the sake of reader understanding) discussed in the previous section is not implemented in the equations that follow for the sake of consistency with other formulations in the literature and clarity.

The basic wave equation is based on the fundamental law of dynamics given by,

$$F \;=\; \frac{\partial\, T_{ij}}{\partial\, X_j} \tag{2.7}$$

where F is the force density per unit volume, T_{ij} is the stress tensor and X_j are the axes of three co-ordinate direction ($X_x = X, X_y = Y, X_z = Z$). Then the wave equation for displacements in an elastic, homogeneous, anisotropic (characteristics different in different direction) as well as isotropic (characteristics same in all directions) medium is expressed as,

$$\rho\, \frac{\partial^2\, U_i}{\partial t^2} \;=\; \frac{\partial\, T_{ij}}{\partial X_j} \tag{2.8}$$

Where ρ is the mass density of the elastic medium and Ui are the displacements in respective co-ordinate directions. Equation 2.2 can also be written as [23],

$$T_{ij} \;=\; C_{ijkl} \frac{\partial U_l}{\partial X_k} \tag{2.9}$$

and summation over repeated indices implied, the full wave equation is given by,

$$\rho\, \frac{\partial^2\, U_i}{\partial t^2} \;=\; C_{ijkl}\, \frac{\partial^2\, U_l}{\partial X_j\, \partial X_k} \tag{2.10}$$

Equation 2.10 is a set of 3 equations for displacements U_x,U_y,U_z in 3 co-ordinate directions. The $ijkl$ takes all possible combinations of X, Y, Z values and are repeatedly summed in the right-hand side of the equation. The size of the wave equation

depends on the number of stiffness constants existing for a particular material. For instance, many entries are zero for materials that are isotropic or cubic (symmetry) and the equations are smaller, whereas for general piezoelectric materials fewer entries are zero and the equation can be lengthy. The other important thing to note in Equation 2.10 is that it represents wave propagation in a non-piezoelectric medium as noted before, but provides useful information about wave propagation in media and can be directly extended to piezoelectric case.

2.4 Wave Solutions in Unbounded Anisotropic Media

An unbounded medium is one which is infinite in all directions (of three co-ordinate axes) and the simplest solution for the wave equations in such media can be plane waves given by,

$$U_i \;=\; A_i \exp[jk(l_i i - vt)] \tag{2.11}$$

where A_i is the amplitude of displacement, $k.l_i$ is the wave vector (l_i describes the direction cosines of wave vector) and v is the velocity of wave [25].

Equation 2.11 represents three waves with different polarizations propagating in a given direction, i.e, a wave with displacement component only in the wave vector direction, a wave with displacement component in direction perpendicular to the wave vector direction and a wave with displacement component in the direction perpendicular to the plane in which the wave vector exists. The three waves are one quasi-longitudinal and two quasi-shear waves, categorized according to the polarization of the displacement of the corresponding waves. They are called quasi waves because of the fact that almost none (except for certain propagation directions at which modes become pure) of them have displacement components either in the direction of wave propagation or perpendicular to it but rather make a small angle to the propagation vector and its normals. Nevertheless, the polarizations of the three waves are always mutually perpendicular to each other. The velocity of the quasi-longitudinal wave is always higher than that of quasi-shear waves and also the shear waves have different velocities which are in turn classified as fast and slow shear waves depending on their velocities. This kind of wave propagation is true

only for unbounded media and all these modes propagate at all frequencies. But once the medium is bounded or finite, mechanical boundary conditions should be satisfied and these waves cannot propagate independently. This prompts a look into surface wave solutions for bounded finite media [23].

2.5 Surface Wave Solutions in Bounded Media

A co-ordinate system shown in Figure 2.2 is assumed for surface wave solutions with the surface at $Z = 0$ and extending to negative infinity. The wave vector is assumed to be in the XY plane, i.e parallel to the surface of the medium which is unbounded in the X and Y directions.

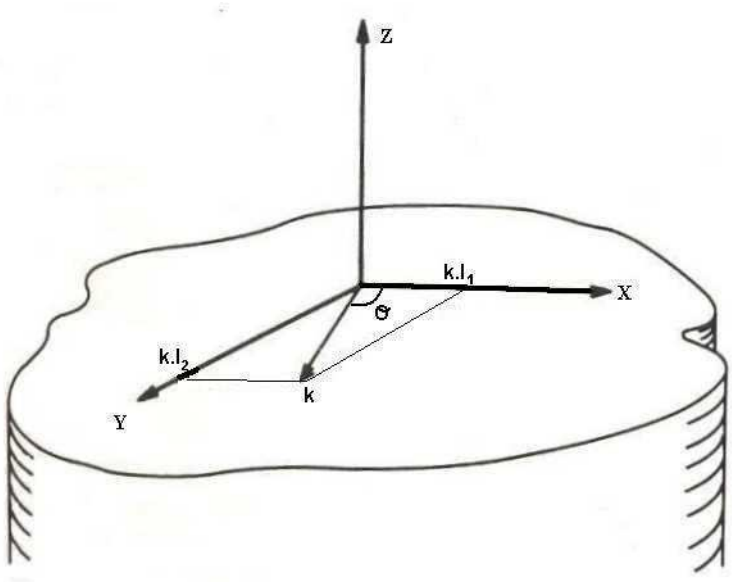

Figure 2.2: Co-ordinate system for surface wave solutions [25]

Surface wave solutions are those in which displacements decay with depth below the substrate surface and are straight crested, i.e there is no dependence of the displacement at any depth on the distance measured perpendicular to the sagittal plane [23] (plane containing wave vector and normal to the surface as shown in

Figure 2.2). Such a solution can be written in the form in which the Z dependence is treated as part of the amplitude term and wavelike properties depending on the X and Y components and is given by,

$$U_i \;=\; A_i \exp(jkl_3\mathbf{z}) \exp[jk(l_1\mathbf{x} + l_2\mathbf{y} - v\mathbf{t})] \tag{2.12}$$

It can also be written in terms of θ as,

$$U_i \;==\; A_i \exp(jkl_3\mathbf{z}) \exp[jk(\cos(\theta)\mathbf{x} + \sin(\theta)\mathbf{y} - v\mathbf{t})] \tag{2.13}$$

These solutions (with l_1 and l_2 or θ known) can be substituted into the Equation 2.10 and a 3×3 matrix is formed which when equated to zero (for non-trivial solutions), results in a sixth order equation in l_3 with v as a parameter. A sixth order equation has six roots with three complex conjugate pairs. For surface wave solutions, the value of l_3 must lead to displacement components vanishing as $z \to -\infty$. The roots in the upper half of the complex planes leads to solutions which makes displacements grow to infinity at $z = -\infty$. Contrastingly, the other three roots on the lower half complex plane leads to surface wave solutions for which the displacements vanish at infinite depth. The phase velocity is the same for each value of l_3 and is determined from the boundary condition matrix. A linear combination of the solutions in Equation 2.12 or 2.13 for each l_3 value in the lower half complex plane forms the assumed solution and is given by,

$$U_i \;=\; \sum_{r=1}^{3} A_{i,r} \exp(jkl_3^{(r)}\mathbf{z}) \exp[jk(\cos(\theta)\mathbf{x} + \sin(\theta)\mathbf{y} - v\mathbf{t}) \tag{2.14}$$

From Equation 2.14 it can be seen that there are 3 displacement amplitudes for each root and for 3 displacements there are totally 9 amplitudes. To determine these amplitudes and the phase velocity of the surface wave the boundary conditions should be satisfied at the surface.

2.5.1 Surface Boundary Conditions

The boundary condition that should be satisfied for the surface wave solution is that the surface at $z = 0$ should be stress free, i.e, no surface forces should be acting on

it. The stress free condition can be written from Equation 2.9 for stress as,

$$T_{i3} \;=\; C_{i3kl}\,\frac{\partial u_l}{\partial u_k} \;=\; 0, \quad at\; z = 0\; for\; i = 1, 2, 3 \tag{2.15}$$

or simply as,

$$T_{13} \;=\; T_{23} \;=\; T_{33} \;=\; 0, \;\; at\; z = 0 \tag{2.16}$$

Substituting the assumed solution (Equation 2.14) into the set of boundary conditions gives rise to another set of three homogeneous equations in terms of unknown displacement amplitudes. A 3×3 boundary condition matrix is formed and for non-trivial solutions to exist, the determinant must be equated to zero. The displacement amplitudes that ought to be found may be complex and as a consequence the boundary matrix determinant is also complex. For any particular value of v (in the l_3 component), it is almost improbable to give a determinant value equal to zero. The equation can be algebraically very complex to give an explicit analytic expression for the amplitudes. Instead, a set of successive values of velocities is substituted in the equation to find a particular value for which the determinant vanishes (both the real and imaginary parts should vanish). Nevertheless, explicit relations can be found out in certain special cases such as in isotropic media as reported by Farnell [25].

The velocity of surface waves remains constant in the case of isotropic media, whereas it is a function of propagation direction in the anisotropic case. For each direction a set of velocities should be successively checked for the boundary condition to vanish in order to find out the correct velocity. A plot of variation of phase velocity in XY plane of $LiNbO_3$ is shown in Figure 2.3 [25]. In the plot, the phase velocities are normalized to the shear wave velocity in the [100] direction (i.e the X direction). Evaluation of phase velocities for different directions was highly useful for SAW devices because, directions with higher phase velocities are often chosen for device fabrication to attain higher frequencies of operation. For example, in Figure 2.3 the phase velocity of surface wave varies as the direction of propagation is varied from X-axis (0°) and peaks when the direction of propagation is around 30°.

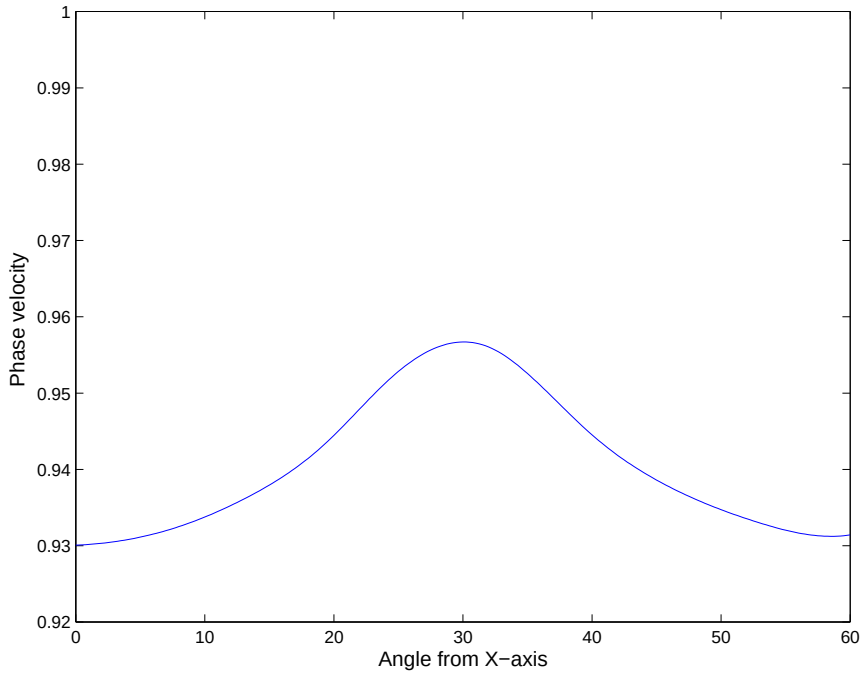

Figure 2.3: Normalized phase velocity as a function of direction in XY plane of $LiNbO_3$ [25]

2.5.2 Displacement Profile for Surface Waves

The homogeneity of the wave solution equations and boundary condition equations allows only for solutions of amplitudes to be found in terms of other amplitude(s). Also, the choice of displacement component to divide through, to find others in terms of it, is compounded by the fact that for certain special directions some displacement components are zero. So, effectively there are only two displacement components, which are confined to the sagittal plane.

In isotropic media, the roots or the values of l_3 are always on the imaginary axis, giving rise to purely exponential decay of displacements in the negative z direction as shown in the Figure 2.4. But in the case of anisotropic media, the roots are not restricted to imaginary axis in complex plane, but rather allowed to take complex values. The real parts in the roots causes the amplitudes of the displacements to oscillate with depth. Even though the real part may be viewed as part of the wave

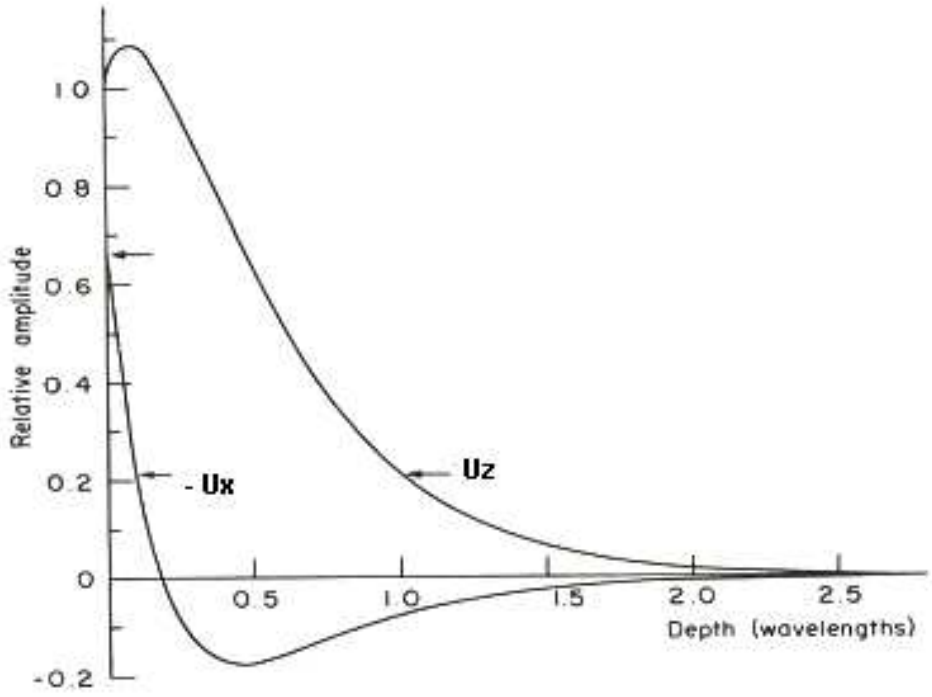

Figure 2.4: Longitudinal and vertical displacement variation in isotropic media [25]

vector, it is convenient to view the propagation vector as one parallel to the substrate and allow the complex root to be part of decaying component. This will allow the displacement amplitudes to be exponentially damped sinusoids as opposed to the simple exponential decay in the isotropic case. A typical variation of transverse and longitudinal displacements with depth for anisotropic case is shown in Figure 2.5.

The surface wave solutions explained until now are called Rayleigh waves, named after their discoverer. These waves die down within 2 to 3 wavelengths and the particle displacements are strictly confined to the sagittal plane as depicted in Figure 2.6(a). The longitudinal and vertical transverse components have a phase difference of $\pi/2$ and their amplitudes do not decrease in the same way as shown in Figures 2.4 & 2.5. Thus the particle displacement at any depth is described by an ellipse and the shape of the ellipse changes with depth due to the change in relative magnitudes of U_z and U_x with depth.

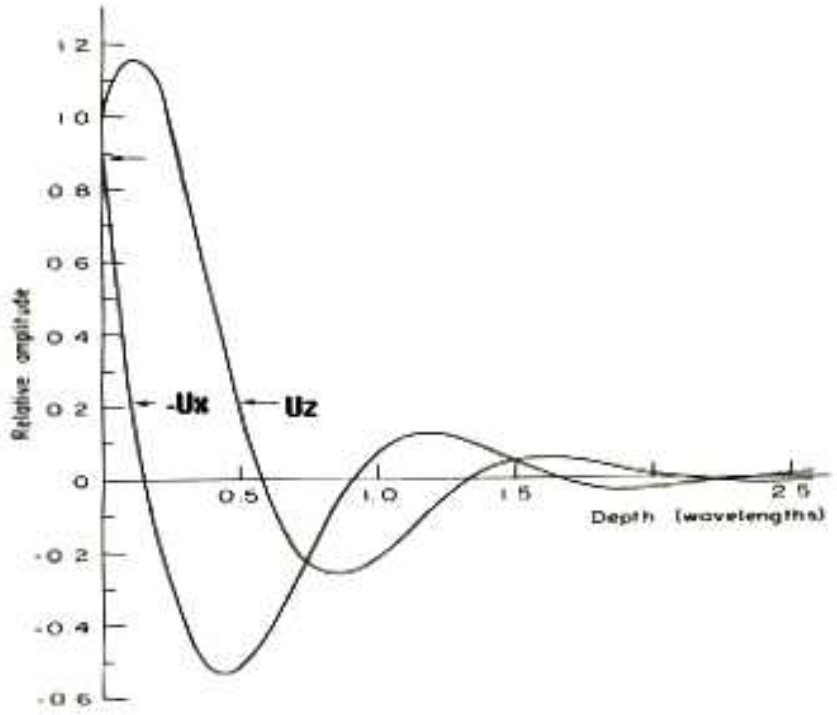

Figure 2.5: Longitudinal and vertical displacement variation with depth. Propagation in [100] axis of anisotropic nickel [25]

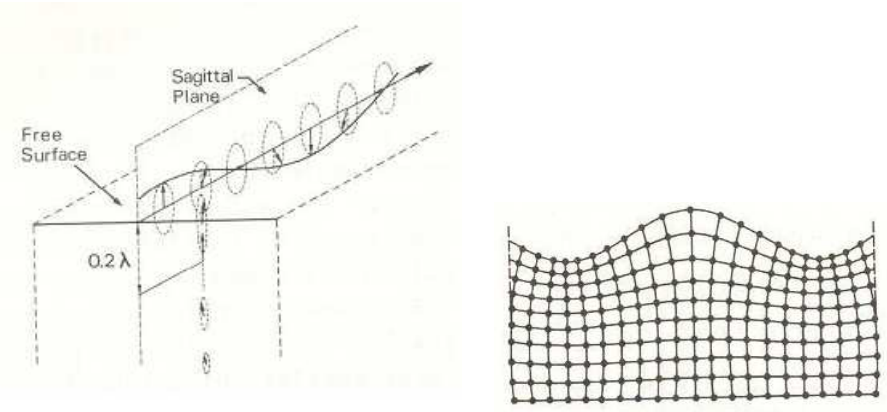

(a) Rayleigh wave (b) Sagittal Plane

Figure 2.6: Rayleigh wave with displacements in the sagittal plane [23]

2.6 Surface Waves With Piezoelectric Effects

The materials used in SAW devices are mostly piezoelectric and hence the piezoelectric effect which makes the wave equation a coupled (between mechanical and electrical domains) one, needs to be considered. In a piezoelectric material, the mechanical equations of motion discussed in the previous sections and Maxwell's equations for the electrical behavior are coupled through two constitutive equations given by,

$$T_{ij} = C_{ijkl}\, S_{kl} - e_{kij}\, E_k \tag{2.17}$$

$$D_i = e_{ikl}\, S_{kl} + \epsilon_{ik}\, E_k \tag{2.18}$$

where S_{kl} is the strain tensor (second rank), e_{kij} is the third rank piezoelectric tensor, E_k is the electric field in three directions, D_i is the component of electric displacement and ϵ_{ik} is the symmetric permittivity matrix. The Equation 2.17 is an extension of Hooke's law which espouses the relation between stress and strain in a material. In a piezoelectric material, the electric field produces an additional mechanical stress which is indicated in the equation as an additional term. Similarly, the inverse effect produces an additional term in the electric displacement relation as shown in Equation 2.18

As the velocity of acoustic waves are five orders smaller in magnitude as compared to electromagnetic waves, the frequency of the electric field waves can be considered to be small enough to categorize them as quasi-static. In such a case, the curl of the electric field can be assumed to vanish reducing the Maxwell's equation to,

$$\nabla \times E = 0, \tag{2.19}$$

enabling us to write electric field as the negative gradient of the scalar potential given by the following equation:

$$E = -\nabla \phi \tag{2.20}$$

Magnetic fields are rarely of interest in surface acoustic wave problems and hence Maxwell's equations concerning them are disregarded. The piezoelectric materials

are almost perfect insulators reducing the remaining Maxwell's equation to,

$$\nabla \, . \, D \;\; = \;\; 0 \tag{2.21}$$

The components of strain in Equations 2.17 and 2.18 are the same as in Equation 2.1. Substituting the relations for S_{ij} and E into the piezoelectric constitutive equations and henceforth into the wave equation and Maxwell's equation provides a system of coupled wave equations given by,

$$\rho \, \frac{\partial^2 U_i}{\partial t^2} \;\; - \;\; C_{ijkl} \, \frac{\partial^2 U_k}{\partial x_j \, \partial x_l} \;\; - \;\; e_{kij} \, \frac{\partial^2 \phi}{\partial x_k \, \partial x_j} \;\; = \;\; 0 \, , \tag{2.22}$$

$$e_{ikl} \, \frac{\partial^2 U_k}{\partial x_i \, \partial x_l} \;\; - \;\; \epsilon_{ik} \, \frac{\partial^2 \phi}{\partial x_i \, \partial x_k} \;\; = \;\; 0 \tag{2.23}$$

Surface wave solutions similar to the ones in non-piezoelectric case is assumed for the piezoelectric case, i.e., straight crested waves with displacements decaying below the substrate surface. A solution is also assumed for the potential in the medium, along with expressions for displacements in three directions. Again, the wave vector is in the XY plane and the Z-dependence of the wave is regarded as part of the amplitude term in the solution. The assumed solutions for the displacements are the same as for the non-piezoelectric case (given by Equation 2.12) and the solution for potential in the medium is given by,

$$\phi \;\; = \;\; A_4 \exp(jkl_3\mathbf{z}) \exp[jk(l_1\mathbf{x} + l_2\mathbf{y} - v\mathbf{t})] \tag{2.24}$$

where A_4 is the amplitude of potential that is to be determined using boundary condition equations. The solutions are substituted back into the wave equations given by Equations 2.22 and 2.23 to get a 4×4 matrix in terms of l_3 with v as a parameter. An eighth order equation thus formed is equated to zero for non-trivial solutions and in general has 8 roots (real or complex pairs). As before, the upper half plane roots that lead to displacements and potentials growing with depth are not taken into account and the four roots in the lower half of the complex plane are only considered as they correspond to surface wave solutions.

The displacements and potential are assumed to be linear combinations of four terms (corresponding to 4^{th} root) as opposed to three terms in the non-piezoelectric

case, as shown in the following equations:

$$U_i = \sum_{r=1}^{4} A_{i,r} \exp\left(jk\, l_3^{(r)}\mathbf{z}\right) \exp\left[jk(l_1\mathbf{x} + l_2\mathbf{y} - v\mathbf{t})\right] \tag{2.25}$$

$$\phi = \sum_{r=1}^{4} A_{4,r} \exp\left(jk\, l_3^{(r)}\mathbf{z}\right) \exp\left[jk(l_1\mathbf{x} + l_2\mathbf{y} - v\mathbf{t})\right] \tag{2.26}$$

The boundary conditions should be satisfied at the surface in order to determine the appropriate phase velocity and amplitudes of surface waves. Being a piezoelectric case, mechanical and electrical boundary conditions need to be satisfied simultaneously. The mechanical boundary condition is given by stress-free surfaces, i.e.

$$T_{i3} = C_{i3kl}\frac{\partial u_l}{\partial u_k} + e_{ki3}\frac{\partial \phi}{\partial u_l} = 0, \quad at\ z = 0\ for\ i = 1, 2, 3 \tag{2.27}$$

The electrical boundary condition is imposed by Maxwell's equations, the normal component of **D** being continuous across the air/substrate interface:

$$D_3 = -\epsilon_0 \frac{\partial\, \phi}{\partial\, x_3} \qquad for\ z > 0$$

$$D_3 = e_{3kl}\frac{\partial\, U_k}{\partial\, x_l} - \epsilon_{3k}\frac{\partial\, \phi}{\partial\, x_k} \quad for\ z < 0$$

Combining both the relations, at $z = 0$, the boundary condition becomes,

$$e_{3kl}\frac{\partial\, U_k}{\partial\, x_l} - \epsilon_{3k}\frac{\partial\, \phi}{\partial\, x_k} - k\epsilon_0\phi = 0 \tag{2.28}$$

When the assumed solutions are substituted into the mechanical and electrical boundary conditions, we get a set of four homogeneous equations in terms of unknown amplitudes as before. The search procedure for roots and the appropriate velocity is the same as before for the of non-piezoelectric case, the only differences being four lower half plane roots, 4×4 boundary condition matrix and determination of potential in the medium.

2.7 Leaky Wave Solutions

Surface wave modes can be differentiated from each other by the phase velocity region in which they exist. It was already mentioned that there are 3 types of waves that can propagate in an unbounded anisotropic media, namely two shear (slow and

fast) and one longitudinal (fastest) waves. The surface Rayleigh wave mode which consists of four decaying terms beneath the surface, almost always has its velocity slower than the slowest shear wave. But in certain isolated directions, the Rayleigh mode velocity exceeds the velocity of slowest shear wave. In the neighbourhood of such directions, a special type of 'surface wave' called 'leaky surface wave' propagates in the medium. The leaky waves also possesses velocity that is always higher than the slow shear waves but lesser than that of fast shear waves. The velocities of Rayleigh wave and leaky wave propagating in various directions of $LiNbO_3$ substrate is shown in Figure 2.7.

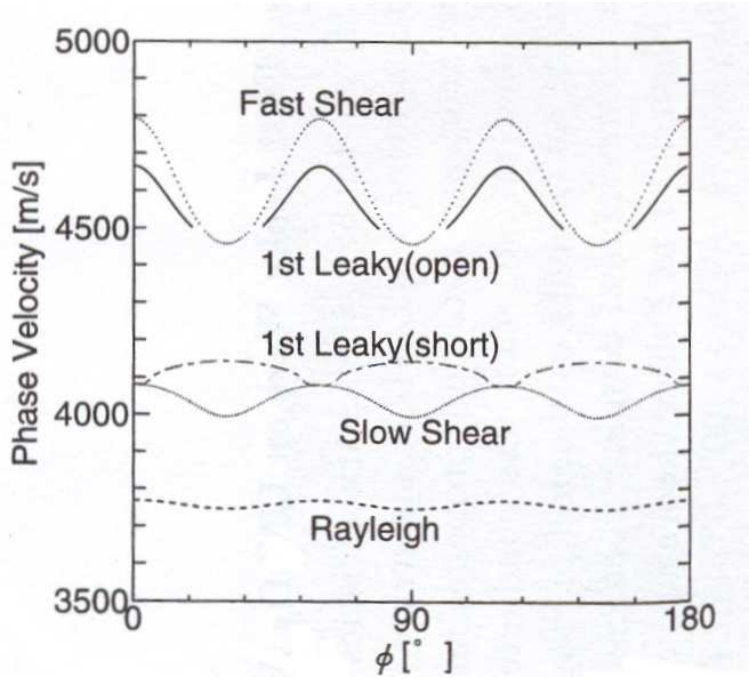

Figure 2.7: Phase velocity of leaky wave, Rayleigh wave propagating on $LiNbO_3$ substrate as a function of angle from x-axis [26]

For the velocities shown in Figure 2.7 the 4×4 matrix discussed before does not reduce to zero, rather a small non-zero imaginary part of the determinant remains (real part reduces to zero). This in turn affects the boundary condition matrix and

the stress-free surface boundary conditions are not satisfied. But if the components of the wave vector in the XY plane (i.e. l_1 and l_2) are allowed to have a small imaginary part, the matrix vanishes completely and satisfies stress free boundary condition. The small imaginary part of the components of wave vector correspond to the attenuation of the wave in the propagation direction. In the isolated direction itself, the Rayleigh wave has only two (or three in piezoelectric case) highly damped terms (imaginary part of last root of l_3 goes to zero), whereas for the leaky wave, a small third term representing a bulk wave radiating into the solid exists. This component of the wave carries some energy away from the surface thus leading to non-conformity to original condition of displacements vanishing at infinite depth. It is because of this small radiating term, these type of solutions are called 'pseudo' or 'leaky' surface waves. A closer look at the roots calculated by Farnell [25] for propagation vector 30° from the [100] axis in copper crystal (non-piezoelectric) reveals a lot of information.

$$\begin{aligned} l_1 &= \sqrt{\tfrac{3}{2}}(1 + i9.1 \times 10^{-5}), \\ l_2 &= \tfrac{1}{2}(1 + i9.1 \times 10^{-5}), \\ l_3^{(1)} &= 0.609 - i0.297, \\ l_3^{(2)} &= -0.609 - i0.297, \\ l_3^{(3)} &= -0.544 + i3.1 \times 10^{-4} \end{aligned}$$

It can be noted that direction cosines l_1 and l_2 have a small imaginary part representing attenuation in the direction of wave propagation. The first two roots (l_1 and l_2) have negative imaginary part (lower half plane) signifying displacements decaying with depth. The third root namely, $l_3^{(3)}$ has a small positive imaginary part (3.1×10^{-4}) causing the amplitude of displacements to increase slowly with depth. The weighting factor (displacement amplitudes) for the first two roots are generally higher than that for the third root causing the overall displacements to be dictated by the rapidly decaying (first two roots) terms. The displacements die down rapidly near the surface and does not regain (due to growing third term) its surface value until a depth of few thousand wavelengths. So these type of waves satisfy the experimental conditions for surface waves and are easily observable. If

piezoelectric effects are taken into account, there are four roots that define surface wave behavior. For leaky wave solutions in piezoelectric media, three of the roots make displacement amplitudes decay with depth (instead of two) whereas the fourth root makes amplitude slowly grow into the substrate.

Longitudinal leaky waves are another type of solution that satisfy experimental conditions for surface waves. They have two components radiating energy in to the substrate (two roots cause displacement amplitudes to grow) [10] as opposed to one root in the leaky wave case discussed before. The longitudinal leaky waves are often called second order leaky SAW which have their phase velocity more than that of fast shear bulk wave and slightly slower than that of longitudinal wave. A small relation showing the phase velocities of various types of waves in a medium is shown as follows:

$$v_R < v_{S1} < v_{L1} < v_{S2} < v_{L2} < v_L$$

where v_R, v_{S1}, v_{L1}, v_{S2}, v_{L2}, v_L are velocities of Rayleigh, slow shear, first leaky, fast shear, second leaky and longitudinal waves respectively. The displacements of particles in longitudinal leaky mode is confined to sagittal plane similar to that of Rayleigh mode(though with dominant longitudinal displacements and hence the name), whereas the first leaky mode generally has displacements in the third direction too.

2.8 Need for Numerical Solvers

The solutions of the partial differential equations described here only provides relative values of displacements and potentials of particles in the medium. Due to the homogeneity of equations, it is difficult to find absolute values for these variables. But usage of numerical techniques provides approximate solutions (absolute values) which are accurate enough (if properly formulated) for all practical purposes. The basic technique can be to divide the continuous domain into discrete sub-domains to get a finite amount of solution data through repeated iterations at finite number of points in the continuum. Such a process is called discretization and is a vital step in many numerical methods to solve partial differential equations.

The wave solutions discussed in the previous sections are waves that propagate on the free surface of the material. It can be quite complex to incorporate the effect of disturbances such as electrical/mechanical perturbations in the analytical solution. Effect of the mass of the electrode which is generally made of a material other than the substrate, is to slow the propagating wave mode. Such effects due to finite electrode mass which affect wave propagation are called mass loading effects. Similar effects can also be seen in the case of electrical open or shorting of the electrodes. Incorporation of such effects is fairly straight forward in numerical techniques which might not be possible without it. Also, the calculation of electrical properties such as admittance of the structures is possible with the implementation of numerical techniques.

3. Modeling of SAW Devices

The development and evolution of present day SAW devices has been possible only due to simultaneous efforts to simulate these devices. The physical development and theoretical modeling of devices go hand-in-hand, both contributing to the other. Various models have been used since the introduction of SAW devices in the late 1960's to the present date and it has been a constantly evolving process. In this chapter, the underlying assumptions, abilities, pitfalls, and potentials of various models are discussed, eventually leading into finite element modeling for SAW resonators.

3.1 Early SAW Models

3.1.1 Delta Function Model

The delta function model is one of the earliest and simplest of SAW models to be developed for bi-directional IDT response prediction. The model is a very basic one, and cannot determine input/output impedance level, bulk wave interference or harmonic operation of devices [3]. It can only provide relative insertion loss of the device as a function of frequency. Nevertheless, it provides excellent preliminary design information regarding bandwidth, rejection levels, and sidelobes.

In the delta function model, each electrode on top of the piezoelectric substrate is assumed to be a delta function source. The voltage on the electrode fingers alternate in polarity with their centres spaced $\lambda/2$ at the centre frequency. The complex electric fields are assumed to be normal to the substrate with distribution approximated as two delta function sources (due to opposite voltage polarity, opposite charges move to the edges of the electrode) or can be simplified to one source per electrode as shown in the Figure 3.1. It should also be noted that the arrows in the

Figure 3.1 are not electric field lines but are delta function sources (direction indicates positive and negative). These delta sources are summed to get the resultant

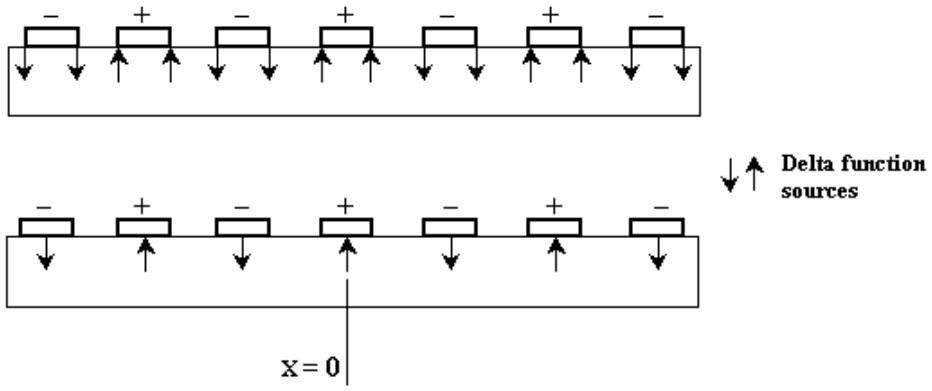

Figure 3.1: Delta function model - Electric field lines approximated as delta function sources

response of the input, output or both IDTs together.

A reference point at the centre of the centre electrode ($x = 0$) is assumed for summing the distributed delta function contributions and the summation yields the frequency response of one set of IDT (input or output). The amplitudes of delta sources are assumed to be constant but the phase contribution changes for each electrode according to the distance from the reference point. The frequency response for the IDT modeled using the delta function approximation (using simplified representation) is given by,

$$H_{in}(f) = \sum_{-n}^{n} (-1)^n A_n \exp(-j\beta x_n) \tag{3.1}$$

where, $H_{in}(f)$ is the frequency response of the input IDT, n is the number of electrode pairs, $(-1)^n$ signifies the alternating electrode polarity, A_n is the weighting factor given by the finger apodization overlap. The $\exp(-j\beta x_n)$ term gives the phase contribution of each electrode with β the propagation constant and x_n the distance from the reference point. The relation given in Equation 3.1 is simplified using trigonometric identities and close to the centre frequency, the response is often

approximated to a sinc function given by $\sin x/x$. The total frequency response of the input and output IDT pairs is given by,

$$H\left(f\right) \;=\; \left|H_{in}\left(f\right)\right| \;\cdot\; \left|H_{out}\left(f\right)\right|, \tag{3.2}$$

where, $H_{out}(f)$ is the response of the output IDT and is given by,

$$H_{out}\left(f\right) \;=\; \sum_{-m}^{m} \left(-1\right)^{m} A_m \exp\left(-j\beta x_m\right) \tag{3.3}$$

where m is the number of electrode pairs in the output IDT.

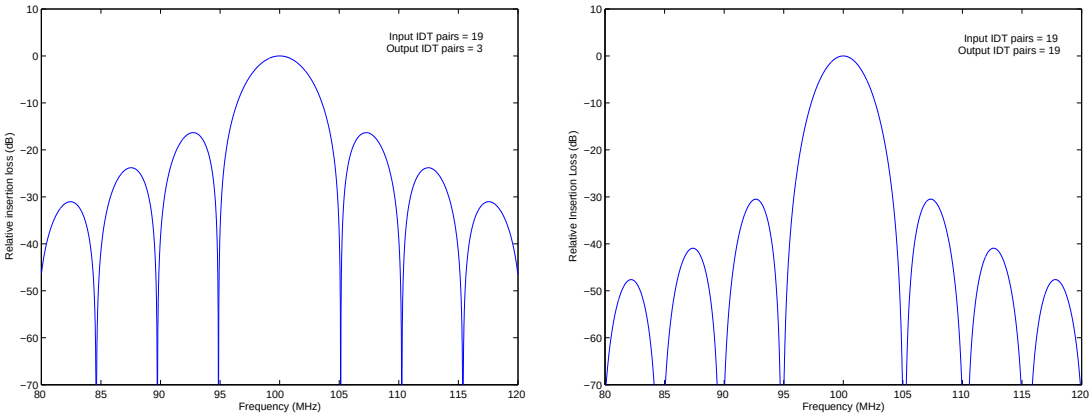

(a) Filter response with 3 output IDT pairs (b) Filter response with 19 output IDT pairs

Figure 3.2: Sample IDT filter response with 19 input IDT pairs using delta function modeling

It should also be noted that the responses calculated using the delta function model have no acoustic path effects and are determined only by the IDT pairs. Sample IDT SAW filter responses with 19 input IDT pairs were calculated using the delta function model and are shown in Figure 3.2. It can be observed from the responses that, with increase in the number of output IDT pairs, the side lobes decrease in magnitude and also the response becomes narrower.

3.1.2 Equivalent Circuit Model

The equivalent circuit model is a three port model, two acoustic and one electric ports to describe the response of a SAW device. The electrical equivalent of the two acoustic ports is represented as a SAW transmission line and the third electrical port is the one in which voltages are applied and sensed. The electric field is assumed to be crossed field, i.e., the field lines are assumed to be normal to the piezoelectric substrate surface similar to the one in a parallel plate capacitor. The real electric field and the cross-field approximation is shown in Figure 3.3.

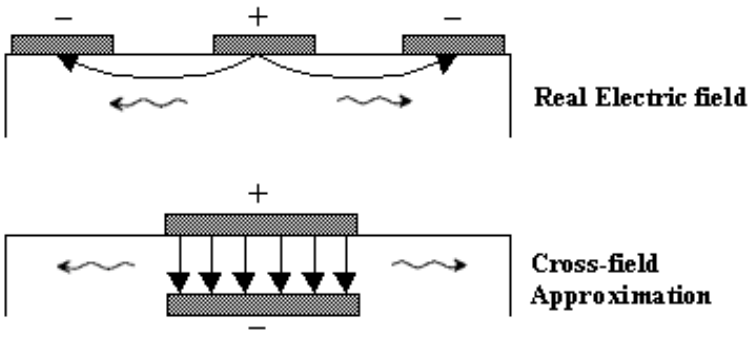

Figure 3.3: Electric field - Real case and approximation

Smith et al. formulated an equivalent circuit model for SAW devices based on the crossed field model developed by Mason for launch and detection of bulk acoustic waves [27]. In this model, the acoustic forces are converted into electrical voltages and SAW velocities are converted into equivalent currents. These transformations allow the mechanical characteristic admittance (similar to the transmission line characteristic impedance which is expressed in ohms) to be expressed as an equivalent transmission line characteristic admittance in mhos as,

$$G_0 = \frac{\omega_0 C_s k^2}{2\pi} \tag{3.4}$$

where, $\omega_0 = 2\pi f_0$, f_0 is the centre frequency, k is the electro-mechanical coupling

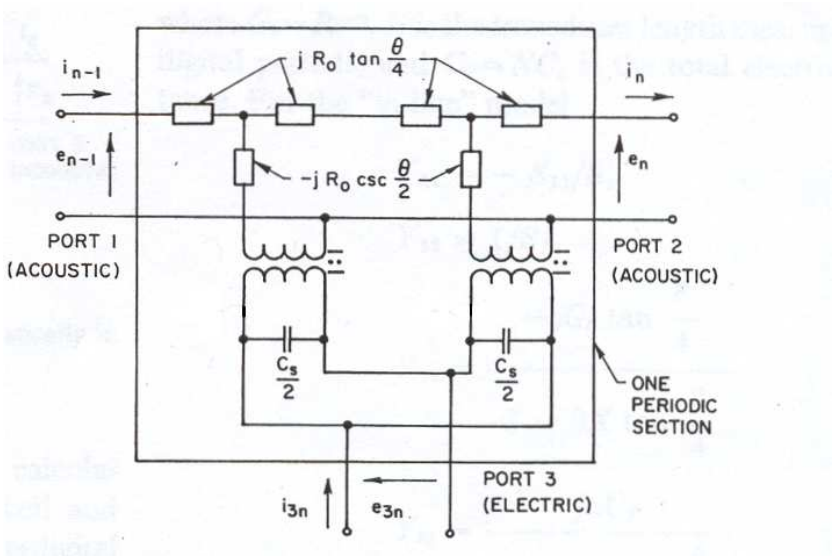

Figure 3.4: Mason equivalent circuit used by Smith et al. for SAW equivalent circuit model [27]

coefficient and C_s is the static electrode capacitance of one periodic section. The centre frequency can be determined from the known surface wave velocity (v) and period of the IDT, the capacitance can be experimentally or theoretically determined and the k^2 values can be approximated by $-2\Delta v/v$([27], [3]), where Δv is the perturbation in wave velocity when the piezoelectric surface is electrically shorted by a thin metal film and it can be theoretically determined.

The equivalent circuit shown in Figure 3.4 is just that of one period and the equivalent circuit of the entire section of IDT is formed by connecting acoustic ports in cascade and electrical ports in parallel. If the IDT is a generator, the emergent acoustic waves are assumed to be absorbed completely (without reflections) by the receiver and has a matched termination at its acoustic ports and vice versa. The 3-port matrix equation is given by [27],

$$\begin{bmatrix} I_1 \\ I_2 \\ I_3 \end{bmatrix} = \begin{bmatrix} -jG_0\cot N\theta & jG_0\csc N\theta & -jG_0\tan(\theta/4) \\ jG_0\csc N\theta & -jG_0\cot N\theta & jG_0\tan(\theta/4) \\ -jG_0\tan(\theta/4) & jG_0\tan(\theta/4) & j\omega C_T + 4jNG_0\tan(\theta/4) \end{bmatrix} \begin{bmatrix} V_1 \\ V_2 \\ V_3 \end{bmatrix} \tag{3.5}$$

where, $C_T = NC_s$ (total IDT capacitance), N being the number of electrode pairs and $\theta = 2\pi f/f_0$ the electrical transit angle through one period (centre to centre distance of successive electrodes), expressed in radians. The overall equivalent circuit of a SAW IDT is shown in Figure 3.5. The input admittance for this circuit is given as:

$$Y_3(f) \;=\; G_a(f) \;+\; B_a(f) \;+\; j\omega C_T \tag{3.6}$$

$G_a(f)$ and $B_a(f)$ is defined as the radiation conductance and susceptance respec-

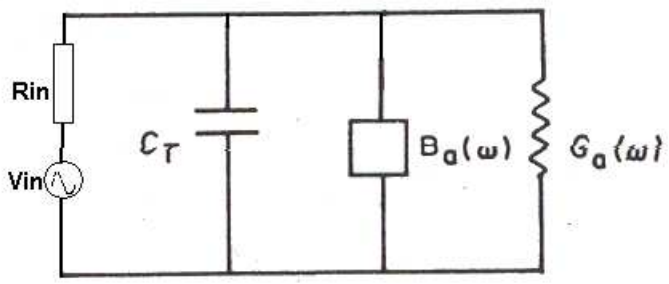

Figure 3.5: Equivalent circuit for a SAW IDT using crossed-field model

tively which are given by:

$$G_a(f) \;\approx\; 8N^2G_0\left|\frac{\sin X}{X}\right|^2 \tag{3.7}$$

$$B_a(f) \;=\; 8N^2G_0\frac{[\sin(2X) - 2X]}{2X^2} \tag{3.8}$$

where $X = N\pi(f - f_0)/f_0$. The radiation susceptance is a reactive parameter ($\pm jB$) that goes to zero at the centre frequency. This term is often omitted in calculations near the centre frequency because it is often negligible when compared to the total IDT capacitance term.

More recently, improvements have been made to the equivalent circuit model to incorporate various second order effects. The reflectivity of the electrodes is

incorporated by differing the characteristic admittances for the metallized and non-metallized regions. Energy storage in electrodes/discontinuities is important in the case of leaky SAW based devices and harmonic operation of SAW IDTs. This is accounted for by including shunt susceptances at the electrode discontinuities (of the equivalent circuit). Also, the unidirectional SAW devices, arbitrary metallization ratios and different polarity sequences (of electrodes) can be modeled by extension of the equivalent circuit model to a more generalized form [3].

3.2 Current SAW models

3.2.1 Coupling-of-Modes (COM) Model

The coupling of modes model is a one dimensional model which gives solutions to the differential equations outlined in the previous chapter in one dimension. The depth of penetration is not considered in the COM model; only the wave amplitudes, variation of acoustic properties and interaction of waves in the propagation direction are taken into account. The one dimensional wave equation for a freely propagating medium without electrical coupling is given by,

$$\frac{d^2}{dx^2}\,\varphi\,(x,t) \;=\; \frac{1}{v^2}\,\frac{d^2}{dt^2}\,\varphi\,(x,t) \tag{3.9}$$

The field $\varphi(x,t)$ in the equation can be described as displacement, stress or electrical potential but generally it is normalized to the power flow [28]. The direction X is the direction of propagation as shown in Figure 3.6 and v is the velocity of the freely propagating SAW. The wave equation being an unloaded one (wave propagating on a free surface) yields a set of unperturbed solutions to the propagation problem. In this model, only two counter-propagating modes are considered, i.e., the forward ($\varphi^+(x)$) and backward ($\varphi^-(x)$) propagating modes as shown in the Figure 3.6.

When the wave equation becomes loaded due to the presence of transducer (grating) or a periodic perturbation, the forward and backward propagating waves couple due to the presence of reflections. The loaded wave equation is given by [28],

$$\left(\frac{d^2}{dx^2} \;+\; \beta_0^2\right)\,\varphi(x) \;=\; -\zeta(x)\beta_0^2\varphi(x) \tag{3.10}$$

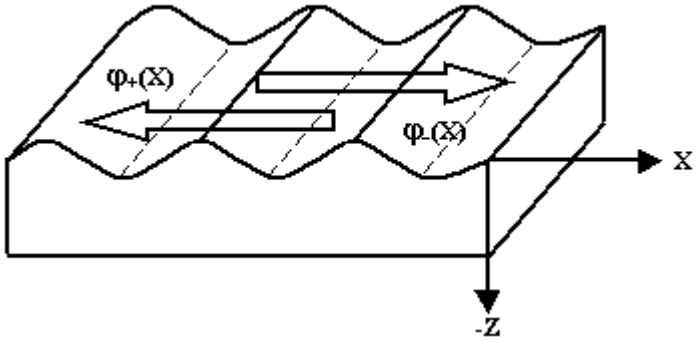

Figure 3.6: Counter-propagating waves in COM model

where, $\beta_0 = \omega/v_0$ is the propagation constant for the free surface, $\zeta(x)$ the periodic load density. Also, the quantity β is the unknown wave number or propagation constant of the solution. The solutions to the equation are the eigenmodes propagating in the medium and they consist of infinite set of discrete harmonics (fundamental harmonic has the wavenumber β). The harmonics involved are not independent of each other but rather coupled. When solutions of this kind are substituted back into the loaded wave equation (Equation 3.10), it results in an infinite number of linear homogeneous equation to be solved [28].

There are two approaches to reduce it into a finite system of equations. They are the algebraic and the differential approach respectively. The algebraic method reduces it to finite system of equations by considering only few harmonics and in general numerical methods (like FEM) are employed to solve the system of equations. The differential approach involves transformation of the reduced algebraic equations into linear differential equations and then solving them. It should also be noted that the Equation 3.10 is an ordinary differential equation which is used for simplicity and for developing the differential form of the COM model which is one dimensional. But it is worth mentioning that the algebraic method mentioned solves the partial differential equations outlined in Chapter 2.

In general, coupling is strong between incident and reflected waves, if the period

of the grating (p) is close to half of the wavelength ($\lambda = 2p$). The waves traveling in either direction get reflected constructively and destructively at two discrete frequencies forming a stopband. This characteristic is fundamental to waves propagating in a periodically perturbed medium. This condition is known as the Bragg condition and the reflections are known as Bragg reflections.

Since the two waves (traveling in either direction) have a strong coupling, other interactions are negligible and only these two counter-propagating waves are considered in the differential form of the COM model. Close to the centre frequency, the propagation constant β can be written as a small deviation from the propagation constant at the centre frequency ($2\pi/\lambda = \pi/p$). It is given as,

$$\beta \;=\; \frac{\pi}{p} + q \tag{3.11}$$

The counter-propagating waves $\varphi_+(x)$ and $\varphi_-(x)$ can be separated into slow ($R(x)$ and $S(x)$) and fast (exponential terms) varying phase oscillations as,

$$\begin{aligned} \varphi_+(x) \;&=\; R(x)\exp(-j\pi x/p) \\ \varphi_-(x) \;&=\; S(x)\exp(j\pi x/p) \end{aligned} \tag{3.12}$$

Since we are considering only two counter-propagating modes in this model,

$$\varphi(x) \;=\; \varphi_+(x) + \varphi_-(x) \tag{3.13}$$

Substituting this expression for φ into the loaded wave equation, and assuming the perturbations to be weak (which is valid in case of typical gratings which are weak reflectors), eliminates the second order derivatives of the wave equation and presents a set of two first order differential equations to solve [28]. The piezoelectric effect generates the SAW in devices and should be taken into account. This adds another electrical coupling term to the differential equation and the voltage drop in the grating is assumed to be negligible making it spatially independent. Also, due to the inverse of piezoelectric effect, a charge develops on the electrodes due to the propagation of SAW. The induced charge causes a current $I(x)$, to flow through the electrodes which can also be written in a differential form. The three first order

differential equations derived from COM model is presented as follows [28]:

$$\begin{aligned} \frac{dR(x)}{d\,x} &= -j\delta R(x) + j\kappa S(x) + j\alpha V, \\ \frac{dS(x)}{d\,x} &= -j\kappa^{*} R(x) + j\delta S(x) - j\alpha^{*} V, \\ \frac{dI(x)}{d\,x} &= -2j\alpha^{*} R(x) - 2j\alpha S(x) + j\omega C V. \end{aligned} \tag{3.14}$$

where δ is the de-tuning factor given by,

$$\delta = \frac{2\pi(f - f_0)}{v} - j\gamma.$$

In the equations, the independent parameters κ, α, v, γ, and C are reflectivity due to perturbations, transduction coefficient, SAW velocity, attenuation and capacitance per unit length respectively. The asterisk symbol signifies the complex conjugate of the concerned parameters.

The first order differential equations (in Equation 3.14) are inhomogeneous in nature and the final solution consists of two parts namely homogeneous and particular solutions. For the homogeneous solutions, the driving force or voltage are not considered and they provide the eigenmodes and the dispersion curves for the system. The dispersion relation gives the dependence of the propagation constant on the frequency and the quantity q is given by,

$$q = \pm\sqrt{\delta^2 - \kappa^2} \tag{3.15}$$

The particular or forced solution deals with the generation problem and the wavelength corresponding to this solution is always $2p$ or λ [28]. Though the separation of solution into two parts is applied to the reduced first order differential equations, it remains the same for all inhomogeneous differential equations and the solutions found out using numerical methods would also have similar properties.

In some of the cases, say structures with constant independent parameters, closed form solutions can be found for the SAW devices using the COM equations (Equation 3.14), owing to its simplicity. In the following section, an important result (admittance of the periodic structure) arising from the solution is presented. This

feature enables fast simulation of device responses using the COM model and is reasonably accurate for Rayleigh and leaky SAW modes. Also, it can be used to model a variety of SAW devices such as SAW resonators, low-loss filters, ladder filters, etc.

But the parameters outlined above cannot be determined from the theory itself and need to be initially introduced from outside. The parameters can be extracted by physically fabricating the device and measuring from it [22] or theoretically determined from numerical simulations [28]. Quite often, a one port synchronous (the reflecting grating extends as a continuation of the transducer) SAW resonator is built as a test structure to extract the parameters. The prime disadvantage of experimental measurement is that these COM parameters are a function of structure (width and height of the electrodes) and orientation/material of the substrate. So, when a range of structures (with differing electrode heights and widths) and substrates need to be modeled for optimized device response, it becomes necessary that devices with different structures and substrates be fabricated every time to measure the parameters. Also, the process of fabricating the device involves considerable time, effort and resources making it an expensive one. For this reason, extraction of COM parameters using numerical techniques is an attractive option.

3.2.2 P-matrix Model

The P-matrix model can be considered as an extension of the COM model, wherein the linear COM equations (given by Equation 3.14) are described by a matrix of elements. Alternatively, it can also be seen as a matrix representation of three ports (similar to the equivalent circuit model shown in Figure 3.4), two acoustic and one electric ports. The acoustic ports are characterized by a scattering matrix (upper left 2×2 matrix) [29] and the electric port is characterized by admittance terms. The P-matrix representation of an IDT shown in Figure 3.7 is given by,

$$\begin{bmatrix} b_1 \\ b_2 \\ I \end{bmatrix} = \begin{bmatrix} P_{11} & P_{12} & P_{13} \\ P_{21} & P_{22} & P_{23} \\ P_{31} & P_{32} & P_{33} \end{bmatrix} \begin{bmatrix} a_1 \\ a_2 \\ V \end{bmatrix} \tag{3.16}$$

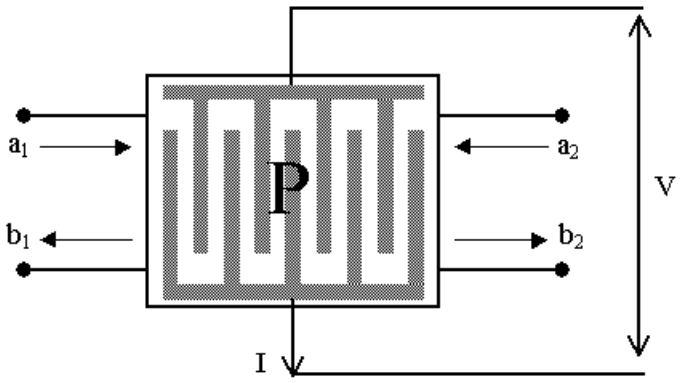

Figure 3.7: P-matrix representation of an IDT

where a_1, a_2 and b_1, b_2 are the incident and reflected waves at the two acoustic ports respectively. P_{11} and P_{22} are the reflection coefficients whereas P_{12} and P_{21} are the transmission coefficients (similar to the scattering matrix). The remaining terms P_{13} and P_{23} correspond to the excitation coefficient of the IDT and the term P_{33} clearly represents the admittance of the structure relating the current in the electrode (I) and the drive voltage (V). P_{31} and P_{32} terms represent the current generated by the waves arriving at the acoustic ports.

Admittance or P_{33} that could be calculated from simulations is the most useful in device design and P_{33} for the case of structure with symmetry and constant parameters is presented in this section. For information on other elements of the matrix, the reader is directed to [28]. The admittance component P_{33} consists of two parts namely, homogeneous (HS) and particular solution (PS) parts. For the highly important case of bi-directional uniform structures, the transduction and reflectivity constants are not complex but real. For this case the admittance is given by,

$$P_{33} \;=\; P_{33}^{HS} + P_{33}^{PS} \tag{3.17}$$

where,

$$P_{33}^{HS} \;=\; -\frac{4\alpha^2(\delta+\kappa)[(\delta+\kappa)(1-\cos(qL)) - iq\sin(qL)]}{q^3(q\cos(qL) + i\delta\sin(qL))} \tag{3.18}$$

$$P_{33}^{PS} \;=\; -i\frac{4\alpha^2}{\delta-\kappa}L + i\omega CL \tag{3.19}$$

In Equation 3.19, L is the length of the device and clearly for long structures, the particular or excited solution part dominates the whole admittance. The resonance and anti-resonance pattern of the response is dictated by the excited solution part of the admittance. A simple COM module was developed using MATLAB for the 36° Y-cut X propagating $LiTaO_3$ resonator using the independent parameters published in [30]. The values of the parameters are $v = 4149$ m/s, $\kappa_p = 5\%$, $\alpha_p = 79 \times 10^{-5}$ $\Omega^{-1/2}$, $\gamma_p = 2.9 \times 10^{-4}$ dB/λ and $C_n = 57 \times 10^{-5}$ pF/μm/period. The period of the simulated structure is $3\mu m$, the length $L = 200\lambda$, and the results are presented in Figure 3.8. It can be seen from the plot that the effect of the homogeneous solution contribution is negligible to the overall admittance of the device even for a nominal device length of 200λ. In general the device length is much longer and effectively the excited solution part can be taken as the admittance of the device for all practical purposes unless the device is short in length.

In SAW devices it is common to have different substructures such as IDTs, reflectors and absorbers. The substructures can be treated independently for which the P-matrices are determined individually and then cascaded to get the P-matrix for the whole device. The expression for admittance presented in this section is valid for a long device, but in general different substructures are modeled separately and cascaded together to get better results without resorting to closed form solutions. The COM model is more suitable and easier to handle if the structures are uniform throughout the device, whereas if the reflection and transduction vary in the structures, it is convenient to calculate the device response using P-matrix model [28]. Nevertheless, it should be kept in mind that the P-matrix model is similar to COM model and the parameters should be input after experimental or numerical determination for successful simulation of device responses.

3.3 Finite Element Analysis (FEA) for SAW Devices

The SAW propagation problem is governed by differential equations given in equations [2.22 and 2.23] and must be solved along with the complexities in geometry of the device, properties of materials (along with that of electrodes) and boundary

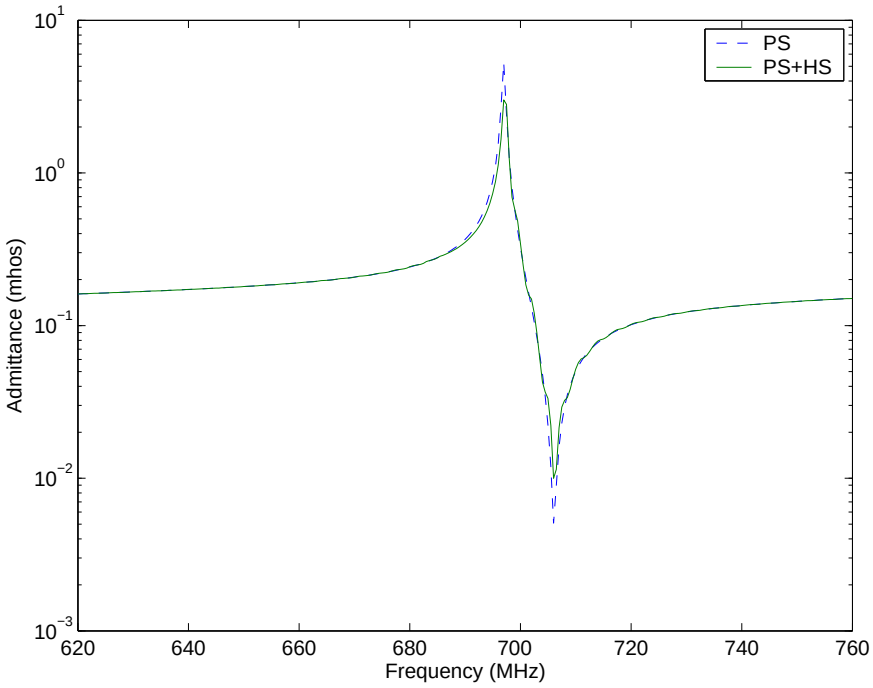

Figure 3.8: Admittance of the YX-36° $LiTaO_3$ resonator using COM model showing the importance of particular solution over homogeneous solution(Period = $3\mu m$, Length = 200λ)

conditions. The finite element method provides numerical solutions to such problems defined by differential equations. Only some basic procedures and techniques used in finite element formulations will be presented here and a detailed theory can be found in [31].

In the finite element method, the problem domain is discretized into smaller regions called elements which are connected at specific points called nodes (shown in Figure 3.9). The elements created may be two or three dimensional and can have triangular,quadrilateral, tetrahedral or brick shapes depending on the dimesionality. The solution to the unknowns (field variables such as displacement, potential, stress, etc) are determined at these nodes and these unknowns are known as degrees of freedom (DOF). The continuum has infinite degrees of freedom, whereas the discretized domain has finite number of DOF, contributing to the name finite element

method. The continuity of the solution (since solutions are determined at specific points, the nodes) is taken care of by introduction of shape functions or interpolation functions. The choice of these functions determines or approximates how the field varies across a single element domain. Normally, a polynomial function is chosen as a shape function and the number of nodes assigned to a particular element defines the order of the polynomial. For instance, a linear element has two nodes per side whereas a quadratic element has 3 nodes per side or edge. The approximation of the field by the interpolation function is given by,

$$\phi(x) \ = \ \sum_{i} N(x)_i \phi_i$$

where $\phi(x)$ is the field approximation across the element, $N(x)$ is the shape function and ϕ_i is the unknown field value at the node. The difference in using a linear shape function and quadratic shape function is shown in Figure 3.10. In the Figure 3.10, an element and its nodes are shown along the X axis and the displacement in X direction (field variable) is shown in Y direction. Clearly, the approximation is quite different in the two cases presented and element type should be chosen according to nature of the correct solution. Choosing an element type is thus a matter of sound engineering judgment and deeper understanding of the problem at hand. The effects of using linear and quadratic elements for SAW propagation problem are discussed in the coming chapters. Also it is important that the data defining the material

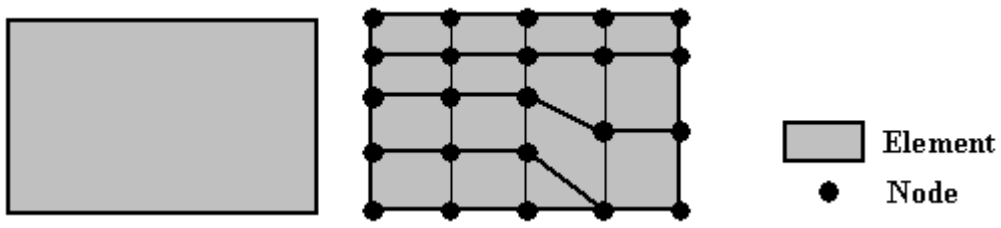

Figure 3.9: Discretization of problem domain in FEM

properties such as density, stiffness, etc., be specified at the start of the analysis.

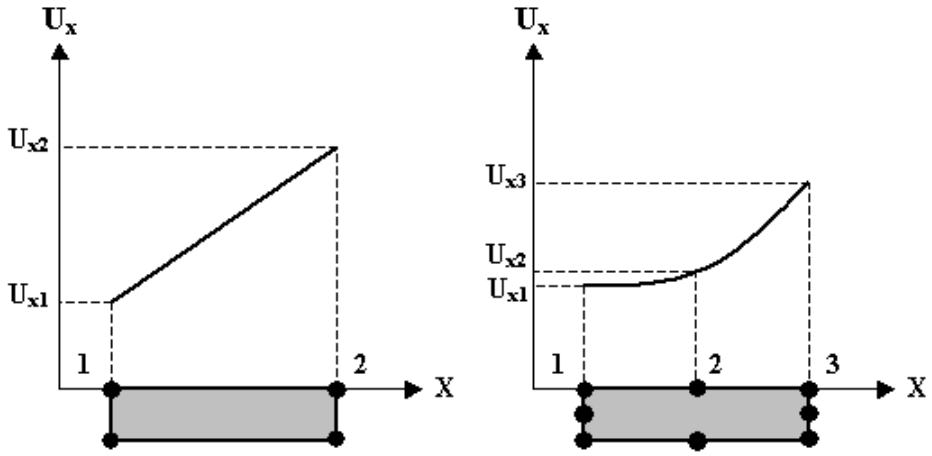

Figure 3.10: Field approximation by linear and quadratic elements

Once the element type is defined, the solution to the differential equation is approximated to the continuous function and expressed in terms of the unknown nodal values ϕ_i for a single element. A system of equations in terms of unknown nodal values is formulated for that element and subsequently for the whole domain. This assembly of algebraic equations should conform with the practical rule that nodes shared by the elements should have the same values for the field variables. The system of equations thus formed cannot be solved without the application of boundary conditions because the system remains indeterminate. All the boundaries need to be addressed properly before the final solutions could be relied upon. And finally, the resulting system of equations are solved by appropriate numerical techniques. The numerical technique used in ANSYS for solving the system of equations, is not the focus of this research and will not be discussed in this thesis.

3.3.1 ANSYS as Simulator

The finite element method is a numerical method which is not of much value without the use of a computer due to the number of equations that need to be solved in order to arrive at a solution. There has been some efforts by engineers and scientists to simulate SAW devices using finite element methods and can be seen in [32], [33], [34].

Most of the results have been accomplished after writing custom codes based on the early work done by Allik and Hughes [35] on variational formulation for piezoelectric analysis. Commercial software for FEA had been in use for quite sometime but the level of maturity required for successful simulation of piezoelectric devices had not been possible until recently. The finite element method in itself is a straight forward one, but it requires considerable amount of time and effort to develop a finite element program from scratch. For this reason, one of the most popular finite element software, ANSYS has been used in this research work. Also, the following features prompted the usage of ANSYS for development of a finite element model:

- Well developed piezoelectric coupled field solver.
- Good graphical user interface (GUI) for creation of model geometry and solving.
- Excellent post-processing capabilities to sort and display results.
- Well scripted user's help and tutorial kit.

The steps involved in development and solving of a problem using ANSYS are:

- **Pre-processing:** The geometry of the model is drafted in this step along with the selection of element type (essentially the shape function) for meshing the structure. This is the most time consuming part of the work with much emphasis going towards proper element selection and input of appropriate material properties. There are a handful of coupled field elements in ANSYS from which an appropriate one (to be discussed in detail) is selected and used for SAW analysis. After the design of geometry, the problem domain is meshed according to the accuracy needs and available computer resources. If the structure is finely meshed, more accurate results are obtained but the memory and time requirements to solve the problem increases proportionately. So, often a balance is achieved between the two conflicting parameters namely, accuracy and size of the problem, the problem is solved optimally.

- **Solving:** The application of boundary conditions can be categorized either under a pre-processing or solving step but it is of utmost importance for achieving an accurate solution. The externally applied loads and excitation are supplied at this stage and it is an electrical voltage in the case of SAW devices. The defining part of the solving stage is the specification of the type of analysis that needs to be done. For instance in a static analysis, a static load is applied to the structure and its response is studied. Such an analysis is of no use in SAW finite element model, but the two following analyses need to be done for some useful results.

  - Modal analysis: This requires the solving of the eigenvalue problem with the aim of achieving the eigenmodes propagating in a structure. External loads (drive voltage) are not applied to the structure in this case with the electrodes either shorted or open. Even if some drive voltage is applied, ANSYS converts it into a short and calculates the eigenmodes. In essence, the modal analysis calculates the homogeneous solution (HS) of the differential equations involved. This analysis can be used as the starting point for other detailed analysis such as transient or harmonic analysis to determine the time step or frequencies of interest [36].
  - Harmonic analysis: Once the frequency around which the required mode exists is determined, a frequency sweep is done to determine the response of the structure or device around those frequencies. The driving voltage applied in the harmonic analysis would be a cyclic one (sinusoidal one) and a steady state response is obtained as an output. Also, the harmonic analysis provides the excited or particular solution (PS) of the differential equation and is highly useful in determining the admittance of the device. The number of frequency points should also be kept optimal because it also determines the time and memory required to calculate the solution.

- **Post-processing:** The finite element solution is given by a set of numbers which needs to be interpreted by the user in a proper way. The ANSYS post-

processor has nice features to help the user in this regard. The results from the modal analysis in ANSYS, not only provides modal frequencies but also the shapes of the modes in a visual manner. Colorful displacement, electric field, stress/strain contours (and many more) can be produced through the ANSYS postprocessor and regions of interest can be zoomed in and investigated. Many built-in mathematical functions are available in ANSYS which are highly useful in calculating quantities such as admittance of the structure.

3.3.2 One Port SAW Resonator

A small introduction to SAW resonators was given in the first chapter but a deeper insight is required in order to establish that one port SAW resonators can be modeled best by the finite element methods. In a one port SAW resonator, surface acoustic waves emitted from either side of the IDT are reflected in-phase at the centre frequency by the reflection gratings giving rise to a standing wave pattern. A synchronous one port SAW resonator is one in which the reflector gratings on either side of the IDT are formed as a continuation of the IDT. The basis of operation for

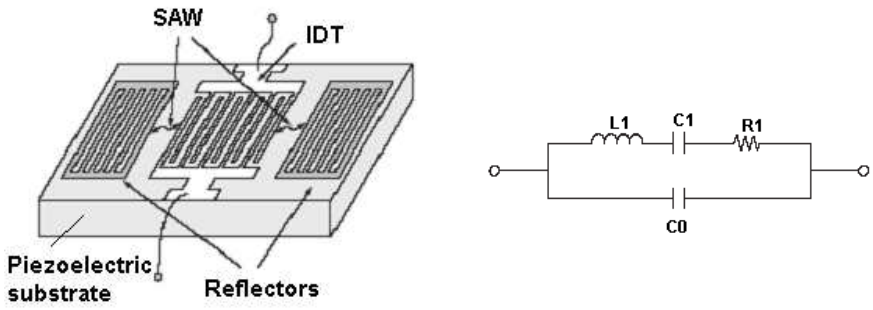

(a) One port SAW resonator (b) Lumped element equivalent circuit

Figure 3.11: SAW resonator and equivalent circuit [37]

a SAW resonator is the Bragg's reflection condition as noted before in Section 3.2.1. The waves get reflected in phase at the centre frequency and the reflectivity can be

close to unity if the number of reflectors is sufficiently large. Under this condition, propagation of waves into the media is prohibited and the frequencies between which it happens is called the stopband.

An ideal lumped element equivalent circuit is shown in Figure 3.11(b), and it should not be confused with the equivalent circuit model discussed earlier in this chapter. The lumped equivalent circuit is just a circuit that gives frequency response similar to that of SAW resonator, rather than a model simulating acoustic wave behavior and consequently describing the electrical response. It consists of a series resonance circuit with L_1, C_1 and R_1 elements shunted by a capacitor C_0. The inductor, capacitor and resistor in the series branch represent the equivalent motional parameters of the SAW series resonance and the shunt capacitance represents the IDT capacitance. The series (resonant) and parallel (anti-resonant) resonant frequencies are given by the following formulae:

$$f_s = \frac{1}{2\pi\sqrt{L_1.C_1}} \tag{3.20}$$

$$f_p = f_s.\sqrt{1+\frac{C_1}{C_0}} \tag{3.21}$$

The ratio C_1/C_0 is important in the design of SAW resonators as it determines the separation between resonant and anti-resonant frequencies which are often offset for optimal device performance [3]. A typical admittance curve (magnitude) showing resonant and anti-resonant frequency of a one port SAW resonator is shown in Figure 3.12. One-port SAW resonators with such responses are highly useful in constructing low-loss high frequency filters. They are connected as impedance elements in ladder networks where the location of resonant and anti-resonant frequency is of high importance.

The parameters that determine the centre frequency and performance of the SAW resonator are the metallization ratio, electrode/reflector height, number of IDT pairs/reflectors and acoustic aperture. The metallization ratio is defined as the ratio of the width of the electrode (a) to the period of the structure d (shown in Figure 3.13). The electrode height is always represented as a fraction of acoustic

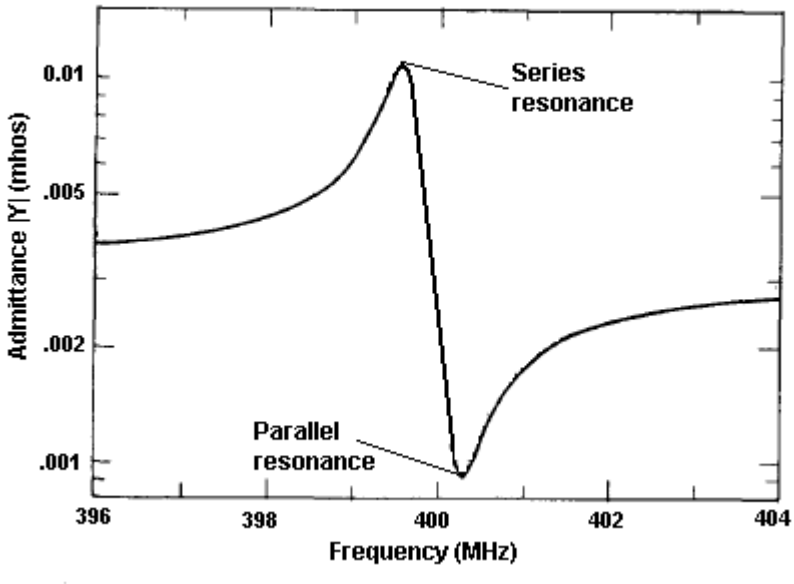

Figure 3.12: Typical admittance curve of one port SAW resonator

wavelength and hence given as a percentage value throughout this work.

$$\text{Metallization ratio} \;=\; \frac{a}{d}$$

$$\text{Electrode height} \;=\; \frac{h}{\lambda} \;=\; \left(\frac{h}{2 \cdot d} \times\; 100\right)\;\%$$

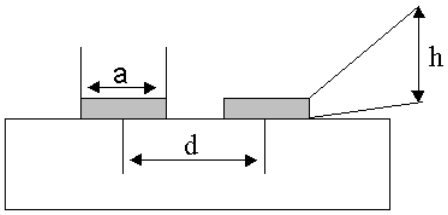

Figure 3.13: Metallization ratio and electrode height

3.3.3 Limitation of the Finite Element Method

A typical one port SAW resonator is on the order of $500 - 1000\lambda$ (transducer and reflectors together) long, $50 - 100\lambda$ wide in the lateral direction (aperture) and a depth of up to 100λ as shown in Figure 3.14. It is a well known that the degree of discretization of the model is directly proportional to the accuracy of the results. In the problem of interest, one might assume to have at least $10 - 20$ first order (linear) elements per wavelength would be required to get reasonably accurate results. Calculating optimistically, the total number of elements required for the whole

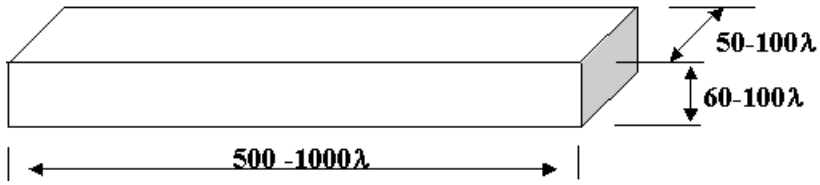

Figure 3.14: Dimensions of a SAW resonator

device (without electrodes and reflectors) gives,

$$\text{Number of elements } = 500 \times 50 \times 100 \times 10 \ = \ 2.5 \times 10^7.$$

A piezoelectric problem has four degrees of freedom namely, displacement in X direction (U_x), displacement in Y direction (U_y), displacement in Z direction (U_z) and potential (ϕ). So the total number of unknowns can be calculated to be,

$$\text{Total number of unknowns } = \ 2.5 \times 10^7 \ \times \ 4 \ = \ 1 \times 10^8.$$

Clearly, this number of equations would need to be solved in order to arrive at a complete solution. Also, it should be kept in mind that this is a conservative estimate and the actual number could be much more if we take into account the IDT, reflectors and more accuracy. Solving this many equations is possible only by powerful super computers whose cost and time required (to solve) is not justified. Some valid approximations are required to reduce the size of the model to a manageable level.

3.3.4 Assumptions for Reduced Finite Element Model

Attempts at simulating SAW using a finite element model has been possible until now only due to some approximating assumptions [32], [33]. The main approximations are presented here as follows:

Reduction to 2 dimensions: The surface acoustic waves are straight crested, i.e., if the profile of the wave is observed at different places in the lateral direction as shown in Figure 3.15, it can be found to be similar. In other words, the waves do not hold much important information as one traverses in the lateral direction. The

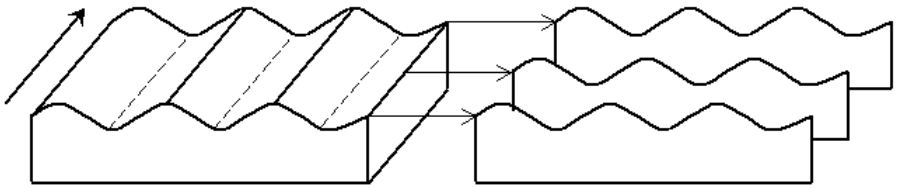

Figure 3.15: Reduction of model to 2 dimensions

effect is almost negligible in most of the useful modes put to use in the SAW devices, and the entire characteristics can be described by a 2 dimensional model.

Reduction of model depth: The depth of penetration of SAW was discussed in Chapter 2 and a plot of various displacement components against depth was shown in Figure 2.5 for anisotropic nickel. It can be seen that the displacements die down to less than 5% of the initial values within 3 wavelengths for purely surface mode solutions. This feature of SAW enables us to model only $5 - 10$ wavelengths of the substrate depth and reduce the amount of unnecessary calculations in solving a model with full depth.

Periodicity of the structure: If the waves propagating on the substrate and structures on top of it are spatially periodic as shown in Figure 3.16, then one wavelength or period is enough is to characterize the whole device [33]. The synchronous uniform one port resonator satisfies this criteria and can be readily modeled using

finite element method using this approximation. The modeling of one wavelength of the device is possible only if the boundaries are treated in a proper way, i.e., either a infinite periodic boundary condition or an absorbing boundary condition need to be applied. The boundary conditions are discussed in a greater detail in the coming sections. A typical resonator has about $500 - 1000$ periodically arranged electrodes

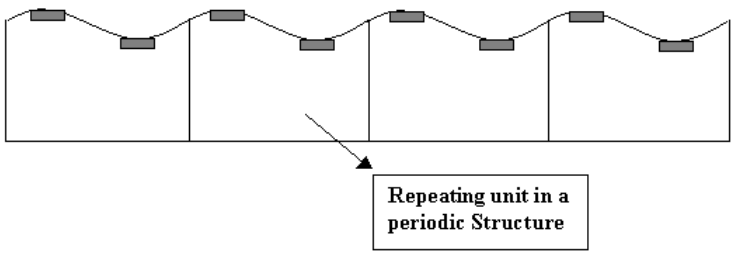

Figure 3.16: Periodic structure in a resonator

and can thus be modeled as an infinitely extended periodic structure with a single wavelength as the base (simulated) structure. Even a single electrode (or half wavelength) is enough to model the device, but one full wavelength has been simulated throughout this work both for clarity and ease of implementation.

3.3.5 Crystal Cuts - Conventions and Implementation

Various crystal types and angles at which they are cut to form a substrate were mentioned in Table 1.1. Crystal cuts and angles are of prime importance in the design and modeling of SAW devices as they dictate the material properties and ultimately the device response. Piezoelectric crystals have their own crystal axes (X', Y' and Z') and they are different from the cartesian axes X, Y and Z. The direction of cut is specified with the name of the substrate and for instance, if a substrate is X-cut, then the cut face is perpendicular to the X' direction of the piezoelectric crystal. The axes and orientation of two crystals, X-cut and 64° Y-cut orientations are shown in Figure 3.17.

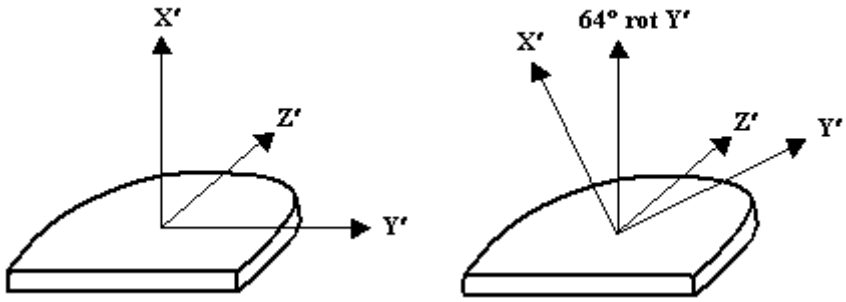

(a) X-cut crystal (b) 64° rotated Y-cut crystal

Figure 3.17: Different crystal cuts

The piezoelectric crystals are generally rotated about their axes by certain angles and then cut. They are specified by a set of angles called Euler angles. These are a set of three angles $(\varphi, \vartheta, \psi)$ specifying consecutive rotations about the crystal axes. There are various conventions for specifying the order of rotation and the one followed in this work is consecutive rotations about Z', X' and Z' axes respectively as followed in [24]. The rotations specified by the euler angle sets are shown in Figure 3.18.

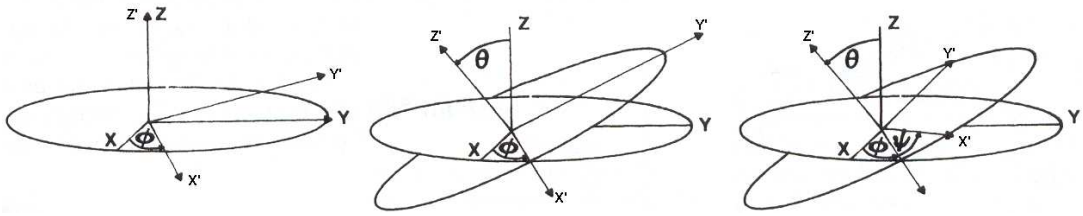

Figure 3.18: Euler angles - Crystal cut rotations

The properties of crystals are different in different directions and they need to be implemented in the FEM for different crystal cuts. The properties that need to be input for successful finite element solution are 6×6 stiffness matrix, 3×6 piezoelectric matrix, 3×3 dielectric matrix, and density. Density remains the same

for all crystal cuts but all other properties change for each distinct crystal cut. Material properties for modeling were taken from [24] and the values given in the book are for Euler angles $(0°, 0°, 0°)$. But with a procedure called transformation of co-ordinates, it is possible to calculate the transformed matrices for differing crystal cuts. The procedure is explained in detail by Auld [24] and the transformed matrices for a specific case of YX-128° cut $LiNbO_3$ is presented in Appendix A. A separate program was written in MATLAB software for transformation of the matrices which were then used in the ANSYS model. In ANSYS, direct implementation of crystal cuts is possible, but it follows a different convention (Z',X',Y' rotations) and it cannot be implemented for 2 dimensional models. For this reason, the prominent (Z', X', Z') convention is used throughout this work.

3.3.6 Modeling of Periodic Structures

The development of finite element model for SAW propagation is bounded by approximations discussed previously and involves the following steps:

1. **Design of Geometry:** The periodic structure is modeled as an infinite grating and only a wavelength of the substrate is created for simulation purposes. Firstly, the type of element (2D) is chosen from the coupled field element library of ANSYS and its physical properties are defined. The plane strain condition should be specified for the element type, i.e., all the gradients in the third direction should be assumed to be zero. The depth of the substrate is limited to 10 wavelengths to limit the size of the problem. Also electrodes of required height are defined on top of the substrate and Aluminum has been used in this work throughout unless otherwise specified. Also, a vacuum or air could be modeled above the substrate but is not considered here due to the fact that only materials with high dielectric constants ($\epsilon_r \approx 40$), Lithium niobate and lithium tantalate has been used [34]. If materials like quartz (have low dielectric constant) are modeled, vacuum layer may be considered. The surface charge on the air-electrode interface becomes quite important due to the fact that it is calculated as $1/\epsilon_r$ times the charge on the electrode-substrate

interface and has been included in the finite element calculations by Hofer and Lerch [38]. The relative permittivity of quartz is approximately equal to 4.5 which would introduce a considerable error if air layer is not considered.

2. **Material properties:** The material properties of the piezoelectric substrate are input as matrices after the required transformation for crystal cuts. ANSYS uses a convention that is different from the widely used method [24] for matrix ordering. The required corrections were made to conform to the ANSYS conventions [36]. Also the material properties such as density, modulus of elasticity and poisson ratio must be specified for the electrode material.

3. **Meshing:** The shapes of the elements used in simulations are either rectangular (2D elements) or brick (3D elements) throughout. Also, the fact that the displacements are largest near the substrate surface for SAW has been considered in minimizing the size of the problem. The domain is discretized to higher densities near the surface than near the bottom. Also, the electrodes are meshed to higher degrees of density. ANSYS 8.0 (intermediate university version) has been used which has the maximum node limit of 32000 and the size of the problem had to be kept within that limit throughout. A one wavelength solid and meshed model is shown in Figure 3.19. Only 2 wavelengths is shown in the depth direction for the sake of clarity and it can be seen that the meshing density decreases with depth. But the meshing density is kept constant in the direction of propagation.

4. **Boundary conditions:** The application of boundary conditions is the most critical part of arriving at finite element solutions. The four boundaries (Γ_L, Γ_T, Γ_R, Γ_B) shown in Figure 3.20 need to be treated with care. Stress-free boundary conditions should be specified at the top of the substrate and electrodes as discussed in Chapter 2; i.e., there should be no mechanical constraints on that surface. Dirichlet boundary condition can be applied at the bottom surface Γ_B, with displacements dying down within 3 to 4 wavelengths. The left and right boundaries Γ_L and Γ_R can be allowed to have phase differences

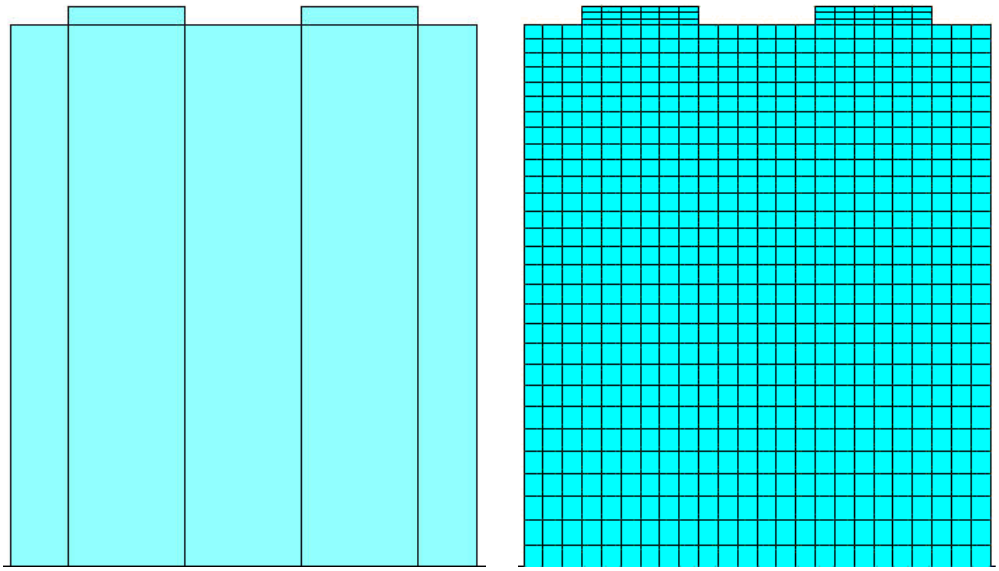

(a) Solid model (unmeshed) (b) Meshed periodic structure

Figure 3.19: Meshing

to allow arbitrary propagation of waves in the medium. This formulation would require an absorbing condition at both the boundaries which is beyond the capability of ANSYS at this moment. This kind of absorbing boundary could also be applied to the bottom surface if available. Also, if a FEM/BEM (Boundary element method) coupling is available, the electrodes could be modeled using FEM and the substrate could be modeled using BEM and the whole device could be simulated. Nevertheless, a stricter periodic boundary condition wherein the left and right boundaries are forced to have the following constraints [32] was assumed,

$$U_L = U_R \tag{3.22}$$

$$\phi_L = \phi_R \tag{3.23}$$

where U_L, U_R and ϕ_L, ϕ_R are displacements and potential at left and right boundaries respectively. If only one period (half wavelength) of the structure is modeled, the boundaries are forced to have opposite values (In Figures 3.19(b) and 3.20 full wavelength is shown).

This boundary condition restricts the results to waves with wavelengths twice the period of the structure. This approximation is similar to the COM model (which is considered quite accurate for SAW and LSAW based devices) wherein only two counter-propagating modes are considered. Consequently, the results of both the FEM (with infinite periodic boundary condition) and COM are very accurate only around a small frequency band around the resonance. The resonance anti-resonance pattern that is important for device design lies within this band of frequencies. Even outside this band of frequencies, the electrical response of the device purely depends on the electrical characteristics (capacitance of the transducer, contact pads, inductance of connecting wires, etc) rather than on acoustic activity [28]. So, the electrical response (due to acoustic activity) determined by applying this boundary condition can be quite useful in device design. These simulations can also be highly useful in extracting parameters for the COM model which otherwise might require fabrication of the device and measurement of parameters. Also, this boundary condition assumes that there are infinite number of electrodes extending on either side of the boundaries which is also quite valid considering that there are hundreds of electrodes in a typical SAW resonator.

After the application of boundary conditions, a modal analysis is performed to determine the eigenvalues and vectors of the problem. The modal analysis gives the two stopband edges of the resonator (dispersion) and the harmonic analysis (particular solution) can be used to determine the admittance of the device similar to the discussion in Section 3.2.2. Since the length of the device in infinite in this finite element formulation, the contribution of the homogeneous solution is negligible to the device admittance (as seen from Equation 3.19) and thereby neglected in this work. Only the particular solution (with $\lambda = 2p$) is taken into account and utilized in calculation of admittance.

The absolute displacements and electric field distribution can be determined only through harmonic analysis. The electric field (intensity) vectors calculated using ANSYS for a YX-128° $LiNbO_3$ single wavelength structure are shown in Fig-

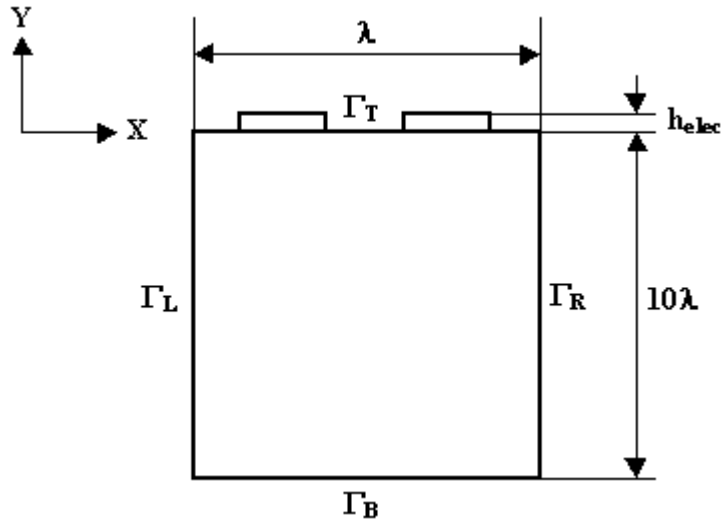

Figure 3.20: FE model of periodic structure

ure 3.21. The calculated electric field (intensity) vector shown in Figure 3.21 can be compared to the real electric field in the devices shown in Figure 3.3. It is similar to the real electric field present in the devices and proves that the finite element calculation provides a more realistic representation of electric field as compared to approximations in other models. Further validation of the simulator is presented in the coming chapter and the model is extended to leaky SAW mode propagation.

3.4 Chapter Summary

Some of the early day SAW models such as delta function model and equivalent circuit models were discussed in brief with their accompanying assumptions. It was followed with a description of newer developments such as COM and P-matrix models which are more suitable for present day devices, but the requirement for parameters to be inserted from outside prompts a look at more fundamental wave simulators. The full set of partial differential equations governing the problem are considered in finite element solutions and hence chosen as a simulator in this research work. The admittance of a YX-36° $LiTaO_3$ resonator calculated using COM/P-matrix model with parameters from published results was also presented in this

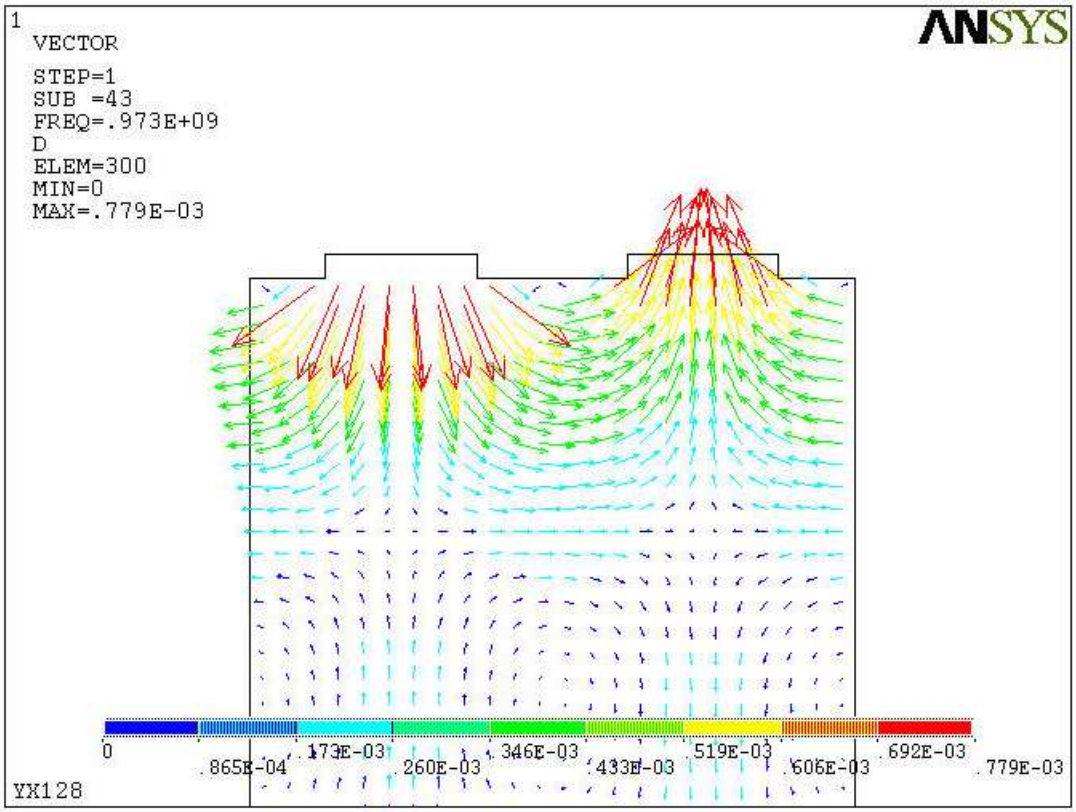

Figure 3.21: Electric field vectors in a periodic structure

Chapter to explain the contribution of homogeneous and particular solutions to the electrical characteristic of the device.

The solution method using finite element analysis was briefly discussed along with the usage of commercial software ANSYS for this work. The size of the problem is extremely huge if a full solution is to be obtained; so the problem was reduced to a 2 dimensional one by considering the straight crested nature of the surface waves. Also, the consideration of periodic structure such as a one port resonator would further reduce the size of the problem by enabling the simulation of just one wavelength of the device. The crystal cut implementation in ANSYS, design of geometry, meshing of the problem domain, application of boundary conditions and the similarity of the electric field representation by FEM were also described.

4. FEM Results for One Port SAW Resonator and Validation of ANSYS Simulator

The finite element models developed using ANSYS in this work are compared to results listed in the literature. Firstly, the simulation results for the relatively simpler case of Rayleigh waves are presented and the simulator is validated against published results. Later the more complex leaky waves are modeled taking into consideration the properties of these waves as described in Chapter 2. Two substrate cuts have been used in modeling of Rayleigh SAW based devices namely, Y-Cut Z propagating lithium niobate (written as YZ-$LiNbO_3$) and 128° Y-Cut X propagating lithium niobate (YX-128°$LiNbO_3$). Also, a 36° Y-cut X propagating lithium tantalate (YX-36°$LiTaO_3$) and YX-42°$LiTaO_3$ substrate cuts have been used for modeling leaky SAW resonators. All the finite element simulations presented in this work were done on a 4 processor (Ultra spark 3), SUN V480R (Sunfire) system (1GHz) with 16 GB of RAM. The modal analyses typically took less than a minute for all simulations and a harmonic analysis with 100 frequency points and 20000 nodes (4 degrees of freedom) took roughly around 2 hours to complete.

4.1 SAW Propagation on a Free Surface

4.1.1 Rayleigh SAW on YZ-$LiNbO_3$

The propagation of Rayleigh SAW on a free surface of Y-Cut Z propagating $LiNbO_3$ was investigated using FEM. A linear 2D element (PLANE13 in ANSYS), was used for the purpose. The PLANE13 element is a general coupled field 2D element in ANSYS for which the piezoelectric degrees of freedom (U_x, U_y and ϕ) can be represented. The plane strain condition specifying the independence of degrees of freedom on the third coordinate should also be explicitly specified for the PLANE13 element. The Euler angle set for this double rotated YZ crystal cut is $(0°, 90°, 90°)$

as specified in [3]. The transformations are done for the material property matrices accordingly as discussed in the previous chapter and in the appendix.

The wavelength of the SAW was set to be $4\mu m$, which is the length of the simulation domain in the propagation direction. The periodic boundary condition, i.e., the nodes at right and left boundaries having the same displacements and potential were applied at the boundaries along with the stress free boundary condition at the top surface. A modal analysis was performed without applying any drive voltage to determine the propagating modes in the substrate. A range of frequencies were checked to identify any propagating modes. The modal analysis gives the frequency at which a particular mode resonates for a given wavelength. The solution consists of a set of increasing eigenfrequencies in the specified range that satisfy the applied boundary conditions. In the solution set there will be a pair of eigenfrequencies representing the Rayleigh SAW. This pair represents the two edges of the stopband and is quite useful in determining the velocity of the SAW. A strong resonance is formed at one edge (frequency) of the stopband due to constructively interfering eigenmodes (propagating in either direction) and they destructively interfere at the other edge. The two stopband edge frequencies are given by f_{sc+} and f_{sc-}. There is no propagation into the media in this band of frequencies and is called the stopband. Once the frequencies are found, the deformed shape of the structure can be viewed using ANSYS. However absolute values of displacement cannot be found, instead relative values can be displayed. For a SAW resonator with electrodes on top, the modal analysis would give two frequencies as Rayleigh SAW modes representing two edges of the stopband. But for propagation on a free or fully metallized surface, the two modes degenerate into one at the same frequency (indicating the absence of stopband in either case).

The velocity of propagation of Rayleigh SAW on the free surface of YZ-$LiNbO_3$ has been published many times and it is used to compare and validate the accuracy of the ANSYS simulator. The calculated free surface velocity has been reported to be around 3488 m/s [3] [39] by Campbell, Adler and others. The Table 4.1 gives the frequencies at which the Rayleigh mode propagates with a wavelength of $4\mu m$ as

determined from the modal analysis. The velocities were calculated using the modal frequency and wavelength for different meshing densities.

Table 4.1: Rayleigh wave velocities calculated using different mesh densities

	Wavelength (μm)	Frequency (MHz)	Velocity (m/s)
12 Elements	4	883	3532.3
16 Elements	4	878.46	3514.0
24 Elements	4	875.2	3500.8
32 Elements	4	874.1	3496.4
40 Elements	4	873.55	3494.2

If the published velocity value of 3488(m/s) is assumed correct,then the error values for various meshing densities can be calculated.These are plotted in Figure 4.1. It can be seen from that the error percentage drops from above 1% to 0.1% if the number of elements is increased from 12 elements per wavelength to 40 elements per wavelength. Clearly, the finite element solutions become more accurate once the number of elements per wavelength is increased.

In ANSYS 8.0 there is also a 2D quadratic coupled field element (PLANE223) that could be used to model the SAW periodic structure. The elements have 8 nodes per element with one mid-side node on each side. There are also results published in literature for which higher order elements (4^{th}) have been used in SAW simulations [40]. But ANSYS does not have higher order elements other than a quadratic element and only its suitability was assessed. The problem domain was kept the same along with boundary conditions and the type of analysis. Only the type of element was changed and the frequency at which the Rayleigh mode propagates was determined. It can be seen from the Table 4.2 that quadratic elements with 24 per wavelength provides a high level of accuracy that is sufficient for all practical purposes. For this reason, quadratic elements have been used throughout this work

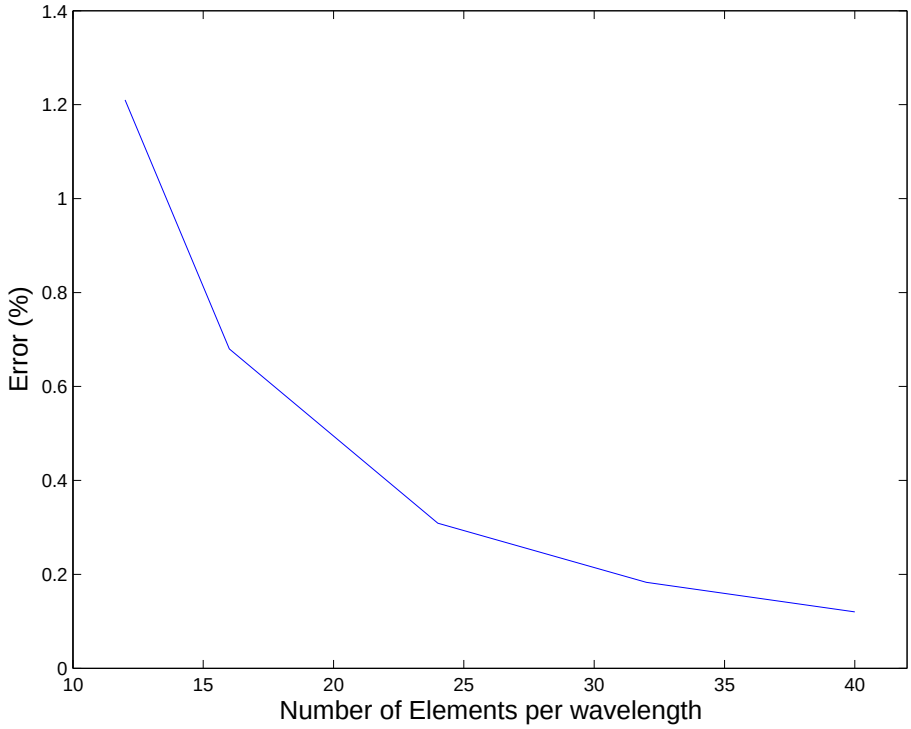

Figure 4.1: Percentage of error in velocities for differing mesh densities

unless otherwise specified.

Table 4.2: Free velocity calculation using quadratic element

	Wavelength (μm)	Frequency (MHz)	Velocity (m/s)	Error
24 Elem	4	872.38	3489.5	0.04%

YZ-$LiNbO_3$ has a moderate velocity for Rayleigh SAW and hence is not a suitable one for development of high frequency SAW devices unless critical sub-micron technologies are applied. But as shown in the coming chapter, a high velocity LL-SAW mode propagates on it which could be highly useful for development of high frequency SAW devices assuming realistic fabrication capabilities.

4.1.2 Rayleigh SAW on YX-128° $LiNbO_3$

Another prominent cut that propagates Rayleigh SAW and is being widely used in SAW devices is YX-128° $LiNbO_3$. It has one of the highest Rayleigh SAW velocities among the crystal cuts in use. The Euler angle set for this cut is given by $(0°, 38°, 0°)$ which transforms and aligns the direction of SAW propagation with the co-ordinate X and Y axes. Because of its higher accuracy with lesser number of elements, the 2D quadratic element was used to determine the free surface velocity of this cut. The modal analysis yielded a modal frequencies of 1 GHz (degenerate) for 4 μm structure. This translates into a velocity of 4000 m/s as compared to a velocity of 3992 m/s found in the literature [3].

A harmonic analysis was performed for this periodic structure around the identified modal frequencies. In a harmonic analysis, an alternating drive voltage is applied on the electrodes to determine the frequency response of the structure. In this case a balanced voltage of ±0.1V (peak to peak 0.2V) was applied.

A harmonic analysis on a free surface is equivalent to a device with electrodes of zero width and height. For simulating electrodes with zero width and height, the driving voltage is directly applied to the surface on one node per electrode. Although such devices do not exist in reality, it is highly useful to study the response of such structures. The displacement profile of the SAW at the resonant frequency, calculated using the harmonic analysis is shown in Figure 4.2(a). The components of displacements in X (propagation) and Y (depth) directions plotted against the depth co-ordinates can be compared to the oscillatory displacement components of anisotropic nickel substrate in Figure 2.5. Both the displacements and the electric potential die down within 2 to 3 wavelengths as seen from from Figure 4.2 and is completely typical of Rayleigh SAW propagation. It can also be seen in Figure 4.3 that on the surface of the substrate, the X and Y displacements are 90° out-of-phase with each other, which is one of the important properties of Rayleigh SAW.

The results presented above substantiates the assumptions made in finite element modeling of SAW propagation and can indeed be extended to model the propagation

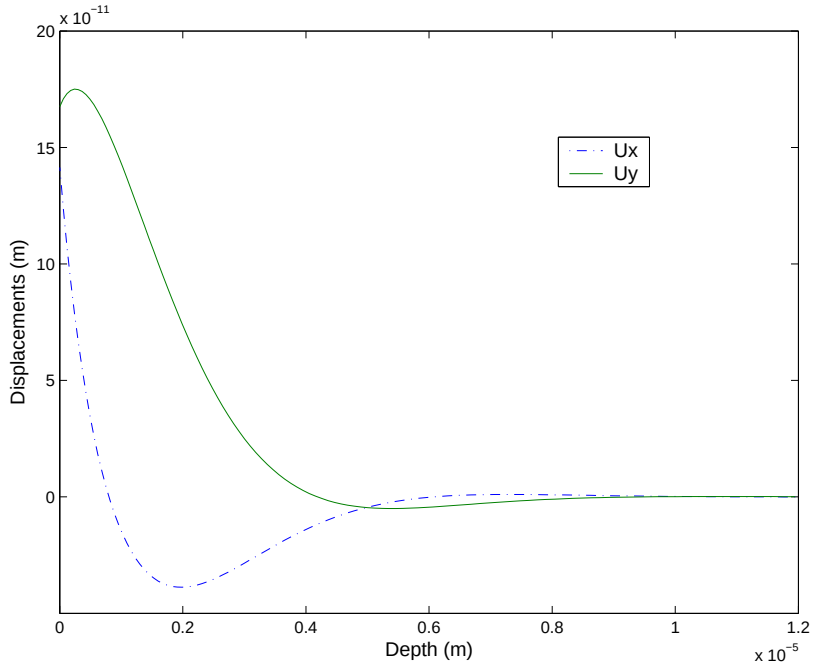

(a) Displacement profile for SAW

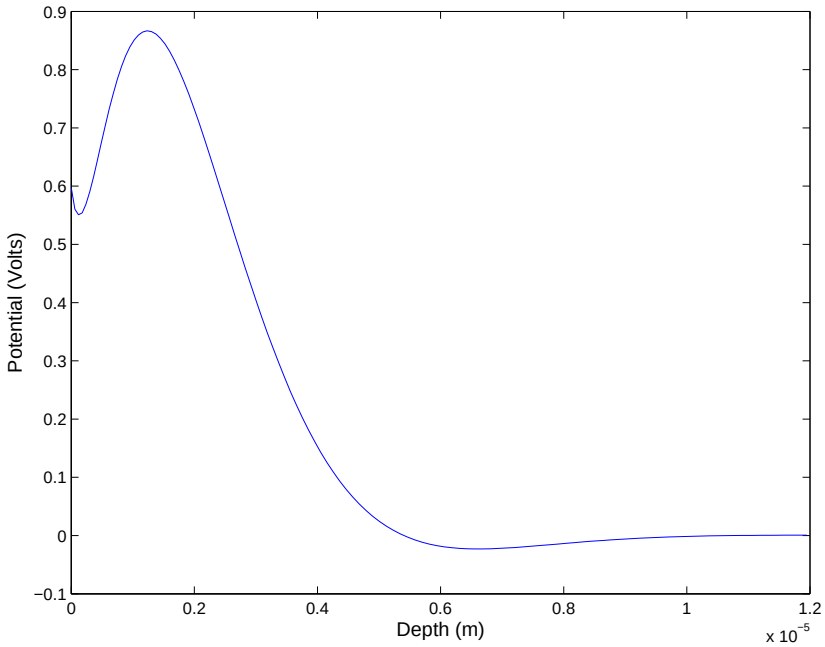

(b) Electric potential for SAW

Figure 4.2: Displacement and potential for SAW in YX-128° $LiNbO_3$ at resonant frequency

of SAW in periodically perturbed structures such as resonators.

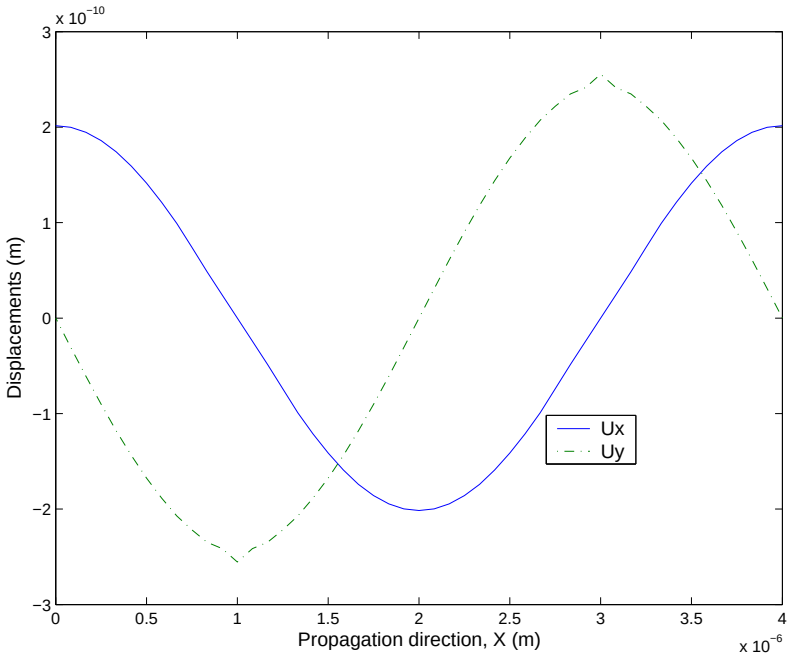

Figure 4.3: Phase difference between displacement components for Rayleigh wave

4.2 Finite Element Results for Periodic Structure

The propagation properties and electrical response of YX-128° $LiNbO_3$ synchronous one port resonator is discussed in this section. A synchronous one port resonator is spatially periodic and only one wavelength of the device is modeled by applying periodic boundary conditions. The modeled structure assumes the electrodes to be infinitely extending on both the sides, which is comparable to the hundreds of electrodes and reflectors originally present in the device. The period of the structure is kept to be $2\mu m$, so that it can be used to compare the free surface velocity value calculated in the previous section with $4\mu m$ wavelength.

The frequency of operation of the SAW resonator determines the electrode dimensions, especially the period of the electrode structure. Apart from the period, metallization ratio and electrode height are also extremely important. They deter-

mine the mass of the electrode on top of the substrate which slows down the velocity of SAW and affects the reflectivity of the electrodes. A modal analysis was performed with varying metallization ratios and electrode heights and the results are compared to values of velocities and reflectivity calculated by Plessky and Koskela [28].

4.2.1 Modal Analysis

The geometry was discretized using quadratic elements (PLANE223) with 40 elements per wavelength. Aluminum was used as electrode material with appropriate properties (desnity, bulk modulus and Poisson's ratio). A modal analysis was performed which gives two eigenfrequencies (f_{sc+} and f_{sc-}) that are the edges of the stopband. Since there is no propagation into the media in this band of frequencies, the velocity is determined from the pair (of eigenfrequencies) using the formula [28]:

$$v \;=\; (f_{sc+} \;+\; f_{sc-})\, p \tag{4.1}$$

where, v is the velocity, p is the period or pitch of the electrode structure and f_{sc+}, f_{sc-} are the two modes (edges of stopband) determined by the modal analysis. The SAW modes cannot be determined from just the list of eigenfrequencies alone, but can be identified from the eigenvectors (mode shapes) displayed using ANSYS. The modes shapes are distinctly different at the two edges as shown in Figure 4.4 with one of the modes having zero displacement component in X direction (f_{sc-}) at both the ends and the other having zero displacement component in Y direction (f_{sc+}) at the ends. These modes have also been referred to as symmetric and anti-symmetric SAW modes [33], depending on the symmetry of the electric potential about the centres of electrodes. The identification of these mode types is important because it determines the sign of the reflectivity per electrode as can be seen from the equation:

$$\kappa p \;=\; \pi \frac{f_{sc+} \;-\; f_{sc-}}{f_{sc+} \;+\; f_{sc-}} \tag{4.2}$$

where, κp is the reflectivity per electrode. This relation is derived as a zero of the dispersion relation given in Equation 3.15. It is found as a zero of the equation due to the fact that the deviation quantity q goes to zero in the stopband frequencies.

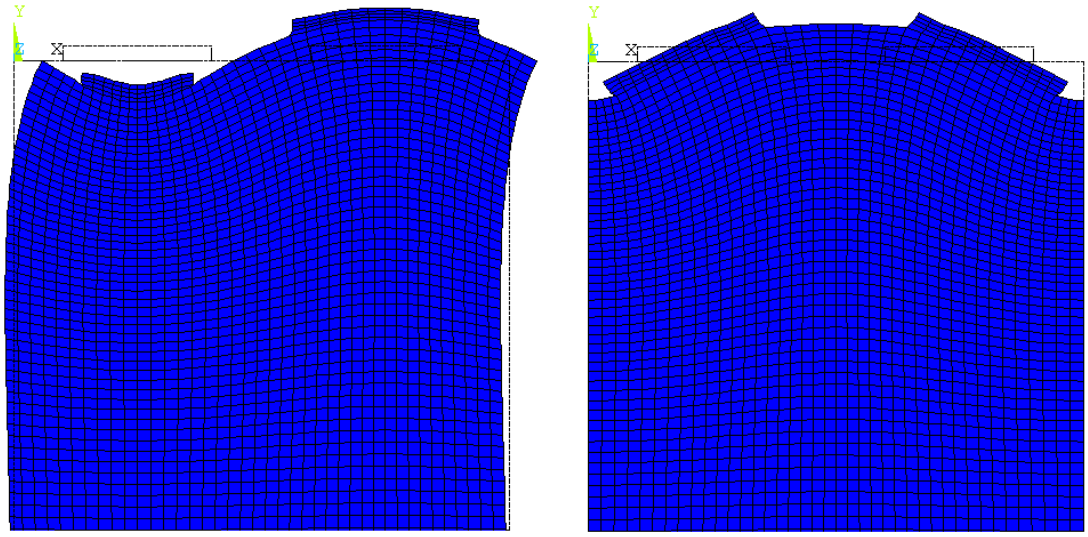

(a) 1^{st} mode (f_{sc+}) at 971.5 MHz (b) 2^{nd} mode (f_{sc-}) at 964.75 MHz

Figure 4.4: Mode Shapes for SAW propagation

A set of simulations were done for varying metallization ratios (MR) and electrode heights. The modes determined by the modal analysis for MR of 0.6 and h/λ of 3% is shown in Figure 4.4. The velocity of SAW and the reflectivity per electrode was calculated using the formulae given in Equations 4.1 and 4.2. The f_{sc-} mode (symmetric) shown in Figure 4.4(b) has a lower frequency than the f_{sc+} (antisymmetric) mode and subsequently has a positive reflectivity as shown in Table 4.3. The sign of the reflectivity (κ) determines the frequency at which the electrical resonance occurs.

The velocity values have a shown a considerable decrease from the free surface velocity of 4000 (m/s) calculated previously. This decrease is due to the mass loading effect described previously and the values computed are compared to the ones calculated by [28] using FEM/BEM calculations. Also, the reflectivity values are slightly different; nevertheless, the trend of decreasing velocities and switching of negative reflectivity to positive values with increasing MR is effectively modeled by the finite element simulations. The two parameters extracted are very useful and can be used in further simulations if a COM model were developed. The other

Table 4.3: Velocity and reflectivity calculated using FEM

MR	h/λ	Velocity (m/s)	Reflectivity	Velocity (m/s) [28]	Reflectivity [28]
0.4	3.0%	3897	−0.008	3875	−0.017
0.4	3.4%	3889	−0.005	3868	−0.012
0.5	2.4%	3894	−0.003	3872	−0.008
0.5	3.0%	3883	+0.002	3861	+0.004
0.6	3.0%	3872	+0.011	3851	+0.019

parameters namely, transduction coefficient (α), capacitance per unit length (C) and attenuation (γ) can be found by using fitting techniques once the admittance of the structure is found. A full COM model would be required for this extraction of parameters using fitting technique and hence is not part of this work.

4.2.2 Harmonic Analysis

An alternating drive voltage was applied on the electrodes around the modal frequencies determined using the previous analysis. As explained in Chapter 3, the harmonic analysis involves finding the particular solution for the problem and the wavelength pertaining to this solution remains $2p$. The complex admittance of the structure representing the response of the one port SAW resonator can be determined from the charge getting collected at the electrode [34]. In the harmonic analysis, the electric potential of the nodes belonging to one electrode are kept constant (coupled to one another to be same). Complete complex charge Q (or current) on the entire electrode can thus be got and the complex admittance of the device can be determined from the following relation [34],[41]:

$$Y = \frac{j\,\omega\,Q}{V} \tag{4.3}$$

where, Y is the complex admittance, j the imaginary number, ω the angular frequency and V the drive voltage.

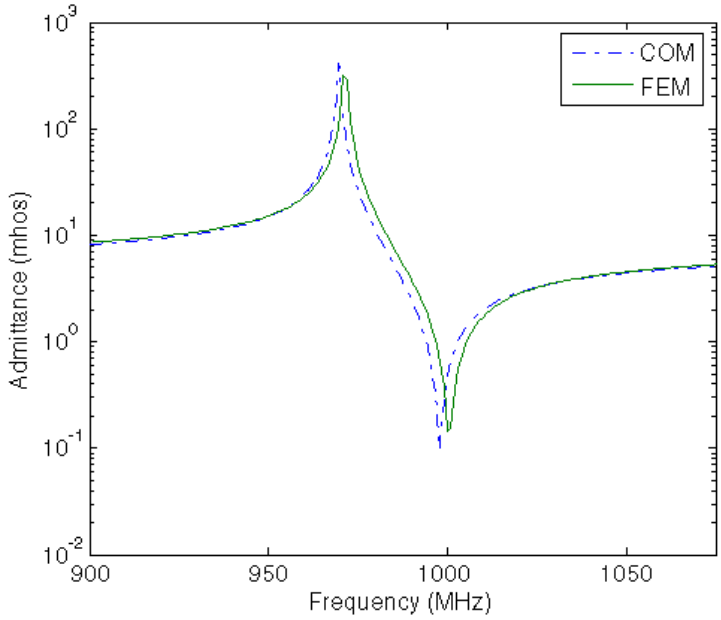

Figure 4.5: Admittance of YX-128° $LiNbO_3$ resonator calculated using FEM and COM model (with MR-0.5 and h/λ=3 %)

Admittance calculated for a resonator with MR of 0.6 and h/λ = 3% using the formula in Equation 4.3 is shown in Figure 4.5. The admittance plotted in the figure is the magnitude of the complex quantity. The plot shows resonance at 971 MHz and anti-resonance at 1 GHz similar to the plot showing a typical SAW resonator response in 3.12 of chapter 3. The centre frequency also matches with the value determined by the modal analysis (f_{sc+} = 971.5 MHz). The results from a COM/P-Matrix model is also presented in Figure 4.5. The parameters for the model were used from FEM modal analysis and partly from published results [28]. The velocity (v) and reflectivity (κ) calculated using FEM for MR= 6 and h/λ=3% (refer Table 4.3) were used in the COM simulation. The transduction coefficient (α) and capacitance parameters were taken from the published results for the same MR and

electrode height. The value of admittance calculated is above 10^2Ʊ at the resonant frequency which in the case of real devices would be a bit lower due to attenuation mechanisms that are unaccounted for here. Although, a small value of attenuation (about 2 dB/λ) was used for the COM model and a small damping ratio (0.0005, using DMPRAT command in ANSYS) was assumed for FEM. Also, the simulations assume that the devices have infinite aperture which in reality might be around 30-50 wavelengths. This will be discussed further in detail, in the following section with 3D finite elements to find out the effect of aperture. The device length (with same p=2 μm as FE model) and aperture were assumed to be really high in COM (L above 2000 and aperture more than 300) to match the results of FEM which assumes infinite boundary condition.

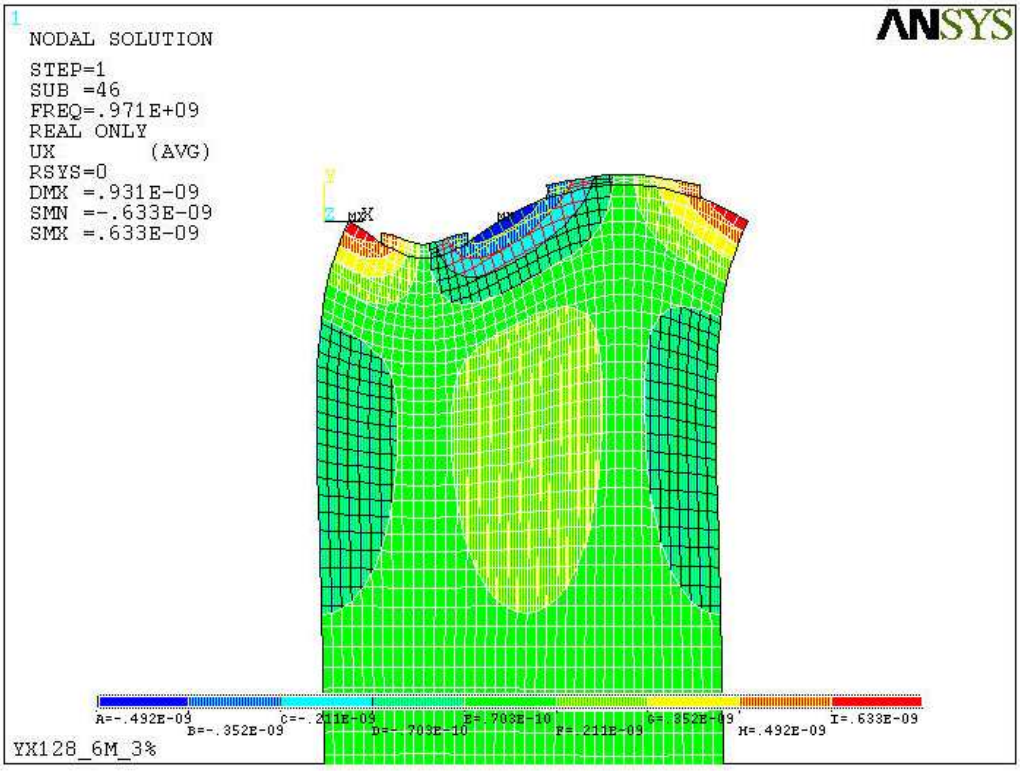

Figure 4.6: U_x displacement contour showing minimum and maximum displacement regions

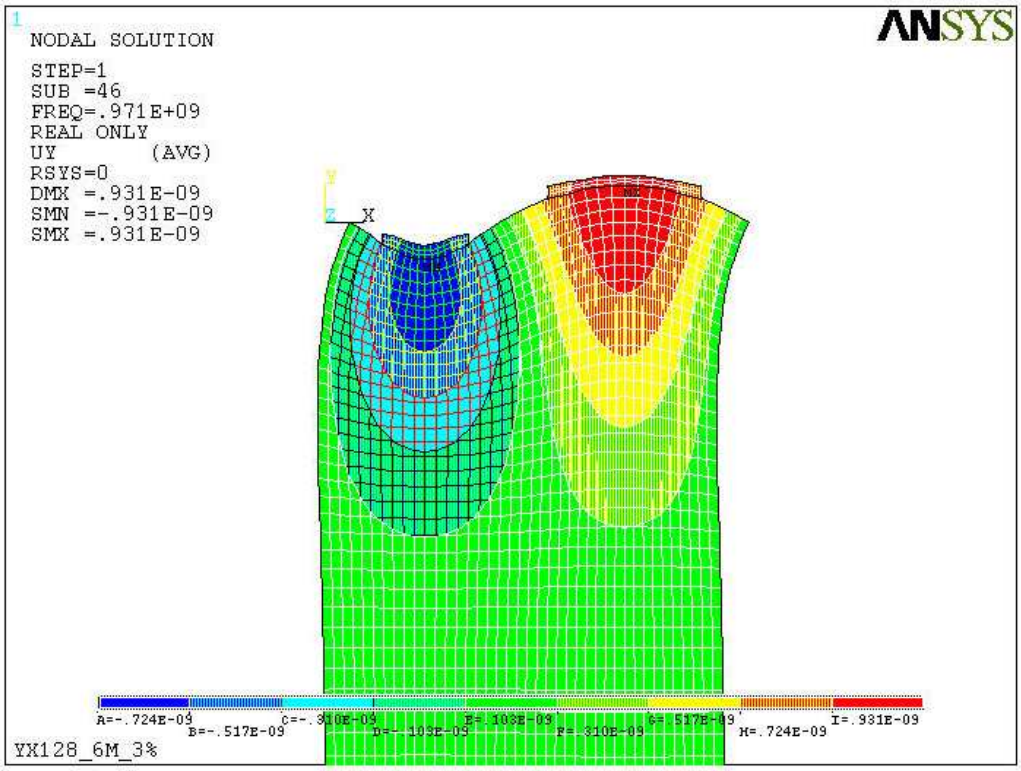

Figure 4.7: U_y displacement contour showing minimum and maximum displacement regions

The displacement and potential contours are shown in Figures 4.6, 4.7, and 4.8 for the single period structure. It can be seen that the displacements are in the order 10^{-10} m with the wavelength being $4\mu m$. Since the displacement is three orders less than the dimensions of the structure, the displacements are multiplied by a factor of 1000 and displayed to view the deformation. Roughly only two wavelengths of depth is shown in the Figure 4.8 and it can observed that both the displacements and potentials die down to near zero values after reaching a maximum within 0.2λ, which is completely typical of Rayleigh SAW waves.

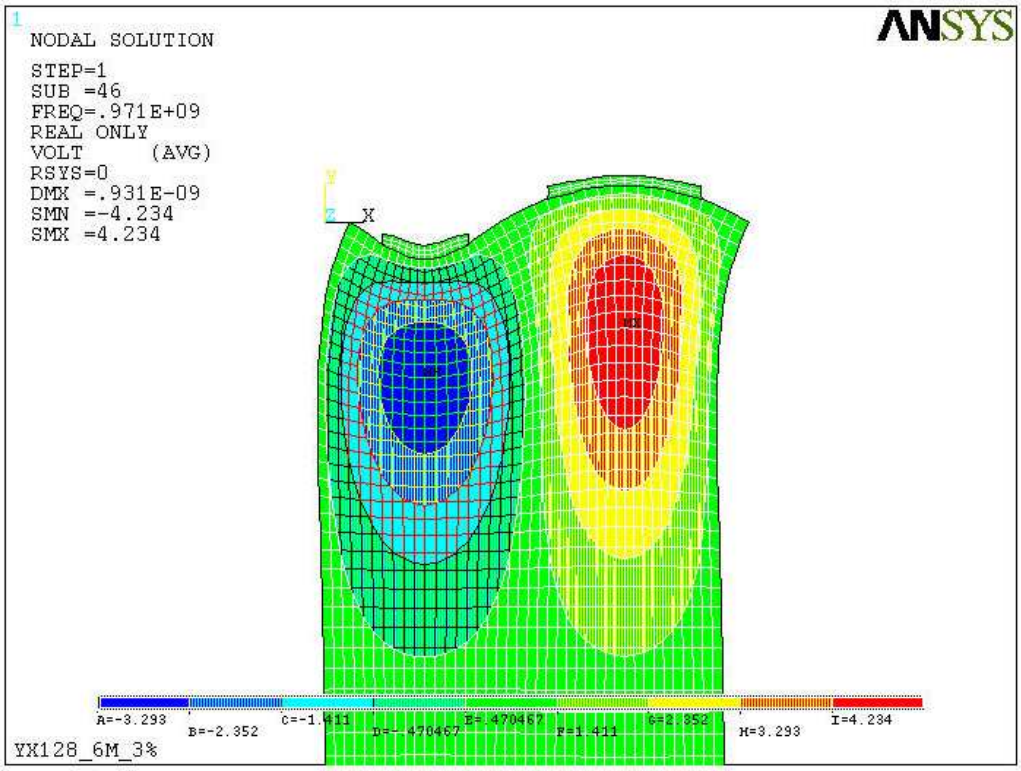

Figure 4.8: Potential contour showing maximum and minimum potential regions

4.3 SAW Resonator Response Using 3D Finite Elements

The results discussed until now were performed using 2D finite elements by considering that the devices are of infinite aperture (extending in the lateral direction). The size of the problem would increase unmanageably if a 3D structure was modeled, even with the consideration of the periodic boundaries in the propagation direction. Therefore, a plane strain condition (built-in to ANSYS for 2D elements) was applied to the 2D structure to model the straight crested SAW.

3D elements can also be used in simulations with plane strain conditions. This is possible by modeling a thin strip of the piezoelectric substrate and applying zero displacement constraint in the third direction. This is valid in the case of Rayleigh SAW as it does not have displacement components in that direction. With this constraint the SAW would still be straight crested and would propagate in the X

co-ordinate direction. The purpose of these simulations is two-fold. It is used to study the effect of aperture and is also useful in extending the model to leaky SAW propagation.

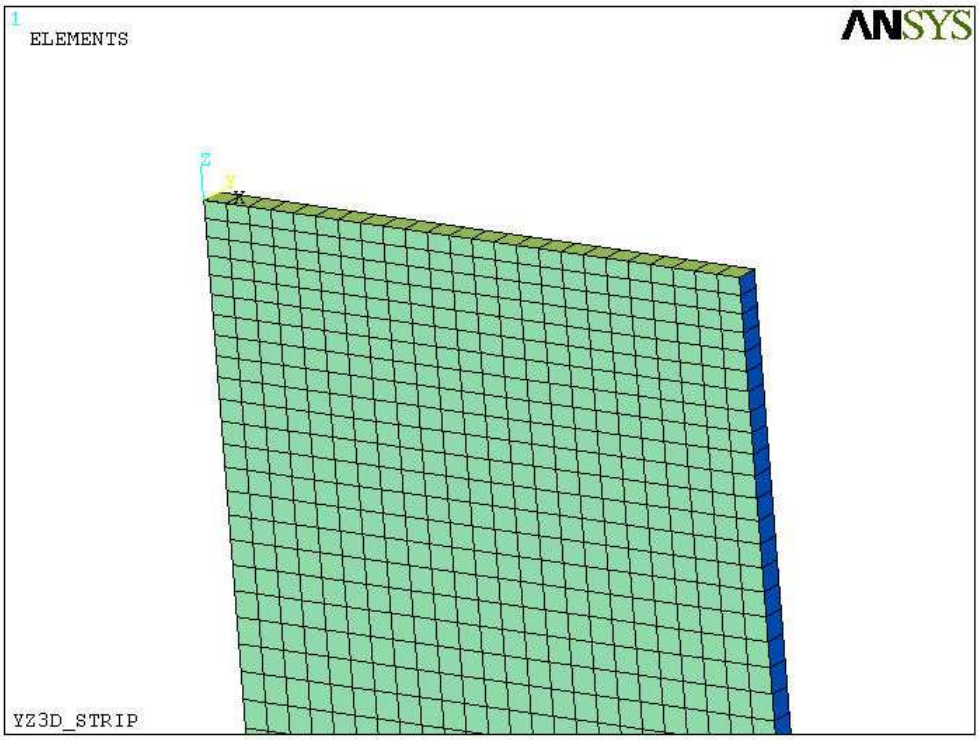

Figure 4.9: 3D mesh of YZ-$LiNbO_3$ resonator

A YZ-$LiNbO_3$ substrate was used in this study and SOLID5, a 3D linear element was used for meshing the structure. Earlier in this Chapter, the velocity of Rayleigh waves in YZ-$LiNbO_3$ was studied, but the electrical response was not presented. Also, this cut is an important one with another type of SAW namely LLSAW propagating on this substrate which is presented in Chapter 5. The calculated electrical characteristic would be used to compare the resonant frequencies of two types of resonators (utilizing different SAWs) with the same IDT periods. The simulations were performed to study the effects of aperture (or strip thickness) and the feasibility of using 3D elements in finite element solutions. For this reason, a simple structure

without metal electrodes was modeled. The drive voltage was directly applied to the substrate through "fictitious" electrodes separated by a period of $2\mu m$. The structure was meshed with a density of 24 elem/λ and the thickness of the strip was modeled to be one such element length. The meshed structure is shown in Figure 4.9. The boundary conditions applied were similar to the 2D model. Also, the full 6×6 stiffness matrix, 3×6 piezoelectric matrix and 3×3 dielectric matrix need to be input for material properties in the 3D modeling of resonators.

The admittance of the structure was calculated as before and is shown in Figure 4.10. The plot shows resonance and anti-resonance at 866 MHz and 875 MHz respectively, similar to the ones calculated for YX-128° $LiNbO_3$ resonator. The value of admittance calculated for this model is in the order of $10^{-5}\mho$ whereas the one in the 2D model was as high as $10^{2}\mho$. The admittance is derived from charge flowing (current) in the electrode as seen from the Equation 4.3. Because only a thin strip was used, the amount of charge flowing through would be small, contributing to the low admittance.

So, to study the effect of this strip thickness, the thickness was increased 6 times by increasing the number of strips to 6 ($1/4^{th}$ of the λ) and the admittance was calculated. It is also plotted in Figure 4.10 (lighter curve) and can be seen that the value of admittance increases with increase in strip thickness. Though the admittance value is exactly multiplied by a factor of 6, the total number of strips suggesting a linear increase, it remains to be studied if the increase in admittance would be linear with increase in aperture of the model. This could not be studied in further detail due to the aforementioned limit on the number of nodes that could be simulated using ANSYS. But nevertheless, this reasonably explains the low value of admittance and suggests that, if modeled to the exact aperture of the resonator, the 3D simulations might provide values that are close to the ones in the real device. The attenuation values in real devices are due variety of effects including temperature, and affect the admittance characteristics of the device. Due to the non-inclusion of these attenuation effects and the low values of admittance in simulations with 3D elements all the admittance values presented henceforth are normalized.

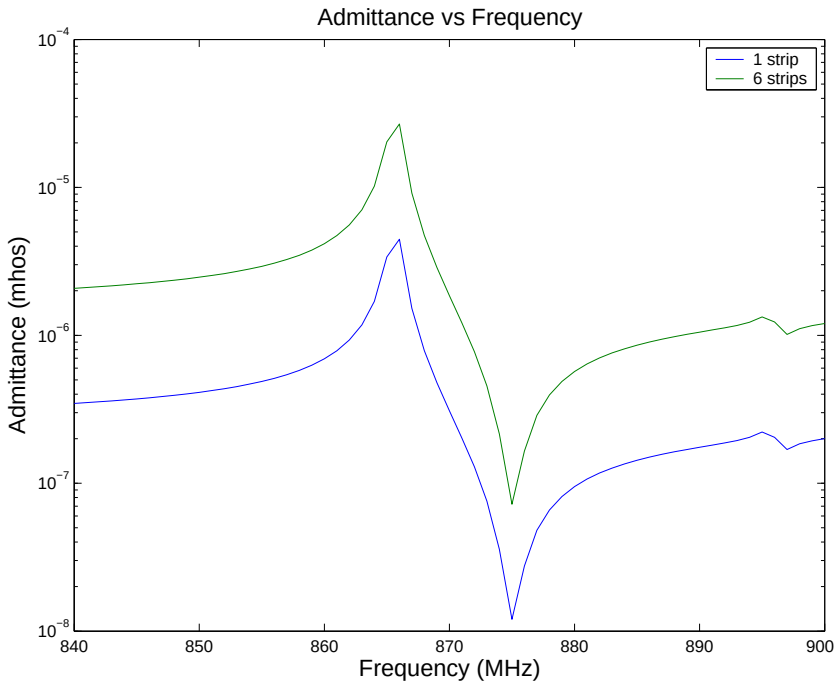

Figure 4.10: Admittance calculated for varying strip thickness

4.4 Leaky SAW Based Resonators

Leaky SAW based devices have become more popular due to the higher velocity and power handling capabilities. A brief introduction to leaky SAW based devices was given in Chapter 1 and physical properties were discussed in the Chapter 2. Together with the advantages of higher velocity and subsequent achievement of higher frequencies comes the challenges in modeling these waves effectively.

4.4.1 Issues in Modeling

Leaky SAW has some properties that are distinctly different from the Rayleigh SAW discussed until now. The essential differences and the changes made in the model due to it are discussed as follows:

- Leaky wave has displacement components in all the three directions [42], [43] and strict 2D elements used in RL wave cannot be used in this case. 3D elements similar to the ones used in the previous section need to be employed.

Though there are displacements in the third direction, the waves are nevertheless straight crested and plane strain conditions (manually) need to be applied. The degrees of freedom (U_x, U_y, U_z and volt) need to be coupled to have the same displacement (unknown) and potential values as shown in the Figure 4.11. The difference in usage of 3D elements for Rayleigh SAW simulation in the previous section was that the displacement in third direction was completely constrained but in this case the displacement is allowed but not the strain.

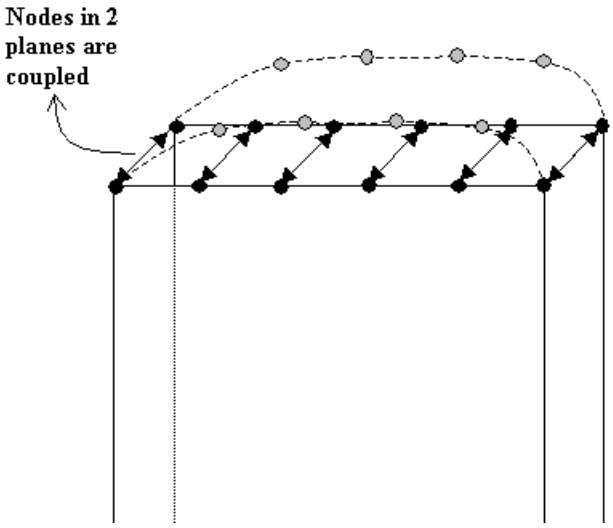

Figure 4.11: Plane strain condition for 3D model

- This wave does not die out completely within 2 or 3 wavelengths as seen in the Rayleigh wave case. This implies that the depth of the model needs to be increased. So, the depth of the model was designed to be 25λ in this simulation for leaky waves.

- In leaky SAW devices, the periodic electrodes apart from launching the waves, serve to trap the energy at the surface and make them behave as a surface wave. For this reason, simulations without the electrodes do not provide results

showing resonant behavior similar to the Rayleigh wave. So all the simulations for the leaky wave based devices were always done with electrodes on top of the substrate.

- Since 3D elements are used in simulations, the property matrices need to be input in full after the required transformation. The transformation of 3×3 dielectric matrix for the required crystal cuts usually results in off-diagonal elements. In ANSYS, only the quadratic element (SOLID226) has the capability to accept off-diagonal elements and hence only quadratic elements have been used in the simulation of leaky waves in this work.

4.4.2 36° YX- Lithium Tantalate Resonator

36° YX- $LiTaO_3$ is one of the most prominent cuts that propagate the first order leaky SAW and has been widely used in the design of SAW resonators for filtering purposes. A resonator was modeled using FEM, similar to the one fabricated by Koskela et al. [44], to compare the frequency response of the modeled resonator to the published results. The resonator was modeled taking into account the issues in modeling leaky SAW discussed in the previous section. The design parameters of the modeled resonator [44] is presented in Table 4.4. The finite element model is of

Table 4.4: Fabricated 36° YX-$LiTaO_3$ LSAW resonator parameters

Number of IDT electrodes	120
Number of reflectors	50 (one each side)
Periodicity(Pitch)	$2.214\mu m$
Metallization ratio	0.5
Electrode height (h/λ)	5.6%(Al)
Aperture	$70\mu m$

the same specifications as the one fabricated by Koskela et al. The number of IDT

fingers and reflectors were not considered in the simulations since periodic boundary conditions were applied and the model was designed for just one wavelength. Also, the full aperture was not modeled due to 'maximum number of nodes' constraint and only a thin strip (one) with thickness $0.276\mu m$ was modeled. This thickness of the strip is the same as the width of the one element in the propagation direction, which was meshed with a density of 16 elements per wavelength.

Modal analysis was performed for the periodic structure, but leaky mode resonant frequencies were not attained as a result. This could be due to a pure numerical limitation of the simulator coupled with the complexity of the leaky wave. Detection of leaky modes have proved to be both elusive and required multiple tries as reported by [40]. Also, there is a possibility of modes that could be missed due to limitations in numerical calculation methods that are used in ANSYS [36]. For this reason, a harmonic analysis was conducted to ascertain the presence of leaky modes and to directly calculate the electrical response of these structures. For the harmonic analysis, the range of frequencies was taken to be same as that of the work to which this model is being compared. The frequency range was from 860 MHz to 960 MHz. A resonance peak was observed in the frequency range at 900 MHz and the displacement profile was observed to ascertain whether it was a leaky mode.

The displacement profile is shown in Figure 4.12. The displacements in the sagittal plane is shown in Figure 4.12(a) and that of the displacements normal to the sagittal plane is shown in Figure 4.12(b). It can be seen that the shear displacements in the normal direction is considerably more than the displacements in the sagittal plane. This is similar to the displacement profile reported by Rosler et al. [42] for leaky waves in 36° YX-$LiTaO_3$. Also the leaky wave property of displacements rapidly decaying in 2 to 3 wavelengths but regaining some of the displacement components after few wavelengths in depth can be seen from the contour plot (Figures 4.13(a) and 4.13(b)) showing X and Y components of displacements. It should also be noted that the entire 25 wavelengths of depth has been shown in the contour and the displacements exist even near the bottom of the model. This type of displacement profile clearly suggests that the mode being excited is a first order leaky

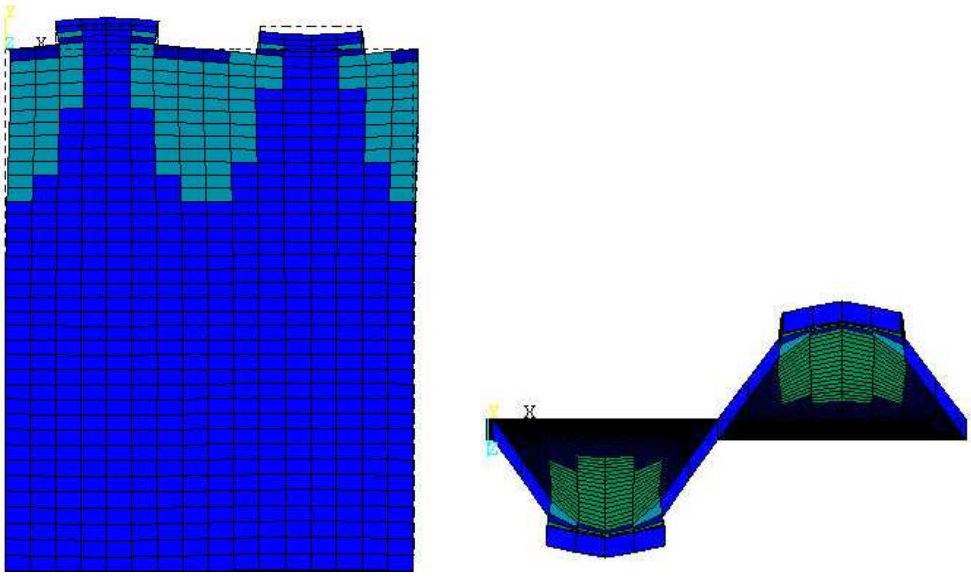

(a) Displacements in sagittal plane (b) Shear displacements in direction normal to sagittal plane

Figure 4.12: Displacement profile for leaky SAW

SAW.

The electrical response calculated and measured by Koskela et al has been compared to the results of the finite element simulation in Figure 4.14. The shape of response calculated using FEM is mostly similar to the fabricated resonator as seen from Figures 4.14(a) and 4.14(b). But some marked deviations do exist between the two results. For instance, the centre frequency of the FEM modeled resonator is at 900 MHz and that of reference is at 906 MHz. The low value of admittance problem had been addressed earlier and hence normalized results are presented. There are also some differences with ripples in the pre-resonant and post-resonant frequencies.

Some of the differences between the FEM modeled structure and the reference resonator regarding the number of electrodes and reflectors has been already outlined. Also, the size of the model could not exceed more than 32000 node due to usage of ANSYS 8.0 intermediate version. So to model 25 wavelength depth in this case, the mesh density in the direction of the wave vector was reduced to 16 ele-

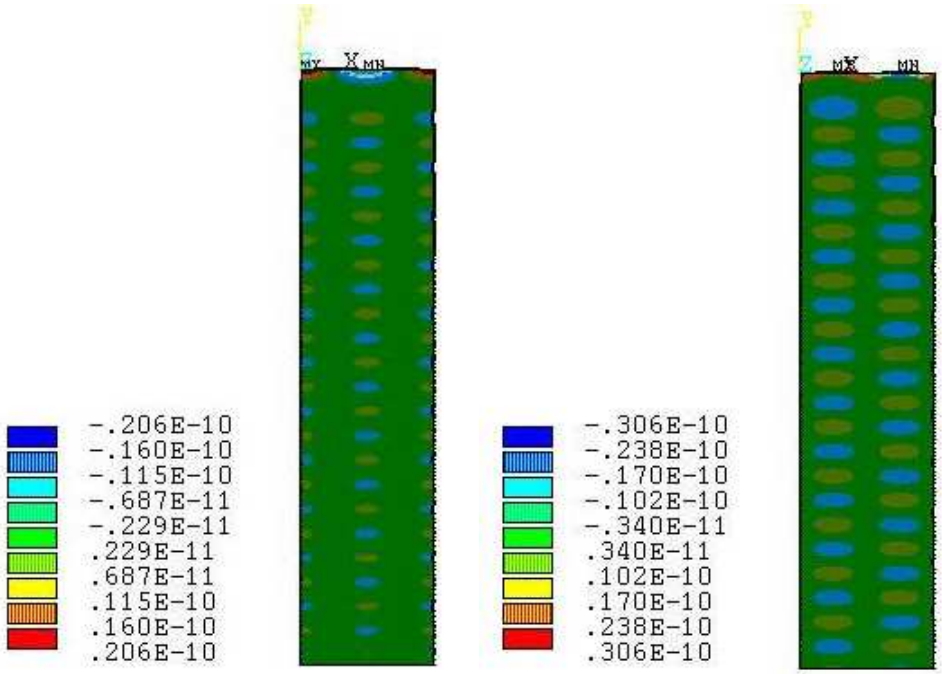

(a) X displacement contour (b) Y displacement contour

Figure 4.13: Contours showing persistent leaky SAW displacements

ments per wavelength. This could have reduced the accuracy of the centre frequency prediction. The measured resonator response in Figures 4.14(a) and 4.14(b) would have contributions from bulk wave excitation and finite resistance (conductance in this case) of the electrodes on top of the substrate that are not accounted for in this FE simulation. The unaccounted conductance value might be the reason for the lower value of the real part of admittance in the FEM calculated response. The application of strict periodic boundary conditions at the left and right boundaries results in excitation of one type of wave only. If all types of waves need to be accounted for in the one wavelength structure, removal of strict boundary conditions and application of absorbing boundary conditions is deemed necessary [34]. This type of boundary condition is currently out of scope for piezoelectric elements in ANSYS and hence was not implemented. In spite of these limitations, the FE results have been relatively accurate indicating the efficacy of the simulator.

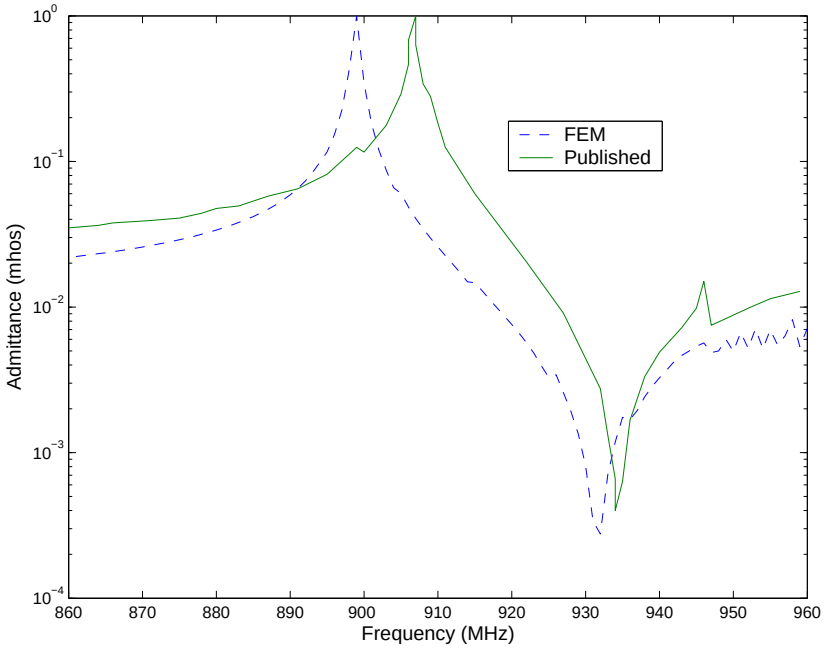

(a) Magnitude of admittance

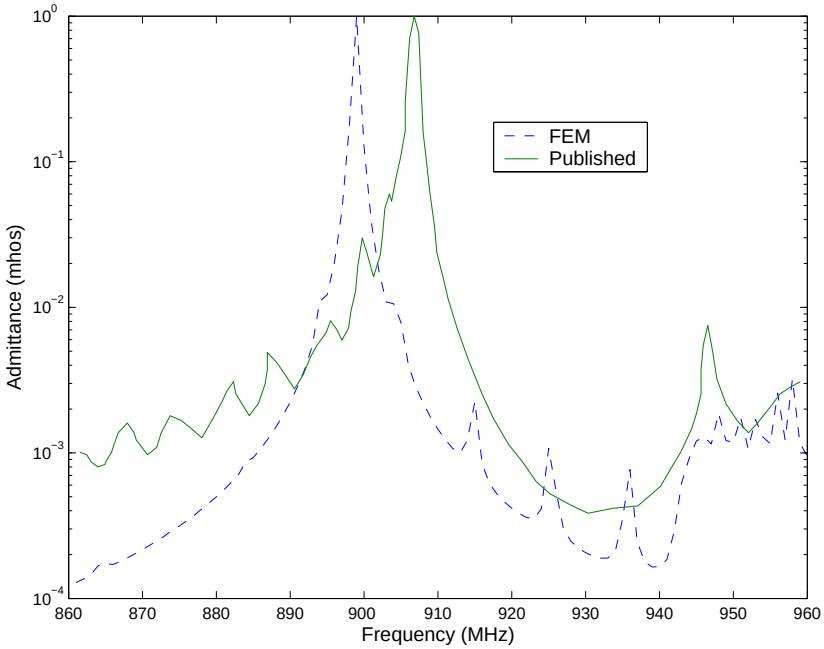

(b) Real part of admittance

Figure 4.14: Comparison of FEM calculated admittance to measured response from [44]

4.4.3 Mass Loading in Leaky Resonators

Thicker electrodes have been used in leaky SAW based devices for attaining better performances. Kawachi et al. [45] have used thick electrodes made of aluminum with h/λ around 10 % for lower losses and better electro-mechanical coupling. Similar results of better performance with thicker electrodes have also been reported by Wallner et al. [46] for these 36°-42° cuts. So, a simulation was performed on YX-42° $LiTaO_3$ resonator to determine the effect of electrode mass loading.

This cut of lithium tantalate is pretty similar to the 36° cut in the sense that both propagate leaky SAW at around similar velocities. 42° YX-$LiTaO_3$ is a relatively newer cut, but is gaining popularity due to its superior characteristics. The propagation loss is minimal and the Q-factor of the resonators fabricated are higher for this cut without affecting other performances [45].

The pitch of the resonator was kept modeled as $3\mu m$, the metallization ratio was 0.5 and h/λ was 5%. To study the effect of mass on LSAW propagation, a material with higher density was considered instead of increasing the thickness of electrodes on top of the substrate. The electrodes used in the simulations until now were aluminum which has a density of 2700 kg/m^3. Gold electrodes were used instead of it, which has a density of 19300 kg/m^3. The reason for using gold in this study is that it is more commonly used in X-ray lithography as explained in Chapter 1, whereas an aluminum metallization process is less well developed. Therefore, it may be easier to build a first proof of principal prototype using gold. Nickel is another material that is common in X-ray lithography, but it has a lower density than gold (but higher than aluminum). The response of the leaky resonator with both aluminum and gold is presented in Figure 4.15.

The admittance plot shows two distinctly different resonant frequencies as expected. The centre frequency has shifted from 668 MHz to 510 MHz signifying the effect of the heavier electrodes on the leaky SAW propagation. The result might look a bit overestimated regarding the shifting down of frequency, but is plausible considering the density of gold being roughly 7 times as that of aluminum. The other

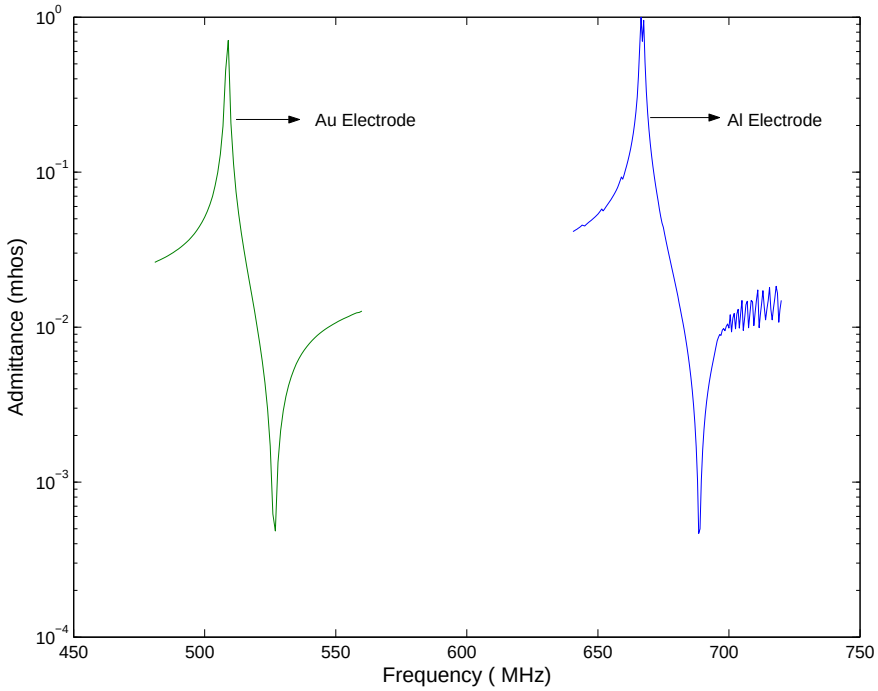

Figure 4.15: Effect of mass loading

interesting difference is the disappearance of ripples present in the aluminum case after the anti-resonance frequency. It suggests that the extra mass could be good for the resonators and can indeed improve the performance of the device. Simultaneously, it should also be considered that the centre frequency shifts down with increase in mass of the electrodes. It clearly is a trade off that should be weighed against the performance during the design of resonators.

4.5 Chapter Summary

Firstly, Rayleigh SAW based resonators on YZ-$LiNbO_3$ and 128° YX-$LiNbO_3$ were investigated. The Rayleigh SAW velocities of both the cuts were determined and the higher velocity of around 3900 m/s (with electrodes) in 128° cut is one of the highest for this type of SAW. This makes it a better choice for attaining high frequency SAW devices. The accuracy of the FE simulations were evaluated based on the results published in the literature. The results suggested that an increase in

mesh density reflects an increased accuracy accordingly. Further, two of the parameters namely velocity (v) and reflectivity (κ) were determined for 128° YX-$LiNbO_3$ based resonators for the one dimensional COM model and results were compared to published results. Also, the parameters extracted from FEM modal analysis, were used in COM simulations to compare the results of the harmonic analysis for 128° YX-$LiNbO_3$ resonator with MR=0.6 and h/λ=3%.

Leaky SAW based resonators modeled using 3D elements were discussed in sections 4.4 and 4.5. The important differences in modeling between the two types of waves (Rayleigh and leaky) was explained and subsequently results were presented for YX-36° and 42° $LiTaO_3$ cuts. The results of the 36° cut resonator was compared to the result published in literature and that of 42° cut was presented to highlight the effect of massloading. The simulation results with regards to prediction of resonance and antiresonance frequencies were within 1%. Considering the limitations of node limit, simplifications, and boundary conditions it could be deemed acceptable. The comparatively low value of admittance was addressed and attributed to the modeling of the periodic structure as a thin strip instead of the full aperture of the device. Also, for this reason the admittance values were normalized and presented.

The leaky SAW based devices can be useful for high frequency SAW devices but is limited by the fact that these waves travel just 200 m/s faster than the Rayleigh waves in YX-128° cut. If materials or modes that propagates SAW at least 1000 m/s faster than these waves could be identified and used, it would be highly useful in achieving higher frequencies of operation. The next chapter discusses one such kind of SAW, along with the modeling issues and results.

5. Longitudinal Leaky SAW for Higher Frequencies

5.1 Introduction

The research approaches to increase the frequencies of operation were listed in Chapter 1 and the one pursued in this work was to look for modes propagating at higher frequencies. Longitudinal waves are the fastest acoustic waves in solids. But they can travel only in unbounded solids and once the solid is bounded (which is the case in devices), the longitudinal waves alone cannot satisfy the stress free boundary condition and are always coupled with the fast shear wave [12]. For this reason, their velocity is between that of fast shear and longitudinal waves.

This type of wave solution has two components growing into the substrate (as compared to one in first order leaky SAW), making it more leaky than the Leaky SAW seen in the previous chapter and are called second order leaky SAW. Also another important difference between the two types of leaky SAWs is that the displacement component is confined to the sagittal plane in the second order leaky SAW. It has a combination of longitudinal and shear displacements that are confined to the sagittal plane similar to that of Rayleigh wave. But the longitudinal component of displacement dominates over the shear component and hence it is also called a longitudinal leaky SAW (LLSAW).

This type of leaky SAW exists in several types of substrate materials but initially they were known to possess a high degree of attenuation and subsequently were ruled out for use in devices. Later, Isobe et al. investigated the propagation of LLSAWs on $LiNbO_3$ and $LiTaO_3$ substrates [47]. They reported thick electrodes (above 8% for Al) on top of substrates could effectively trap the leaky SAWs to the substrate surface and reduce their attenuation into the substrate in the form of bulk acoustic

radiations. More importantly these waves were found to travel at velocities in excess of 6000 m/s in $LiNbO_3$ and around 5800 m/s in $LiTaO_3$ presenting brighter prospects for high frequency SAW devices.

YZ-$LiNbO_3$ substrates that propagate Rayleigh SAW also propagates LLSAW, albeit at a different velocity therefore showing up as a resonant peak at a different frequency. Devices based on LLSAW have been investigated by Makkonen et al. on YZ-$LiNbO_3$ substrates. Devices have been fabricated [12] and simulated [48] from 1.5 GHz to 2.5 GHz by them. For simulation purposes, they have used FEM for the electrodes alone and the Green's function method for the substrate part as compared to the pure FEM in this work. The displacement profile and frequency response of LLSAW has also been calculated [48] to which results of the pure FEM model in this work would be compared.

Since the displacement components of LLSAW are confined to the sagittal plane, they can be modeled using 2D elements similar to the Rayleigh wave devices. But this mode being a leaky one, the displacements do not die down completely within 3 or 4 wavelengths. Instead, they exist even at depths around 40 wavelengths similar to the first order leaky SAW observed in the previous chapter. For this reason, the depth of model was increased to 40 wavelengths or more in these simulations. The effect of reducing the model depth was also analyzed before deciding on the depth of the model. Only one wavelength of the resonator was modeled and periodic boundary conditions similar to other cases was also applied. Before analyzing the effect of depth of the model, metallization ratio and electrode width, the displacement profile of the LLSAW was investigated to confirm the excitation of LLSAW during the simulations.

5.2 Displacement Profile of LLSAW

A harmonic analysis was conducted for a range of frequencies and at the frequency of resonance (when displacements are maximum), the deformed shaped of the single wavelength structure is shown in Figure 5.1(a) and the general schematic of LLSAW given in [48] is shown in Figure 5.1(b). The deformed shape and the general

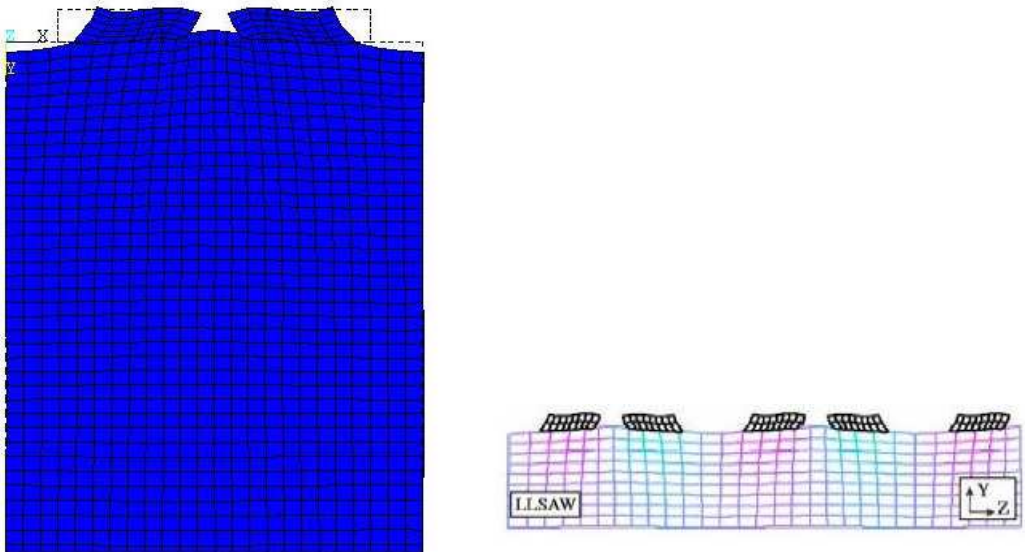

(a) LLSAW displacement displayed using ANSYS

(b) LLSAW schematic from [48]

Figure 5.1: LLSAW displacements

schematic are quite similar suggesting that the excited mode is indeed LLSAW. Also, the longitudinal and shear components of displacements are plotted against the depth in Figure 5.2. It can be seen that the longitudinal displacement component dominates near the top of the substrate and dies down rapidly (but not to zero) whereas the shear displacement component is smaller as compared to it. The displacement profile is shown only for four wavelengths for the sake of better comparison to that of published results. Though not shown in figures, the displacement components does not die down until the whole depth of the model due to the leaky nature, validating the idea of modeling more than 40 wavelengths in depth. The displacement in third direction is shown to be zero in the published result which was not taken into account in FEM simulation due to the usage of 2D elements. The effect of reducing the model depth to lesser number of wavelengths on the electrical response of the LLSAW resonator model is discussed in the next section.

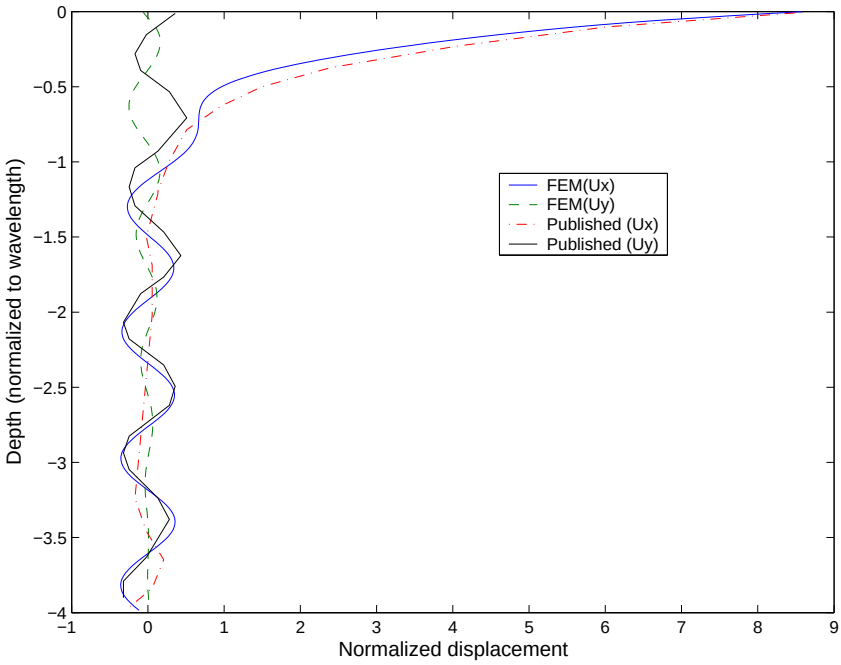

Figure 5.2: LLSAW longitudinal and shear displacement variation with depth (FEM calculated and published FEM/BEM result [48])

5.3 Effect of Depth on LLSAW Resonator Model

FEM simulations were done for LLSAW based models on YZ-$LiNbO_3$. The periodicity of the resonator was 2 μm, the metallization ratio was 0.5 and the electrode height was 7.5 %. The depth of the model was varied from 40 wavelengths to 20 wavelengths and its effect was investigated. The admittance of the structure was calculated for varying depth and it is shown in Figure 5.3. When the depth was 40 wavelengths the resonance was at 1570 MHz and it increased to 1580 MHz when depth was reduced to 30 wavelengths. It was also accompanied by increased ripples in the response. When the model depth was further reduced to 20 wavelengths, the peak of resonance was affected which split into two and the ripples also increased. This clearly suggest that reducing the model depth would adversely affect the response of the resonator structure due to leaky nature of the waves. For this reason, the simulations were performed with a model depth of more than 50 wavelengths in

the responses discussed in the following sections.

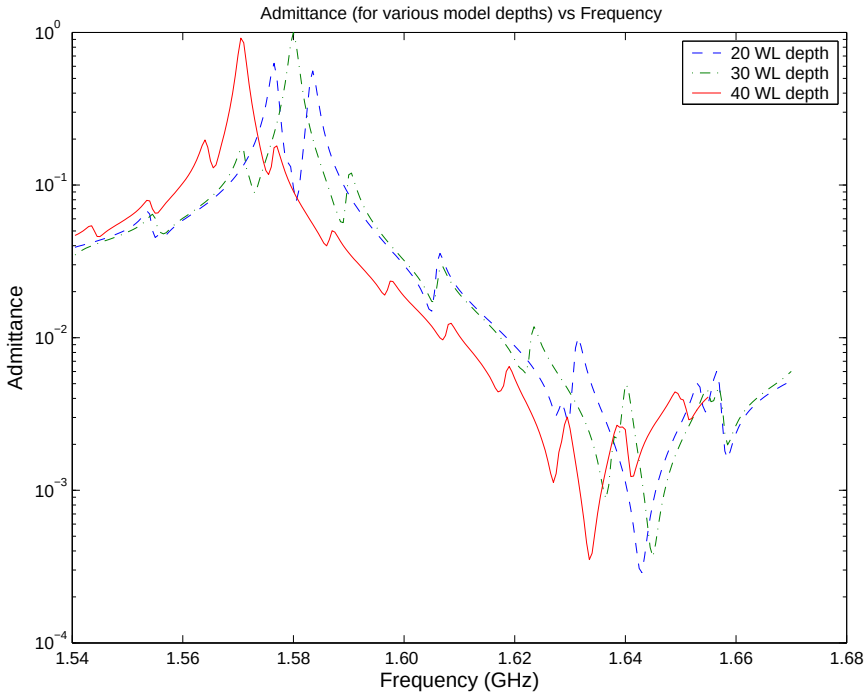

Figure 5.3: Effect of reducing model depth on LLSAW resonator model response

5.4 LLSAW resonator on YZ-$LiNbO_3$

A LLSAW resonator was modeled using FEM similar to the resonator fabricated and tested by Holmgren et al. [49]. The specifications of the resonator are given in table 5.1. The FEM model was also designed for such specifications except for the electrode height being 8 %. Also, the number of electrodes, reflectors and aperture are immaterial to the simulations due to its periodic and 2D nature.

The published test resonator results and FEM calculated results are shown in Figure 5.4. The FEM results show the resonant peak at 1535 MHz and anti-resonance at 1600 MHz as compared to resonance at 1540 MHz and anti-resonance at 1610 MHz of the published measured result. The slight difference might be due to minor difference in electrode heights and simulation artifacts. The ripples in the FEM cal-

Table 5.1: YZ-$LiNbO_3$ LLSAW resonator parameters

Number of IDT electrodes	151
Number of reflectors	37 (one each side)
Periodicity(Pitch)	$2\mu m$
Metallization ratio	0.6
Electrode height (h/λ)	7.9%(Al)
Aperture	$64\mu m$

culated result might be due to artificial termination model depth and the reflections arising out of it. The resonance curve calculated by FEM is also sharper than that of published result, due to the fact that losses occurring in the real device due to thermal effects and resistive losses are unaccounted for in this simulation.

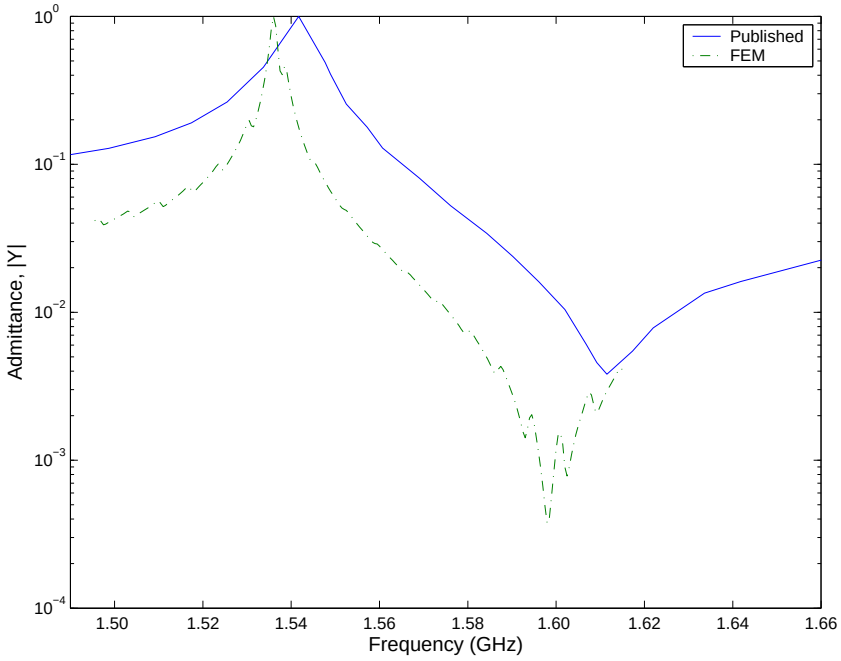

Figure 5.4: YZ-$LiNBO_3$ LLSAW resonator results compared to published result in [49]

From the centre frequency of the resonator the velocity of these LLSAWs can be calculated to be around ≈ 6150 m/s on the YZ-$LiNbO_3$. The Rayleigh SAW on the same substrate travels around ≈ 3400 as seen in the previous chapter. Thus the same substrate can be used to attain frequencies as high as 1.8 times with the same electrode widths, when LLSAW mode is as a resonant mode. Another interesting feature of these modes is that they have a higher bandwidth than other modes. It can be calculated using the formula,

$$BW = \frac{f_a - f_r}{f_a} \tag{5.1}$$

where f_a andf_r are resonant and anti-resonant frequencies. The bandwidth of the modeled resonator was thus calculated to be 0.0406. For the Rayleigh wave on the same resonator it could be calculated to 0.011. With the high velocity and bandwidth these LLSAW modes can be highly useful in the design of wide bandwidth high frequency filters.

5.4.1 Effect of Metallization Ratio and Electrode Height

To study the effect of the metallization ratio on centre frequency and in general the response of the LLSAW FEM model, a series of simulations were done. The pitch of the periodic structure was kept as 2 μm, the electrode height (h/λ) was kept constant at 8 % and the metallization ratio was varied from 0.7 to 0.3 in steps of 0.1. The model depth was kept above 50 wavelengths for all the simulations. One of the main effects of varying the MR is mass loading and the results are presented in Figure 5.5.

From the plot, it can be seen that the centre frequency decreases from 1542 MHz to 1535 MHz and 1528 MHz with the increase in MR to 0.6 and 0.7 respectively. This downshift in frequency was expected and can be attributed to the increase in mass of the electrode which tends to slow the wave velocity and subsequently decrease the frequency. When the MR was further reduced to 0.4, the centre frequency did increase, but very marginally as can be seen from the Figure 5.5. Importantly, for the MR of 0.3 the centre frequency had shifted down to around ≈1530 MHz. This

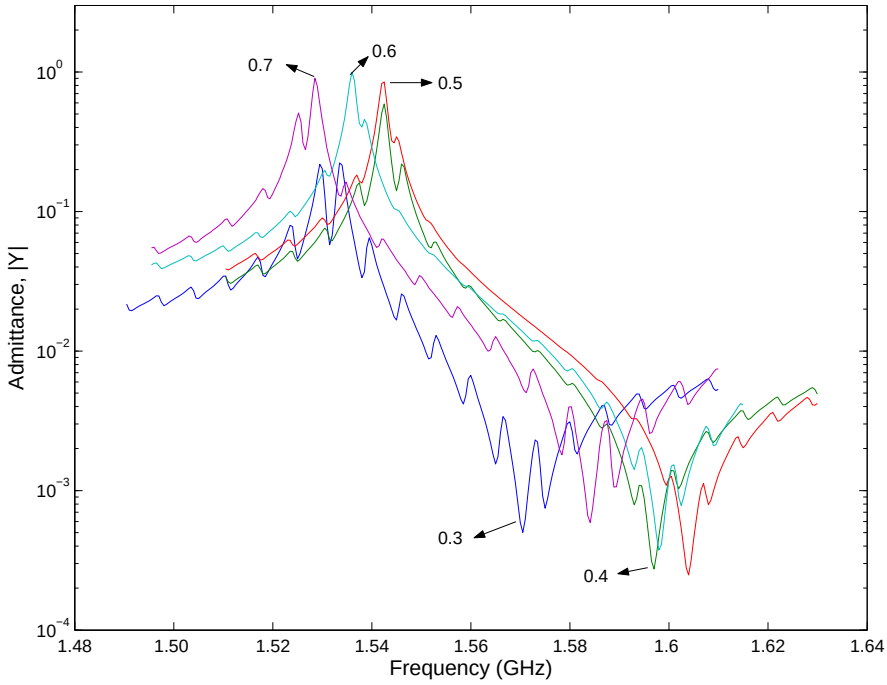

Figure 5.5: Resonator response for varying metallization ratios with $h/\lambda = 8\%$

could be due to the fact that there is less contact area between the electrode and substrate which might lead to less intense excitation of LLSAW causing a downshift of frequency. Also, it could be seen that the ripples in the response increases for both increasing and decreasing metallization ratios. This is due to the limitations of the simulator discussed before. But the ripples are the lowest for the MR of 0.5 with electrode height of 8 %. It suggests that there is an optimal height for which the simulator gives ripple free response. So, the simulator can very well be used to find this optimal electrode height for the corresponding metallization ratio.

Another interesting effect of varying the MR of the electrode structure results in variation of the bandwidth of the resonators. It can be observed that the bandwidths are maximum when the MR is 0.5 and 0.6 with a decrease in value for both metallization ratios greater and lesser than them. It is the lowest for the MR of 0.3. This study clearly suggests that the centre frequency reduces both with the increase and decrease of MR from around 0.4 to 0.5 and also the bandwidth is maximum at

around 0.5 to 0.6.

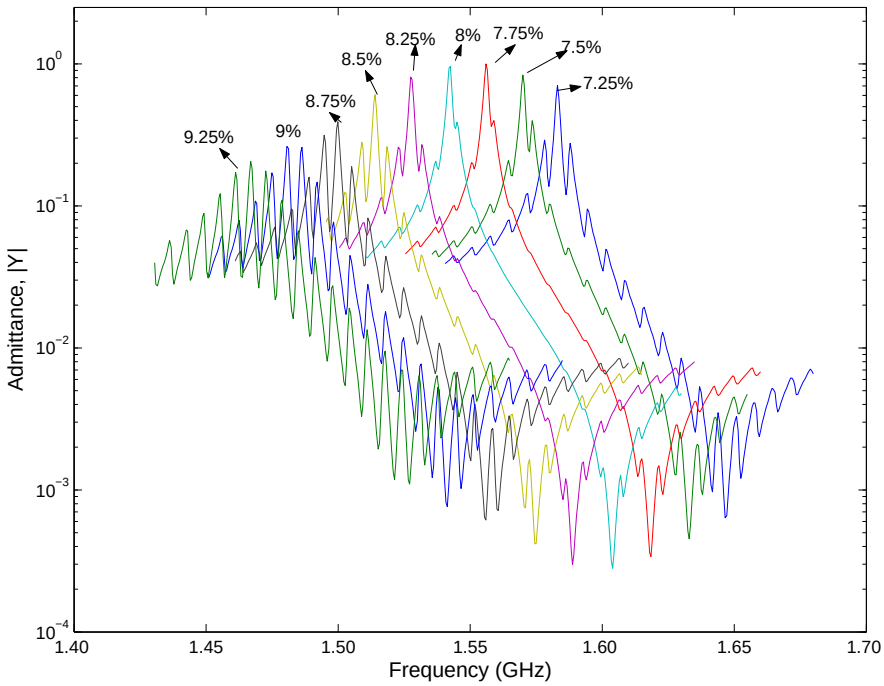

Figure 5.6: Resonator response for varying electrode heights with MR of 0.5

The study of varying metallization ratios suggested that there are optimal electrode height values for each MR. So a set of simulations were conducted for varying electrode heights (keeping MR constant). The results for MR of 0.5 is presented in Figure 5.6. The electrode heights were varied from 7.25 % to 9.25 % in steps of 0.25 %. It can be seen that there is a consistent decrease of centre frequencies with increase in electrode heights due to the effect of mass loading. Also, the resonant and anti-resonant frequencies reduce in frequency level similarly as the electrode heights are varied, suggesting that the bandwidth of the devices remains fairly constant with increase or decrease in electrode heights. But the values of maximum admittance drops on either side of the optimal value of electrode height accompanied by increased ripples in the response.

The optimal height for the case of MR=0.5 was 7.75% to 8%. The ratio of

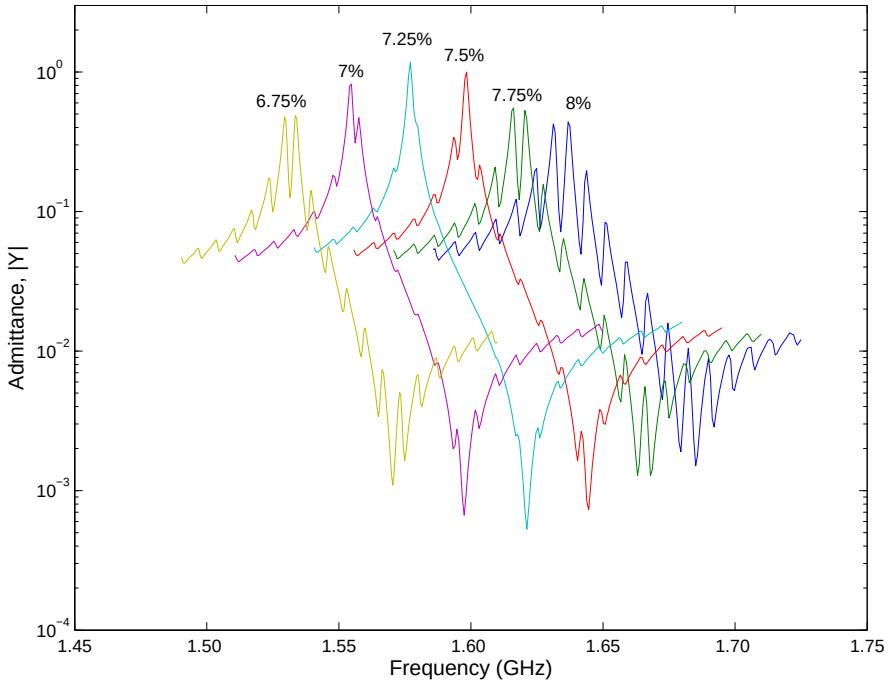

Figure 5.7: Resonator response for varying electrode heights with MR of 0.3

electrode height to width for this case can be calculated to be 31% to 32%. So, a set of simulations were conducted to find the optimal electrode height for the case of MR=0.3. The results are presented in Figure 5.7. The response is similar to the case of MR=0.5 that the centre frequencies decreased with increase in electrode heights. It can also be observed that the optimal height (h/λ) for this MR=0.3 is around 7.25%. The electrode height to width ratio can then calculated to be $\approx 48\%$. Such high ratios are more critical at smaller electrode widths for high frequency devices and present good prospects for XRL fabrication of LLSAW devices.

From these studies it can be concluded that the MR ratio affects the bandwidth of the device and electrode height affects the centre frequency more consistently. So, in the design of filters using these resonators, the MR with required bandwidth need to be determined at first, followed by determination of an optimal electrode height for this MR. Also, the results of these FEM simulations being consistent with the published results, they can be trusted in device design.

5.5 Chapter Summary

The LLSAW propagation on YZ-$LiNbO_3$ substrate was investigated with an objective of increasing the frequency of operation without changing the period of the electrodes. The LLSAW being a high velocity mode, increased the centre frequency of the resonator from 865 MHz to 1535 MHz with the same electrode period of $2\mu m$. This 2 μm (electrode width - 1 μm) can be easily fabricated using contemporary technology. The newly emerging technology, LIGA, presently has the capability to fabricate 400 nm structures [17], and could take the operating frequencies to the 4 GHz range. The displacement profile calculated using FEM was compared to the published results calculated using FEM/BEM technique. The LLSAW mode being highly leaky, the depth of the model was increased to above 50 wavelengths after studying the effects of reducing the model depth.

A LLSAW resonator was modeled using FEM with the same parameters as the test resonator for which the results were published in literature. The responses were mostly similar and the minor differences were attributed to simulator limitations and subsequent approximations. The effect of metallization ratio and electrode height were separately studied by keeping the other parameter a constant. The metallization ratio had a pronounced effect on the bandwidth of the device in addition to changing the effect on the centre frequency. In contrast, the electrode height had a more consistent effect on the centre frequency of the resonator and did not seem to affect the bandwidth of the device. Also, if the MR was decreased to 0.3 the optimal height does not reduce proportionally, but decreases only marginally. This in turn increases the electrode height to width ratio and presents good prospects for XRL fabrication of such SAW devices.

6. Summary, Conclusions and Future Work

6.1 Summary

This main purpose of this research was to provide a finite element model for one port SAW resonators. Even though the accuracy of the finite element method was known to designers, it was not pursued due to the huge computing requirements and time. Consequently, very few FE results were published for the SAW devices. For most of the FEM models in the literature, custom FE codes have been written to accomplish the published results. But after careful research and necessities for modeling SAW using FEM, the well developed commercial FE software ANSYS was used in this work.

In the course of this thesis, various models that are in use for the design of SAW devices such as delta function model, equivalent circuit model, COM model and P-matrix model were discussed. The inadequacies of these models were also briefly outlined and were attributed to the simplifying assumptions. A Finite element model which considers the full set of partial differential equations describing the problem possibly eliminates the simplifying assumptions of other models.

Development of a full level SAW model using FEM was not possible due to the node limit of the software (which in turn is dependent on computing requirements) and the size of the problem. So, the properties of Rayleigh wave, Leaky SAW and LLSAW were discussed in detail to aid in the model size reduction. Due to the uniform nature of the SAW and absence of displacement in the third direction, the model was reduced to quasi two dimensions for modeling the Rayleigh SAW based devices. Due to the periodic nature of the SAW resonators, only one wavelength of the device was modeled. Also, the depth of the model was determined according to

the nature and type of the SAW device that was being modeled. For instance, only ten wavelength depth was considered for the case of Rayleigh SAW propagation, whereas it was increased to 25 wavelengths for 1^{st} order leaky SAW and above 50 wavelengths for 2^{nd} order leaky SAW.

The accuracy of linear and quadratic elements in FEM were determined by comparing the computed free velocities of Rayleigh SAW on YZ-$LiNbO_3$ substrate. The accuracy was found to increase with increasing mesh density of linear elements and similar accuracy could be achieved by using lesser number of quadratic elements. So for most of this work quadratic elements were used in the simulations. The velocity of Rayleigh SAW was determined to be around 3480 m/s for YZ-$LiNbO_3$ and 4000 m/s for YX-128° $LiNbO_3$. Considering the fact that Rayleigh SAW was the slowest acoustic wave in a solid, 4000 m/s (free surface, loaded surface around 3850-3900 m/s) is quite high which led to the further analysis of the wave in YX-$LiNbO_3$. A set of simulations were done for resonators with various metallization ratios and electrode heights to find out the velocity (v) and reflectivity (κ) of the structures. These values were compared to the published literature results for verification and validation. Also, models based on phenomenology such as COM and p-matrix methods, require parameters to be introduced from outside for their operation. The velocity and reflectivity values calculated using FEM could be used in these phenomenological models for further simulations and device design.

The finite element model developed for the Rayleigh SAW based device was extended to leaky SAW by making appropriate adjustments to the model. The first order leaky SAW generally has displacements in the third direction also to satisfy the boundary conditions; so 3D elements were used in the analysis of leaky SAW based devices. A leaky SAW based resonator on YX-36° $LiTaO_3$ was simulated and its response was compared to a result published in the literature for a resonator with the same specifications. Also the results of a 42-YX° $LiNbO_3$ resonator was used to study the effects of electrode mass loading. The resistance of the electrodes, capacitance of the IDT fingers and other bulk wave effects were not added to the simulations. Nevertheless, the predicted response was reasonably similar to the measured results

with respect to velocity and resonance anti-resonance frequencies (both within 1%). The velocity of these first order leaky waves were only marginally faster (around 4050 m/s on loaded surface) than the high Rayleigh SAW wave velocity in YX-128° $LiNbO_3$. Clearly, these waves cannot increase the frequencies of operation to very high values unless fine structures are fabricated. So the research approach was directed towards analysis of modes traveling at higher velocities. Second order leaky SAW or LLSAW mode was found to travel at velocities in excess of 6000 m/s and hence FE model was developed for LLSAW resonators.

A FEM model was developed for YZ-$LiNbO_3$ LLSAW resonator with design specifications similar to the test resonator whose results were published in the literature. The centre frequency of this resonator was 1535 MHz, which is 1.8 times that of a Rayleigh SAW resonator (centre frequency-865 MHz) fabricated with the same period. Also, the bandwidth of the LLSAW resonator was higher than that of Rayleigh SAW resonator suggesting that these modes could help in the design of high frequency wide band filters. To determine the parameters which affect the bandwidth and centre frequencies, a series of simulations were done for various metallization ratios and electrode heights. Also, the case of MR=0.3 was studied in particular to investigate the possibility of using XRL for fabrication of LLSAW devices because of the high electrode height to width ratio required.

6.2 Conclusions

A finite element model has been developed using Commercial software ANSYS, that reduces the time to write custom codes for numerical simulations. It has also been proved that the results obtained using FEM are reasonably accurate considering the fact that quite a few approximations and assumptions were made in order to bring the size of the problem to a reasonable level. A brief review of current modeling methods also revealed that almost all of them required parameters to be introduced from outside. The FEM calculated responses are from first principles and the only inputs to the FE simulator were material properties and the geometry of the device. In fact, some of the results calculated using FEM were used in simulation of a SAW

resonator response using the COM model.

The resonance anti-resonance pattern of SAW resonators have generally been well predicted by the FEM model, but the prediction of the exact admittance has not been possible due to the application of infinite boundary condition and non-inclusion of various attenuation effects. Also, contributions to the admittance due to other propagating modes in the medium have not been included in the model which could have made the calculated results to vary from that of published results. The limitation of this simulator is mainly due to the constraint on the computing resources but not due to the (FE) method itself. The variation of the resonant (centre) frequency with changing electrode mass has been predicted well and is one of the main highlights of the FEM model. This effect can only be modeled by a numerical method and could be highly useful in design of ladder filters and networks.

The literature and reports indicated that usage of FEM for leaky SAW based resonators has been scarce and it was found that by modeling a greater depth for these kind of devices, results that could be useful in device design can be attained. The second order leaky SAW was investigated in a greater detail using FEM because of its high velocity and the potential to increase the frequencies of operation to the 5 GHz range and beyond. The results of LLSAW resonators indicated that greater depths need to be modeled in order to get ripple free responses and also other attenuation effects need to be accounted for in order to get more accurate results. Nevertheless, the preliminary results indicated that LLSAW devices present good prospects for high frequency SAW device fabrication using X-ray lithography.

6.3 Recommendation for Future Work

This research work can be extended in the following directions to achieve the full advantages of the finite element methods and to study some new exciting structures:

1. A COM/P-matrix model could be developed that is dependent on finite element solution for the required external parameters. The velocity and reflectivity of resonatord were determined in this work and other required parameters could be obtained from the admittance of the resonator determined from the

FEM, by using appropriate fitting techniques.

2. The FE model was developed for a single wavelength structure by applying a strict periodic boundary condition which allowed excitation of only one mode at a time. This was due to the non-availability of absorbing boundaries for piezoelectric elements in ANSYS. If absorbing boundary conditions could be implemented in the future, it would help in studying the interaction of SAW and bulk acoustic waves.

3. Non-traditional transducer architecture such as slanted electrodes, electrodes entrenched into the substrate, etc., could be analyzed and investigated.

4. Though a full level FEM SAW model could not be implemented immediately, the imminent usage of 64 bit computing and advances in memory technology presents good prospects for bigger FE models for SAW devices. Then the full aperture of the device could be modeled and the effects of beam steering could be studied.

5. The effect of the metallization ratio, electrode height, and height to width ratio could be studied in a greater detail with a perspective for fabrication capabilities. Also, newer materials for electrodes could be investigated and their mass loading effects could also be studied.

REFERENCES

[1] J. Koskela, *Analysis and Modeling of Surface-Acoustic Wave Resonators*. Doctor of Science, Helsinki Universtiy of Technology, Helsinki, Finland, Jan 2001.

[2] R. Weigel, D. P. Morgan, J. M. Owens, A. Ballato, K. M. Lakin, K. Hashimoto, and C. C. W. Ruppel, "Microwave Acoustic Materials, Devices and Applications," *IEEE Transactions on Microwave Theory and Techniques*, vol. 50, pp. 738–748, March 2002.

[3] C. K. Campbell, *Surface Acoustic Wave Devices for Mobile and Wireless Communications*. San Diego, California: Academic Press, 1998.

[4] D. P. Morgan, "A History of Surface Acoustic Wave Devices," *International Journal of High Speed Electronics and Systems*, vol. 10, no. 3, pp. 553–602, 2000.

[5] T. Makkonen, *Numerical Simulations of Microacoustic Resonators and Filters*. Doctor of science, Helsinki University of Technology, Helsinki, Finland, April 2005.

[6] F. S. Hickernell, "Thin-films for SAW Devices," *International Journal of High Speed Electronics and Systems*, vol. 10, no. 3, pp. 603–652, 2000.

[7] H. Nakahata, H. Kitabayashi, T. Uemura, A. Hachigo, K. Higaki, S. Fujii, Y. Seki, K. Yoshida, and S. Shikata, "Study of Surface Acoustic Wave Characteristics of SiO2/Interdigital-transducer/ZnO/ Diamond Structure and Fabrication of 2.5 GHz Narrow Band Filter," *Japanese Journal of Applied Physics*, vol. 37, pp. 2918–2922, May 1998.

[8] S. Lee, H. Jeong, S. Bae, H. Choi, J. Lee, and Y. Lee, "Epitaxially Grown GaN Thin-Film SAW Filter with High Velocity and Low Insertion Loss," *IEEE Transactions on Electron Devices*, vol. 48, pp. 524–528, March 2001.

[9] I. D. Avramov, "High-Performance Surface Transverse Wave Resonators in the Lower GHz Frequency Range," *International Journal of High Speed Electronics and Systems*, vol. 10, no. 3, pp. 735–792, 2000.

[10] T. Sato and H. Abe, "Propagation Properties of Longitudinal Leaky Surface Waves on Lithium Tetraborate," *IEEE Transactions on Ultrasonics, Ferroelectrics, and Frequency Control*, vol. 45, pp. 136–151, Jan 1998.

[11] T. Sato and H. Abe, "SAW Device Applications of Longitudinal Leaky Surface Waves on Lithium Tetraborate," *IEEE Transactions on Ultrasonics, Ferroelectrics, and Frequency Control*, vol. 45, pp. 1506–1516, Nov 1998.

[12] T. Makonnen, V. P. Plessky, W. Steichen, and M. M. Salomaa, "Surface-Acoustic Wave Devices for the 2.5-5 GHz Frequency Range Based on Longitudinal Leaky Waves," *Applied Physics Letters*, vol. 82, pp. 3351–3353, May 2003.

[13] T. Makonnen, V. P. Plessky, W. Steichen, and M. M. Salomaa, "Fundamental Mode 5 GHz Surface-Acoustic-Wave Filters Using Optical Lithography," *Applied Physics Letters*, vol. 83, pp. 3596–3598, Oct 2003.

[14] U. Knauer, J. Machui, and Clemens C. W. Ruppel, "Design, Fabrication, and Application of GHz SAW Devices," in *IEEE MTT-S International Microwave Symposium Digest*, pp. 1821–1824, 2001.

[15] A. Springer, F. Hollerweger, R. Weigel, S. Berek, R. Thomas, W. Ruile, Clemens C. W. Ruppel, and M. Guglielmi, "Design and Performance of a SAW Ladder-Type Filter at 3.15 GHz Using SAW Mass-Production Technology," *IEEE Transactions on Microwave Theory and Techniques*, vol. 47, no. 12, pp. 2312–2316, 1999.

[16] H. Odagawa and K. Yamanouchi, "10 GHz Range Extremely Low-Loss Ladder Type Surface Acoustic Wave Filter," in *Proceedings of the IEEE Ultrasonics Symposium*, pp. 103–106, 1998.

[17] S. Achenbach, T. Mappes, R. Fettig, J. Kando, and J. Mohr, "Process Conditions for the Fabrication of Sub-Wavelength Scale Structures by X-ray Lithography in PMMA Films," in *Proceedings of SPIE- The International Society for Optical Engineering*, no. v 5450, pp. 86–94, 2004.

[18] N. Yoshioka, A. Sakai, H. Morimoto, k. Hosono, Y. Watakabe, and S. Wadaka, "Fabrication of Surface Acoustic Wave Devices by Using X-ray Lithography," *Journal of Vacuum Science and Technology B. Microelectronics Processing and Phenomena*, vol. 7, pp. 1688–1691, Nov-Dec 1989.

[19] R. Lerch, "Simulation of Piezoelectric Devices by Two-and-Three-Dimensional Finite Elements," *IEEE Transactions on Ultrasonics, Ferroelectrics and Frequency Control*, vol. 37, pp. 233–247, May 1990.

[20] T. Makonnen, A. Holappa, J. Ellä, and M. Salomaa, "Finite Element Simulations of Thin-Film Composite BAW Resonators," *IEEE Transactions on Ultrasonics, Ferroelectrics and Frequency Control*, vol. 48, pp. 1241–2001, Sep 2001.

[21] SGI, INTEL, and ANSYS, "Solving 111 million degrees of freedom." www.sgi.com/pdfs/3691.pdf.

[22] S. N. Kondratiev, T. Thorvaldsson, S. A. Sakharov, O. A. Buzanov, and A. V. Medvedev, "Extraction of COM Parameters on Langasite Susbstrates and the Application to Design of a SAW Filter," in *Proceedings of the IEEE Ultrasonics Symposium*, pp. 53–56, 2001.

[23] E. Dieulesaint and D. Royer, *Elastic Waves in Solids.* Great Britain: Wiley-Interscience Publication, 1980.

[24] B.A. Auld, *Acoustic Fields and Waves in Solids*, vol. 1. Malabar, Florida: Robert E. Krieger Publishing Company, 2 ed., 1990.

[25] W. P. Mason and R. N. Thurston, eds., *Physical Acoustics - Principles and Methods*, ch. 3, pp. 109–166. New York: Academic Press, 1970. "Properties of Elastic Surface Waves" by G.W. Farnell.

[26] S. Tonami, A. Nishikata, and Y. Shimizu, "Characteristics of Leaky Surface Acoustic Waves Propagating on $LiNb0_3$ and $LiTaO_3$ Substrates," *Japanese Journal of Applied Physics*, vol. 34, pp. 2664–2667, May 1995.

[27] W.R. Smith, H. M. Gerard, J.H. Collins, T.M. Reeder, and H.J.Shaw, "Analysis of Interdigital Surface Wave Transducers by use of an Equivalent Circuit Model," *IEEE Transactions on Microwave Theory and Techniques*, vol. 17, pp. 856–864, Nov 1969.

[28] V. Plessky and J. Koskela, "Coupling-of-Modes Analysis of SAW Devices," *International Journal of High Speed Electronics and Systems*, vol. 10, no. 4, pp. 867–947, 2000.

[29] C.C.W. Ruppel, W. Ruile, G. Scholl, Karl Ch. Wagner, and O. Männer, "Review of Models for Low-Loss Filter Design and Applications," in *Proceedings of IEEE Ultrasonics Symposium*, pp. 313–324, 1994.

[30] J. Koskela, V.P. Plessky, and M.M. Salomaa, "SAW/LSAW COM Parameter Extraction from Computer Experiments with Harmonic Admittance of a Periodic Array of Electrodes," *IEEE Transactions on Ultrasonics, Ferroelectrics and Frequency Control*, vol. 46, pp. 806–816, July 1999.

[31] K.J. Bathe, *Finite Element Procedures*. New Jersey: Prentice Hall, 1996.

[32] M. Buchner, W.Ruile, A. Dietz, and R. Dill, "FEM Analysis of the Reflection Coefficient of SAWs in an Infinite Periodic Array," in *Proceedings of IEEE Ultrasonics Symposium*, pp. 371–375, 1991.

[33] Y.K. Yong, "Analysis of Periodic Structures for BAW and SAW Resonators," in *Proceedings of IEEE Ultrasonics Symposium*, pp. 781–790, 2001.

[34] M. Hofer, N. Finger, G. Kovacs, J. Schöberl, U. Langer, and R. Lerch, "Finite Element Simulation of Bulk and Surface Acoustic Wave (SAW) Interaction in SAW Devices," in *Proceedings of IEEE Ultrasonics Symposium*, pp. 53–56, 2002.

[35] H. Allik and T.J.R. Hughes, "Finite Element Method for Piezoelectric Vibration," *International Journal for Numerical Methods in Engineering*, vol. 2, pp. 151–157, 1970.

[36] Ansys 8.0 Documentation, ANSYS, Inc. Theory Reference.

[37] http://www.murata.com/catalog/p36e.pdf.

[38] M.Hofer, R. Lerch, N. Finger, G. Kovacs, J. Schöberl, S. Zaglmayr, and U. Langer, "Finite Element Calculation of Wave Propagation and Excitation in Periodic Piezoelectric Systems," in *Proceedings to WCCM V Fifth World Congress on Computational Mechanics*, July 2002.

[39] E.L. Adler, "Bulk and Surface Acoustic Waves in Ansiotropic Solids," *International Journal of High Speed Electronics and Systems*, vol. 10, no. 3, pp. 653–684, 2000.

[40] Y.K. Yong and S. Kanna, "Analysis of High Velocity Pseudo-Surface Acoustic Waves (HVPSAW) in Quartz Periodic Structures With Electrode Fingers," in *Proceedings of the Annual IEEE International Frequency Control Symposium*, pp. 301–306, 2000.

[41] Ansys Training Manual, "Introduction to Piezoelectric Analysis," Aug 2002.

[42] U. Rösler, D. Cohrs, A. Dietz, G. Fischerauer, W. Ruile, P. Russer, and R. Weigel, "Determination of Leaky SAW Propagation, Reflection and Coupling on $LiTaO_3$," in *Proceedings of IEEE Ultrasonics Symposium*, pp. 247–250, 1995.

[43] M. Hofer, N. Finger, S. Zaglmayr, J. Schöberl, G. Kovacs, U. Langer, and R. Lerch, "Finite Element Calculation of the Dispersion Relations of Infinitely Extended SAW Structures Including Bulk Wave Radiation," in *Proceedings of SPIE - The International Society for Optical Engineering*, no. v 4693, pp. 472–483, 2002.

[44] J. Koskela, J.V. Knuutila, T. Makkonen, V.P. Plessky, and M.M. Salomaa, "Acoustic Loss Mechanisms in Leaky SAW Resonators on Lithium Tantalate," *IEEE Transactions on Ultrasonics, Ferroelectrics, and Frequency Control*, vol. 48, pp. 1517–1526, Nov 2001.

[45] O. Kawachi, S. Mineyoshi, G. Endoh, M. Ueda, O. Ikata, K. Hashimoto, and M. Yamaguchi, "Optimal Cut for Leaky SAW on $LiTaO_3$ for High Performance Resonators and Filters," *IEEE Transactions on Ultrasonics, Ferroelectrics, and Frequency Control*, vol. 48, pp. 1442–1448, Sept 2001.

[46] P. Wallner, W. Ruile, and R. Weigel, "Theoretical Studies on Leaky-SAW Properties Influenced by Layers on Anisotropic Piezoelectric Crystals," *IEEE Transactions on Ultrasonics, Ferroelectric and Frequency Control*, vol. 47, pp. 1235–1240, Sept 2000.

[47] A. Isobe, M. Hikita, and K. Asai, "Propagation Characteristics of Longitudinal Leaky SAW in Al-Grating Stlructure," *IEEE Transactions on Ultrasonics, Ferroelectric and Frequency Control*, vol. 46, pp. 849–855, July 1999.

[48] T. Makkonen, V.P. Plessky, V.I. Grigorievski, L. Kopp, M. Solal, W. Steichen, and M.M. Salomaa, "FEM/BEM Simulation and Experimental Study of LLSAW Resonator Characteristics on YZ-$LiNbO_3$," in *Proceedings of IEEE Ultrasonics Symposium*, pp. 317–320, Oct 2002.

[49] O. Holmgren, J.V. Knuuttila, T. Makkonen, K. Kokkonen, V.P. Plessky, W. Steichen, M. Solal, and M.M. Salomaa, "Imaging Surface-Acoustic Fields in a Longitudinal Leaky Wave Resonator," *Applied Physics Letters*, vol. 86, pp. 024101–1–024101–3, Jan 2005.

APPENDIX A. Transformation of Matrices with Euler Angles

The Euler angles given by $(\varphi, \vartheta, \psi)$ rotate the crystal axes and align them with the required cartesian co-ordinate axes. During such rotations, the stiffness matrix, piezoelectric matrix and dielectric matrix (described in Chapter 2)also gets transformed accordingly and those values need to be input for successful FE simulations. There are many conventions that could be followed to achieve this purpose and the convention used by [24], has been used in this work. The formulae used in transformation has been adapted from [24] and the interested user is referred to the same. A MATLAB routine was written to accomplish the transformation of matrices and the results for only one of the cuts (YX-128° $LiNbO_3$, a 128° Y-cut X propagating substrate) used in this work has been presented here. The data available in the books apply to Euler angle set $(0°, 0°, 0°)$ and for other rotations transformed matrices need to be found.

$$[c] = \begin{bmatrix} 2.03 & 0.53 & 0.75 & 0.09 & 0.0 & 0.0 \\ 0.53 & 2.03 & 0.75 & -0.09 & 0.0 & 0.0 \\ 0.75 & 0.75 & 2.45 & 0.0 & 0.0 & 0.0 \\ 0.09 & -0.09 & 0.0 & 0.6 & 0.0 & 0.0 \\ 0.0 & 0.0 & 0.0 & 0.0 & 0.60 & 0.09 \\ 0.0 & 0.0 & 0.0 & 0.0 & 0.09 & 0.75 \end{bmatrix} \times 10^{11} \ (N/m^2) \tag{A.1}$$

$$[e] = \begin{bmatrix} 0.0 & -2.5 & 0.2 \\ 0.0 & 2.5 & 0.2 \\ 0.0 & 0.0 & 1.3 \\ 0.0 & 3.7 & 0.0 \\ 3.7 & 0.0 & 0.0 \\ -2.5 & 0.0 & 0.0 \end{bmatrix} \ (C/m^2) \tag{A.2}$$

$$[\epsilon] = \begin{bmatrix} 44 & 0 & 0 \\ 0 & 44 & 0 \\ 0 & 0 & 29 \end{bmatrix} \tag{A.3}$$

The Euler angle for YX-128° $LiNbO_3$ is $(0°, 38°, 0°)$ and the transformed matrices for this Euler angle are given by,

$$[c] = \begin{bmatrix} 2.03 & 0.7 & 0.58 & 0.13 & 0.0 & 0.0 \\ 0.7 & 1.94 & 0.91 & 0.09 & 0.0 & 0.0 \\ 0.58 & 0.75 & 2.45 & 0.086 & 0.0 & 0.0 \\ 0.13 & -0.09 & 0.086 & 0.758 & 0.0 & 0.0 \\ 0.0 & 0.0 & 0.0 & 0.0 & 0.569 & -0.05 \\ 0.0 & 0.0 & 0.0 & 0.0 & -0.05 & 0.781 \end{bmatrix} \times 10^{11} \ (N/m^2) \tag{A.4}$$

$$[e] = \begin{bmatrix} 0.0 & -1.85 & 1.692 \\ 0.0 & 4.44 & -2.672 \\ 0.0 & -1.544 & 2.322 \\ 0.0 & 0.091 & 0.604 \\ 4.455 & 0.0 & 0.0 \\ 0.297 & 0.0 & 0.0 \end{bmatrix} \ (C/m^2) \tag{A.5}$$

$$[\epsilon] = \begin{bmatrix} 44 & 0 & 0 \\ 0 & 38.75 & -7.27 \\ 0 & -7.27 & 34.65 \end{bmatrix} \tag{A.6}$$

The transformed matrices cannot be directly input into ANSYS but need to be rearranged according to ANSYS conventions. The Piezoelectricity chapter of ANSYS documentation discusses this in detail [36].